University of Zurich[UZH]

Effects of plant productivity on soil organic carbon stocks and ecosystem carbon fluxes of an extensively managed Swiss mountain grassland

GEO 511 Master's Thesis

Author
Elisa Rachele Romana Filippini
18-705-848

Supervised by
Matthias Volk (matthias.volk@agroscope.admin.ch)

Faculty representative
Prof. Dr. Michael W.I. Schmidt

25.07.2023
Department of Geography, University of Zurich

Agroscope

University of Zurich[UZH]

Master's Thesis

Effects of plant productivity on soil organic carbon stocks and ecosystem carbon fluxes of an extensively managed Swiss mountain grassland

---

submitted in fulfilment of the requirements for the degree of
Master program

Department of Geography, University of Zurich
Research Group for Climate and Agriculture, Agroscope Zurich

Under supervision of

Dr. Matthias Volk,
Agroscope, Zurich

Prof. Dr. Michael Schmidt,
University of Zurich

Submitted by

Elisa Rachele Romana Filippini
Zurich, 25.07.2023

List of Figures

List of Tables

Abstract

Grassland ecosystems are a dominant land cover worldwide and can be important carbon sinks. Management interventions, such as cutting and fertilising, can influence soil organic carbon (SOC) dynamics. Because agriculture is responsible for substantial greenhouse gas (GHG) emissions, thus contributing to global warming, it is important to understand which is the most suitable management practice to improve the carbon sink capacity of grasslands, or at least to minimise SOC losses to the atmosphere.

The influence of aboveground productivity on SOC stocks and CO_2 exchanges between the biosphere and the atmosphere is still unclear. This Master Thesis aims to understand the relationship between plant productivity, plant CO_2 assimilation (GPP), ecosystem respiration (ER) and the resulting SOC stocks in an extensively managed mountain grassland situated in the canton of Graubünden (CH). For this, six different aboveground productivity categories are obtained by different fertilisation combinations of nitrogen, phosphorus and potassium (NPK). Soil samples (1990-2022) were analysed for SOC stocks and total nitrogen (N_{tot}). Data on annual yield and daily weather conditions are available (1990-2022). Net ecosystem carbon exchange (NEE) was measured between April 2022 and April 2023 on 12 campaigns with transparent chambers. From NEE, ecosystem respiration normalised for 10 °C (ER_{10}) and gross primary productivity (GPP_{pot}) were derived.

This study found a decline in SOC stocks of -14.60 ±1.55 % between 1990 (9.66 ±0.27 $kg\,m^{-2}$) and 2022 (8.20 ±0.18 $kg\,m^{-2}$) because of climate warming. The degree of change of the SOC stock was not correlated with fertilisation driven differences in plant productivity. No differences in mean GPP_{pot} (9.34 ±0.12 µmol CO_2 $m^{-2}\,s^{-1}$), ER_{10} (-2.74 ±0.04 µmol CO_2 $m^{-2}\,s^{-1}$) and their ratio (3.24 ±0.06) were found between different productivity categories. Finally, no relationship was found between SOC stocks and the ratio GPP_{pot}/ER_{10}.

This work provided information on how a possible influence of different aboveground productivity on SOC stocks and NEE could be difficult to detect, since the carbon cycle is also influenced by many other factors, such as weather variability and nutrient availability. Further studies could be conducted in a similar pre-alpine grassland, but one not limited by nitrogen availability, and in a year not affected by drought, also considering possible differences in belowground biomass.

Acronyms and Abbreviations

C_{min}	Mineral carbon
C_{tot}	Total carbon
ER	Ecosystem respiration
ER_{10}	Ecosystem respiration normalised at 10 °C
GDD_{sum}	Sum of growing degree days
GHG(s)	Greenhouse gas(es)
GPP	Gross primary productivity
GPP_{pot}	Potential gross primary productivity
GS	Growing season
GSL	Growing season length
IDM	De Martonne aridity index
K	Potassium
MAP	Mean annual precipitation
MAT	Mean annual temperature
N	Nitrogen
NEE	Net ecosystem (carbon) exchange
NEE_{day}	Net ecosystem (carbon) exchange during the day
NEE_{night}	Net ecosystem (carbon) exchange during the night
NPK	Mineral fertilisation with nitrogen, phosphorus, and potassium
N_{tot}	Total nitrogen
OC	Organic carbon
OM	Organic matter
P	Phosphorus
P_{tot}	Total precipitation
$Reco_{day}$	Ecosystem respiration during the day
$Reco_{night}$	Ecosystem respiration during the night
RelS	Relative sunshine duration
SM	Soil moisture
SOC	Soil organic carbon
SOM	Soil organic matter
ST	Soil temperature
T_{max}	Maximum temperature
T_{mean}	Mean temperature
T_{min}	Minimum temperature

Contents

1 Introduction

1.1 Background

Definition and importance of grasslands

In regions defined as grassland, a minor component of woody vegetation is present and herbaceous vegetation dominates (Pendall et al. 2018). Grasslands cover between 20 and 40 % of the global land surface, excluding Antarctica and Greenland, and almost 70% of the total agricultural land (Bahn et al. 2008, Eze et al. 2018, FAO 2010, Rogger et al. 2022, Scholz et al. 2018). Grassland ecosystems contribute to approximately one-third of the total net primary production and store considerable amounts of organic carbon (OC) (Crowther et al. 2019, Eze et al. 2018, Poeplau et al. 2018). In Europe, especially where highly productive crop production is restricted by climate or topography, grassland is one of the most common land uses (Bahn et al. 2008, Soussana et al. 2007).

Agriculture and carbon cycling

The majority of terrestrial OC, the primary constituent of organic matter (OM), is stored in soils (Crowther et al. 2019, Hofmann et al. 2016, Lal 2004, Paustian et al. 2016, Volk et al. 2011). It represents long-term carbon storage in the soil and plays a crucial role in soil fertility, water holding capacity, and overall soil health (Paustian et al. 2016). In order to achieve positive ecosystem carbon balance, the photosynthetic activity of plants and the related carbon fluxes entering the soil need to exceed the sum of autotrophic and heterotrophic respiration and other carbon losses (harvesting, grazing, methane emissions and leaching) (Davidson & Janssens 2006, Lal 2004, Rogger et al. 2022). Several studies have found grassland ecosystems to be important carbon sinks (Hörtnagl et al. 2018, Pendall et al. 2018, Rogger et al. 2022, Soussana et al. 2007). Management interventions, such as grazing, cutting and mulching, can influence SOC dynamics in grasslands (Poeplau et al. 2018). To alleviate nutrient limitation of plant growth and stimulate primary productivity, nutrients in the form of fertilisers are often applied in agricultural systems (Crowther et al. 2019, Poeplau et al. 2018, Soussana et al. 2007). This practice also influences the carbon cycle. Several studies have found a positive correlation between increased productivity using fertilisers and SOC stocks (Eze et al. 2018, FAO 2010, Poeplau et al. 2018, Sanderman et al. 2017). Because agriculture generates significant greenhouse gas (GHG) emissions, thus contributing to global warming, it is important to understand how the carbon sink capacity of grasslands could be improved (Paustian et al. 2016, Rumpel et al. 2020). Some authors claim that management practices that promote the regeneration of SOC would make it possible to mitigate agriculture's GHG footprint (Lal 2004, Rumpel et al. 2020, Sanderman et al. 2017). This topic is also becoming increasingly relevant, because climate change can alter carbon cycling in grasslands, but it is still uncertain which effects global warming will have on carbon budgets (Davidson & Janssens 2006, Pendall et al. 2018). It is important to find the most suitable management practices in agriculture that can increase SOC stocks globally, or at least mitigate SOC losses to the atmosphere (FAO 2010, Rumpel et al. 2020, Wiesmeier et al. 2013). It is essential to focus on grasslands, as this land cover type is dominant worldwide.

Research gaps and relevance of this research

The influence of productivity on SOC stocks and OM turnover rates is still unclear (Sanderman et al. 2017). It is thus necessary to better understand the interactions between management activities in grassland and climate change, especially if mitigation of global warming through carbon sequestration is intended (Eze et al. 2018). The results of this project will help to fill these knowledge gaps.

The GHG budget of grasslands, with special attention to CO_2 moved into the focus of research, as permanent grasslands store much more SOC compared to arable fields. The exchange of GHG between the grassland ecosystem and the atmosphere is strongly affected by grassland managements, such as the amount and type of fertiliser applied, thus influencing carbon's biogeochemical cycling (Hörtnagl et al. 2018). Therefore, one possible mitigation strategy for the global warming crisis appears to be increasing the storage of atmospheric CO_2 as OC in the soil (Puche et al. 2023, Rumpel et al. 2020). To this end, grasslands and their productivity related to different fertilisation practices are of central importance.

1.2 Research questions

This master thesis aims to understand the relationship between plant productivity, plant CO_2 assimilation, ecosystem respiration (ER) and the resulting SOC stocks in a mountain grassland (Figure 1). The research questions are:

1. Is the SOC stock in the chosen Swiss mountain grassland site shrinking or rising with climate warming?
2. Is the degree of change of the SOC stock correlated with fertilisation driven differences in plant productivity? Does higher productivity translate into lower SOC losses?
3. Are there differences in potential gross primary productivity (GPP_{pot}), ecosystem respiration normalised at 10 °C (ER_{10}) and their ratio (GPP_{pot}/ER_{10}) between different productivity categories?
4. Is there a positive relationship between the SOC stocks and the ratio GPP_{pot}/ER_{10}?

1.3 Objectives and hypotheses

Fertilisation strongly affects yield (FAO 2010). The aim of this project is to investigate if and how above ground productivity affects the SOC stock, respectively, if and how the carbon sequestration depends on the fertilisation management practice. The study aims to show which management is most suited to achieve carbon sequestration in grassland soils, thus mitigating climate change and compensating for GHG emitted by agriculture. Nevertheless, SOC sequestration is only one temporary component of the strategy to mitigate global warming. OC sequestration has a finite lifespan and is only efficient until SOC stocks have reached a new equilibrium (Paustian et al. 2016, Rumpel et al. 2020).

The first hypothesis to be tested is that the SOC stocks may shrink with rising temperatures and subsequently increasing microbial respiration (Davidson & Janssens 2006, Rumpel et al. 2020, Sanderman et al. 2017). The second hypothesis is that the SOC stock increases with increasing productivity in the different management

forms, because the OC input is greater than the combined ecosystem carbon losses (Davidson & Janssens 2006, FAO 2010, Paustian et al. 2016, Poeplau et al. 2016, Rumpel et al. 2020). The third hypothesis is that CO_2 fluxes differ between productivity categories and increase with aboveground productivity, as different yields affect carbon cycling (Bahn et al. 2008). The last hypothesis to be tested is that higher GPP_{pot}/ER_{10} ratios are found in field parcels with higher SOC stocks, indicating a higher net carbon gain by the ecosystem. This could be because either more carbon can be assimilated through photosynthesis or/and less carbon is lost to the atmosphere via ER (Davidson & Janssens 2006).

Figure 1: Grassland in Muldain. Picture taken on 6 June 2023, before the first harvest of the season.

2 Materials and Methods

2.1 Experimental site and treatment design

The research site is located in Switzerland in the Canton of Graubünden in Muldain ($46°41'25.746''N$, $9°31'05.415''E$) at an altitude of 1200 m a.s.l. (Figure 2). The soil at the location is defined as Gleyic Fluvisol (WRB), and the soil texture is characterised by sandy loam (27% clay, 26% silt, 40% sand, 6.5% org. C) (Agroscope 2021). The grassland site is extensively managed and has been receiving the same treatments since 1989. The long-term experiment includes 16 treatment combinations on four replicates, for a total of 64 parcels with an area of 10 m^2 each (Agroscope 2021) (Figure 3).

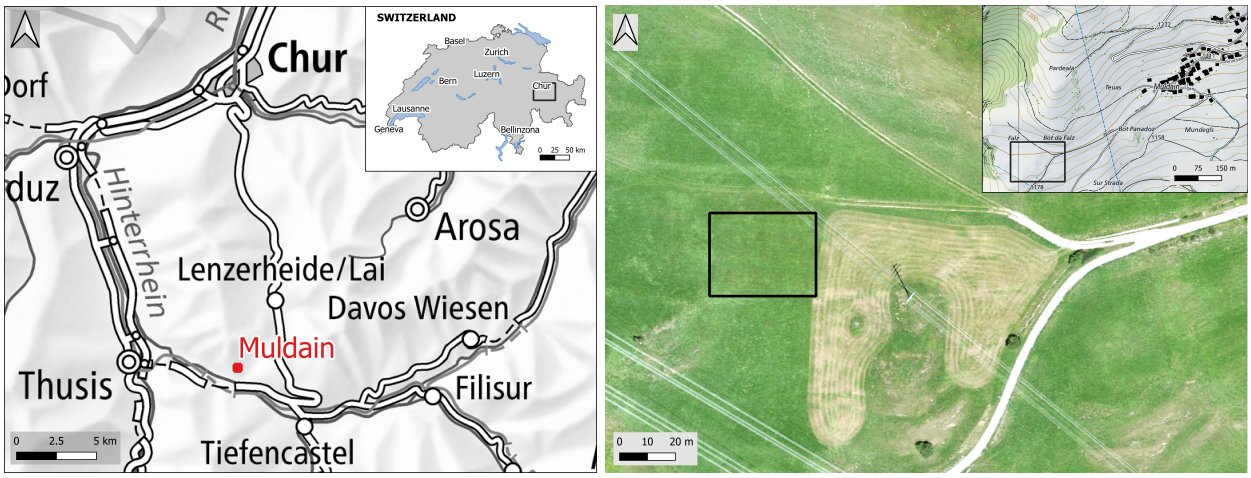

Figure 2: Location of the grassland field under study in Muldain. The image on the left shows the geographical location of Muldain in Switzerland, Canton Graubünden. A zoom shows the exact location of Muldain, south of Chur and Lenzerheide and east of Thusis. The black quadrant in the right-hand image shows the exact location of the investigated grassland field in Muldain. Source: ©swisstopo.

P0K1.5 16	P0.5K0 15	P1.5K0.5 14	P1K0 13	P1K1.5 700 g m^{-2} 12	P0.5K1.5 11	P0K0 450 g m^{-2} 10	P1K0.5 9	P0.5K1 640 g m^{-2} 8	P1.5K1 660 g m^{-2} 7	P0K1 490 g m^{-2} 6	P1.5K0 5	P1K1 680 g m^{-2} 4	P0.5K0.5 3	P1.5K1.5 2	P0K0.5 1	REP 1
P0.5K0.5 32	P1K0.5 31	P1K1.5 700 g m^{-2} 30	P0K0 450 g m^{-2} 29	P1.5K1.5 28	P0.5K0 27	P0K1.5 26	P0.5K1 640 g m^{-2} 25	P1K1 680 g m^{-2} 24	P1K0 23	P0K0.5 22	P1.5K0.5 21	P1.5K1 660 g m^{-2} 20	P0K1 490 g m^{-2} 19	P0.5K1.5 18	P1.5K0 17	REP 2
P0K0.5 48	P0K1 490 g m^{-2} 47	P1K1 680 g m^{-2} 46	P0.5K1.5 45	P1.5K0 44	P1.5K0.5 43	P1.5K1 660 g m^{-2} 42	P1K0 41	P0.5K0 40	P0K1.5 39	P0.5K0.5 38	P1.5K1.5 37	P0.5K1 640 g m^{-2} 36	P1K1.5 700 g m^{-2} 35	P1K0.5 34	P0K0 450 g m^{-2} 33	REP 3
P1.5K1 660 g m^{-2} 64	P0.5K1 640 g m^{-2} 63	P1.5K0 62	P1.5K1.5 61	P1K1 680 g m^{-2} 60	P0K1 490 g m^{-2} 59	P0K0.5 58	P0.5K0.5 57	P1K1.5 700 g m^{-2} 56	P1K0.5 55	P0K0 450 g m^{-2} 54	P0.5K1.5 53	P1.5K0.5 52	P0.5K0 51	P1K0 50	P0K1.5 49	REP 4

Figure 3: Experimental complete randomised block design. The plot is divided into four replicates (REP1, REP2, REP3 and REP4) of 16 fertilisation treatment combinations of phosphorus (P) and potassium (K). The upper replicate faces North and further up the slope. In each cell, the plot number and treatment combination are indicated. In the 24 green-coloured plots selected for this work, the mean productivity (2013-2022) is indicated, and the green colours represent the productivity gradient.

This master thesis will focus on a subset of six treatments that cover the range of productivity and include a phosphorus (P) and potassium (K) fertilisation gradient. The same amount of nitrogen (N), 25 $kg\,ha^{-1}year^{-1}$, is applied to all parcels. In addition, P and K are applied at different rates, from 0 to 1.5, compared to the norm (P_2O_5: 1 = 72 $kg\,ha^{-1}year^{-1}$ and K_2O: 1 = 216 $kg\,ha^{-1}year^{-1}$). The grass is cut three times during the summer period from June to September, and the mean (2013-2022) annual dry yield ranges from 450 $g\,m^{-2}$ for the P0K0 treatment, to 700 $g\,m^{-2}$ for the P1K1.5 treatment. These mean yield values (2013-2022) will be used as names for the six productivity categories (Figure 3). The average productivity of this period was selected, rather than of the whole available time series or of one single year, because it is believed to better represent the current climate and nutrient availability.

2.2 Climate parameters

2.2.1 Historical climate

Available data and parameters calculation

Daily minimum and maximum temperatures (T_{min} and T_{max}, °C), daily relative sunshine duration (RelS, %) and daily total precipitation (P_{tot}, mm) were interpolated for Muldain by MeteoSwiss for the last 47 years (1977-2023) using data from neighbouring meteorological stations. Because data for yield and SOC stocks are available since 1990, the period between 1990 and 2022 was considered for weather parameters. The term calendar year refers to the period between January 1 and December 31 of the same year, while agricultural year refers to the period between the last harvests of two consecutive years, from October 1 of the previous calendar year to September 30 of the following year. From these daily weather parameters, several climatic parameters were calculated:

- Growing season length (GSL, Days): days between the first and the last consecutive five days with a mean daily air temperature higher than 5°C ('5mid' method) (Mesterházy et al. 2018). GSL, especially in a mountain grassland, is an important influencing factor for biomass production (Davidson & Janssens 2006).

- Heat accumulation (GDD_{sum}, °C): accumulation of growing degree days (GDD). In agriculture, the concept of GDD is frequently used to describe the phenological development of plants (Romano et al. 2014). Equation 1 illustrates how GDD was calculated (Mcmaster & Wilhelm 1997). Various researchers have utilised different base temperatures (T_{base}) to calculate GDD for grassland (Bürli et al. 2021, Mcmaster & Wilhelm 1997, Romano et al. 2014). Here, a value of 0 °C was chosen for T_{base}, so GDD_{sum} is equal to the sum of positive (> 0 °C) mean daily temperatures in the chosen period (calendar year, agricultural year, growing season, month).

$$GDD = \frac{T_{max} + T_{min}}{2} - T_{base} \tag{1}$$

- Mean temperature (T_{mean}, °C): the sum of mean daily temperatures (mean between minimum and maximum daily temperature) divided by the number of days in the chosen period.
- Total precipitation (P_{tot}, mm): the sum of daily precipitation during the chosen period.
- De Martonne aridity index (IDM, unitless): the ratio between the total annual precipitation divided by the mean annual temperature with an addition of 10 °C (Equation 2) (Emadodin et al. 2021).

$$IDM = \frac{P_{tot}}{T_{mean} + 10} \tag{2}$$

- Mean relative sunshine duration (RelS, %): mean ratio between the effective sunshine duration and the maximally possible if no clouds were covering the sun during the chosen period.

Overview of the climate in Muldain (1990-2022)

Between 1990 and 2022, the MAP was 939 mm, and the MAT was 7°C (Figure 4). The MAT has significantly increased in Muldain over the last 32 years by about 1.5°C, with a slope of +0.05°C yearly (Figure 4). Temperatures are getting higher, especially during the spring and summer months (from April to July). In contrast, no temperature increases were found for the other seasons (except for November and December). The increased temperatures would be expected to translate into longer growing seasons. The simple linear regression model predicts an increase in GSL of about one day every two years, with important interannual variations. However, this linear model is not statistically significant.

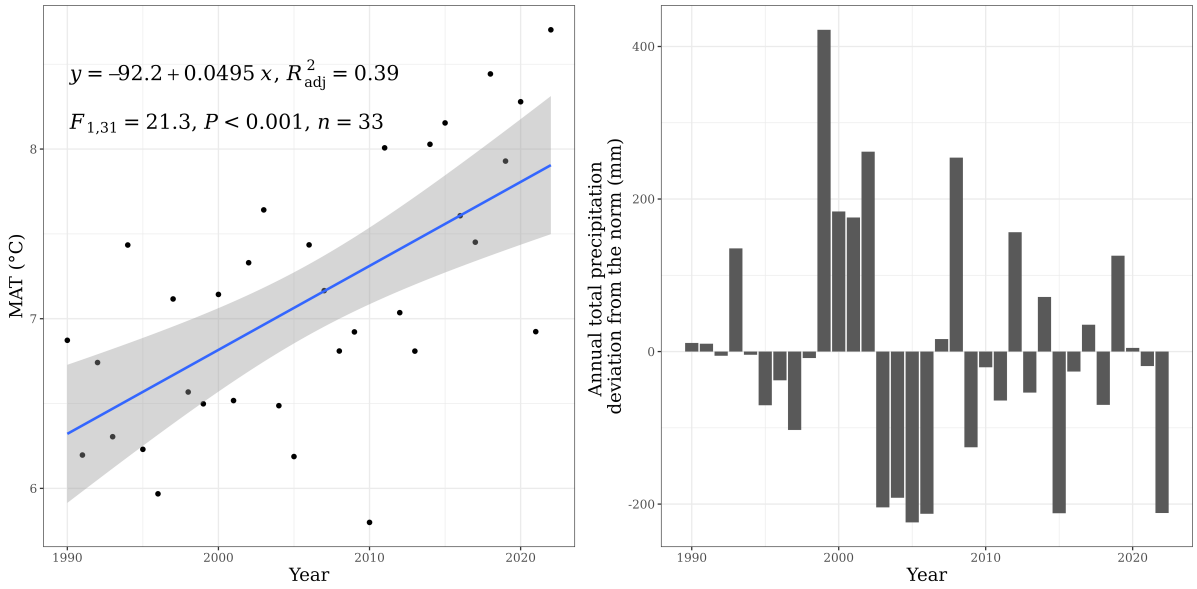

Figure 4: Historical climate in Muldain (1990-2022). The figure on the left shows the significant increase in the mean annual temperature with the results of the simple linear regression model. The graph on the right displays the deviations from the norm (939 mm) of the total annual precipitation.

No trends were found for monthly and yearly P_{tot} over time (Figure 4). Additionally, an increasing

trend was found for the RelS. This means that precipitation is getting less evenly distributed over the year. Because a moderate negative Pearson correlation between annual P_{tot} and mean annual RelS duration was found, years with higher RelS duration could have received less precipitation. This, together with increasing temperatures and with constant precipitation led to increasingly dry conditions, especially during the years with P_{tot} below mean values. A (statistically non significant) decreasing trend in IDM, where lower values stand for more arid conditions, was found over time (Emadodin et al. 2021). This is in line with several studies reporting more pronounced increasing temperatures in Alpine regions and several drought periods in Switzerland because of increased temperature and pronounced precipitation deficits (De Boeck et al. 2016, Rogger et al. 2022, Volk et al. 2021). A summary of the results regarding Pearson correlation coefficients and Mann-Kendall Test for weather parameters over time can be found in the Appendix (Table 9 and Table 10).

2.2.2 Weather in Valbella and the Alpine region between January 2022 and June 2023

The *Alpenklima Sommerbulletin 2022: Klimazustand in den Zentral- und Ostalpen*, created by DWD et al. (2022), proposes an overview of the summer weather in the Swiss Alps in 2022, representative for Muldain. Compared to the reference period of 1991-2020, temperatures between May and August, particularly in October, were generally above normal. In most of the central and eastern Alps during May to August, the amount of sunshine was significantly above average. Furthermore, the precipitation shortfall in these regions was not made up for by the regionally above-average precipitation in June and September. Due to the mainly sunny conditions, the summer also had a protracted period of minimal rainfall. May, July, and August, along with October, were especially dry months in the Alps.

In Table 7 (Appendix), the weather in Muldain from January 2022 to June 2023 is shown in more detail by reporting minimum, maximum and mean monthly temperature, total monthly precipitation and mean monthly RelS duration. The data, provided by MeteoSwiss (IDAweb), are for the nearby meteorological station in Valbella.

2.2.3 Soil temperature and moisture (2022-2023)

Soil moisture (rel-%, where 100% equals field capacity) and soil temperature (°C) were monitored continuously between 19.04.2022 and 29.04.2023, using PlantCare mini-loggers (firmware version 1.34, hardware version C1.0). Two loggers were placed at 10 cm depth in 8 selected plots (10, 12, 29, 30, 33, 35, 54, and 56), representing the four replicates of the highest (700) and lowest (450) productivity categories. Data were recorded hourly until April 26, then four times daily at six-hour intervals (00:30, 6:30, 12:30, and 18:30). All loggers functioned until 03.03.2023; after that, some stopped recording because of empty batteries. Figure 5 shows the time course of soil moisture and temperature. For each time point, data was first averaged for each plot between two repetitions (n=2) and then between the four replicates (n=8).

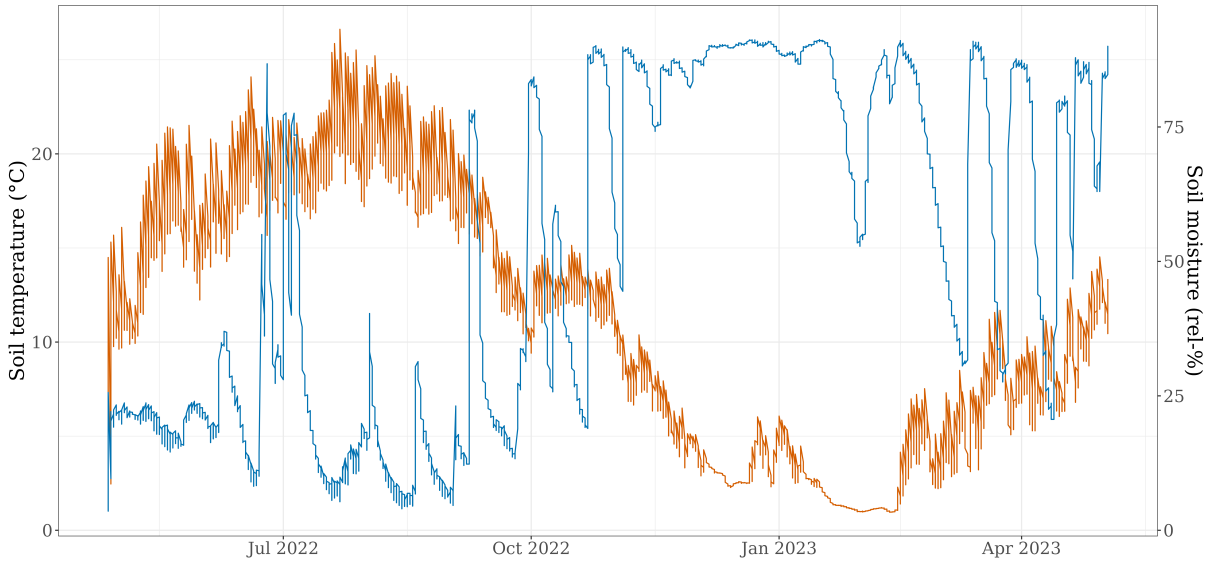

Figure 5: Soil temperature and moisture in Muldain (2022-2023). The graph shows daily average values for temperature (orange line) and moisture (blue line) in the soil from April 2022 to April 2023. The temperature curve follows the seasonal course, with warmer temperatures in summer and colder temperatures in winter. The soil moisture shows maximum values during winter 2022 and spring 2023 and low values during summer 2022, which coincide with the drought recorded for that period (DWD et al. 2022)

2.3 Soil samples

2.3.1 Soil sampling and analysis

Soil sampling 1989-2022

Since the fertiliser management project's begin in 1989, soil samples for the topsoil (depth: 0 - 20 cm) were taken every year at the end of October. The sampling time was always after the last harvest, before fertilisation and before the first snowfall. For each field parcel, 1 kg of soil was randomly sampled by taking seven cores (4 cm diameter) with the Edelmann drill. The soil was oven dried (40°C), sieved (2mm) and archived in plastic jars. For this project, soil samples from 1990 onwards were considered, since the first fertilisation for this experiment took place at the end of 1989 and harvest data starts in 1990.

Additional soil sampling in 2022

In October 2022, soil samples with a defined volume were taken at the upper soil depth (0 to 20 cm) in addition to the usual samples (Figure 25 in the Appendix). Each plot was randomly sampled twice, once towards the north and once towards the south, using sampling tubes (core diameter: 5 cm). The superficial grass was cut off at the top of the soil samples, then separated according to depth (0 to 10 cm, 10 to 20 cm and any remainder). The samples were weighed, oven dried at 105 °C for 48 hours and then weighed again. The samples were then sieved (2 mm) and weighed again after stones and roots remaining in the sieve had been removed.

Total carbon and nitrogen analysis

In 2022, all soil samples were analysed for total soil carbon (C_{tot}) and nitrogen (N_{tot}) using the elemental analyser (LECO, CN928). About 2g of soil were put into ceramic cups, without the need to be milled.

Soil mineral carbon analysis

Since the elemental analyser delivers concentrations for C_{tot}, and not OC, the percentage of mineral carbon (C_{min}) has been determined with the calcimeter (Figure 24 in the Appendix). C_{tot} in soils is the sum of both SOC and C_{min} (Capriel 2013, Nelson & Sommers 1996). In 2022, samples from 2006 to 2021 for the 24 selected field parcels were measured for calcium carbonate ($CaCO_3$) content (%-mass). The method is based on equation (3) of the reaction of calcareous soil ($CaCO_3$) with hydrogen chloride (HCl), where carbon dioxide gas (CO_2) is released. The volume of gas generated is proportional to the carbonate content of the sample. This method to determine calcium carbonate in soil samples is the reference method ("$CaCO_3$") prepared by Diane Bürge under the approval of Thomas Bucheli (version: 17.03.2022, code: B-Kalk). The method can be found for internal use in the Agroscope website (*https://link.ira.agroscope.ch/de-CH/publication/45887*). A detailed explanation of this method is to be found in the Appendix (Section .2.1).

$$CaCO_3 + 2\,HCl \longrightarrow CaCl_2 + H_2O + CO_2 \tag{3}$$

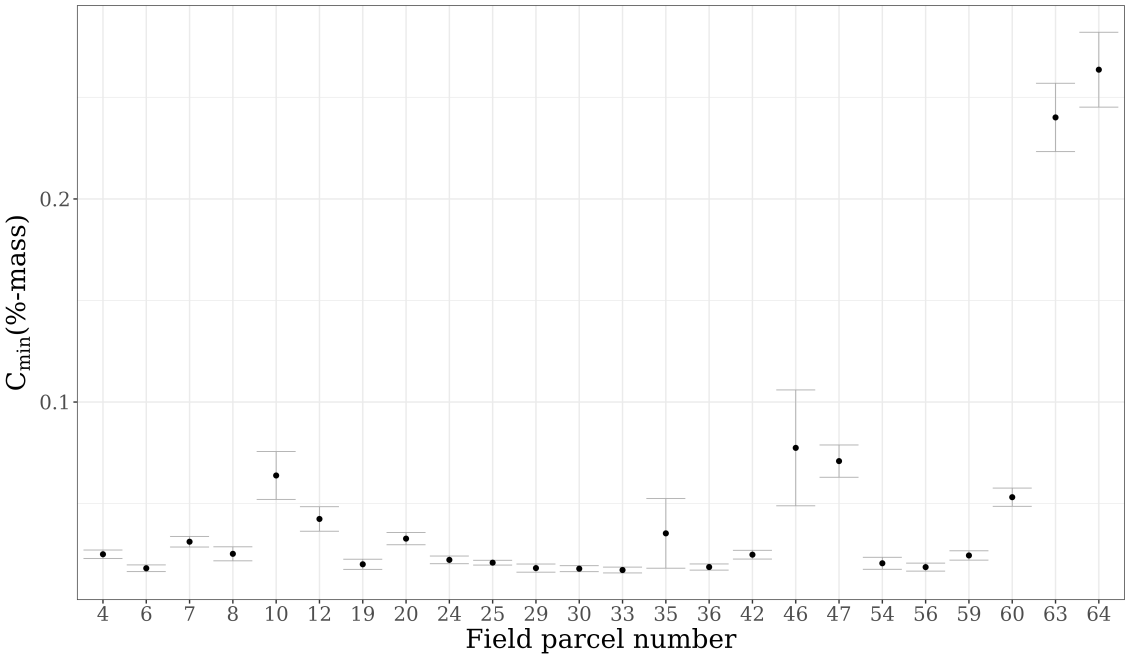

Figure 6: Mean (±SE, n=16, 2006-2021) soil mineral carbon concentration (%-mass) for the 24 selected field parcels.

Figure 6 shows the mean soil C_{min} concentration (±SE, n=16, 2006-2021), which ranges between 0.017 and 0.0264, with a median value of 0.025 (%-mass). For most field parcels, the mean C_{min} concentration is lower than 0.05 (%-mass). Field parcels 10, 46, 47 and 60 show mean values between 0.05 and 0.01 (%-mass). Field parcels 63 and 64 differ strongly from all others regarding C_{min} concentrations, showing values

higher than 0.2 (%-mass). Because of these differences, the percentage of C_{min} is subtracted from the C_{tot} concentration specifically for every field parcel. Calculations of OC concentration were performed slightly differently, depending on the soil sample year. This is because C_{min} was analysed only for soil samples of the period 2006-2021, so for the other years (1990-2005 and 2022), an average C_{min} (n=16, 2006-2021) is subtracted.

- Soil samples 1990-2005 and 2022: SOC (% of field parcel Y in year X) = C_{tot} (% of field parcel Y in year X) - C_{min} (average between 16 years for field parcel Y). Assumption: C_{min} is constant over time.
- Soil samples 2006-2021: SOC (% of field parcel Y in year X) =C_{tot} (% of field parcel Y in year X) - C_{min} (% of field parcel Y in year X)

2.3.2 Soil organic carbon stocks calculation

In order to compare SOC contents over time and between productivity categories, SOC stocks were calculated from the SOC concentrations. Soil density was calculated from the soil samples collected in 2022 with a given core volume. For the samples collected in 2022, a specific soil density was applied to every sample. For the historical samples (1990-2021), the mean soil density (firstly averaged between the two replicates for every parcel and then between all 24 parcels) was used (Poeplau et al. 2016). Based on Equation 4, the calculations assume constant soil density over time and are detailed in the Appendix (Section .2.2) (Eze et al. 2018, Garcia-Pausas et al. 2007, Poeplau et al. 2017).

$$\text{SOC stocks } (\mathrm{kg\,m^{-2}}) = \text{SD (m)} * \text{SBD } (\mathrm{kg\,m^{-3}}) * \text{RA } (1\mathrm{m^{-2}}) * \text{SOC concentration (\%)} \quad (4)$$

where:
SD = Soil depth
SBD = Soil bulk density
RA = Reference area

2.3.3 Soil properties

Soil nitrogen concentration

Soil N_{tot} concentrations have been measured for all historical samples (1990-2022). At the beginning of the experiment, when considering the average of every field parcel for the first five years (n=5 for every of the 24 field parcels), N_{tot} values range from 0.540 to 0.827 %, with a mean (n=24) of 0.641 ±0.015 %. Currently (2018-2022), N_{tot} concentrations range between 0.471 and 0.750 %, with a mean of 0.568 ±0.015 %. Mean yearly N_{tot} (n=24) was found to decrease significantly over time (Mann-Kendall test: p-value < 0.001, tau-statistics = -0.708) (Figure 7). This nitrogen depletion is true for all six productivity categories and applies to all field parcels.

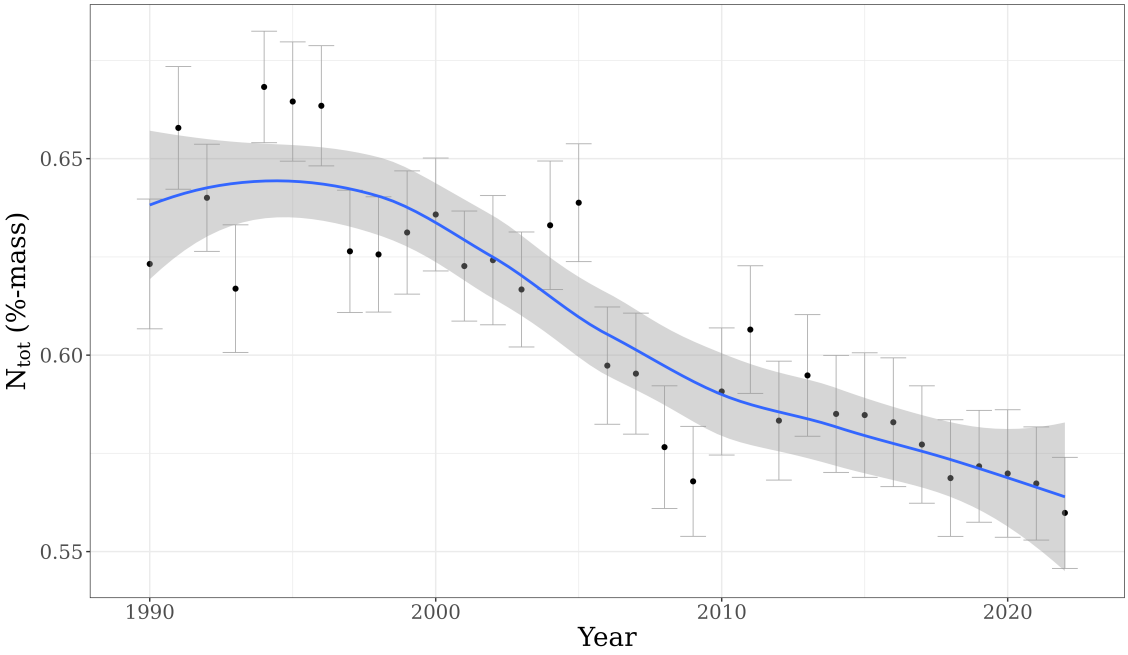

Figure 7: Decreasing mean total nitrogen concentration in soil over time (1990-2022). The black dots represent the mean annual N_{tot} concentrations (n=24), with the standard errors in grey. The blue line is the fitted loess curve (local polynomial regression) with a percentage confidence interval of 0.95 shown in transparent grey.

Clay content, soil pH, bulk density and C:N ratio

In 1989, when the first soil samples were collected at experiment start, clay content and soil pH were measured. Soil bulk density was calculated in 2022 by dividing the dry fine soil mass (<2mm) by the core volume (5cm diameter, 10cm height). Mean values (n=24) and standard error of these selected soil properties are presented in Table 1.

Table 1: Minimum, maximum and mean values for clay content, soil pH, bulk density and C:N ratio.

Soil property	Minimum value	Maximum value	Mean value ±SE (n = 24)
Clay content (%)	24.20	33.70	26.83 ±0.36
Soil pH	6.80	7.20	6.95 ±0.03
Soil bulk density ($kg\,L^{-1}$)	7.62	9.68	8.84 ±0.12
C:N ratio	8.58	8.76	8.67 ±0.01

2.4 Grass sampling and analysis

Every year since 1990, the plant canopy has been mowed three times at 5cm height for a subset of every field parcel (area: 1.25 m x 5m = 6.25 m^{-2}) using a motor mower with a finger bar. After harvest, plant biomass was oven dried at 105 °C and weighed to determine the annual aboveground dry yield. For further analysis in the laboratory, grass samples were oven dried at 60 °C, milled and archived at Agroscope. In

June 2023, the grass samples of 2022 (for all 3 harvests and all 64 field parcels) were analysed for C_{tot} and N_{tot} concentrations with the same procedure as with the soil samples (Elemental analyser, LECO CN928), except that 0.4 g (not 2 g) were weighed in the ceramic cups.

2.5 Ecosystem carbon fluxes

2.5.1 Measuring technique

Figure 8: Ecosystem CO_2 gas exchange measurements technique. In the photo, the transparent cuvette can be seen, fixed to the ground with the red rubber band (secured to the ground with metal stakes) and yellow cell foam band. The humidity and air temperature sensor inside the chamber, the infrared CO_2 probe and the small fan can be seen, in order from the right. Leaning against the cuvette is also the logger, connected to the sensors. The thermometer recording the ground temperature at the time of measurement is not visible.

The ecosystem CO_2 gas exchange of the grassland site was measured according to Volk et al. (2011). Figure 8 illustrates how the measurements were performed in the field. On each of the 24 selected field plots there are two frames, one to the North and one to the South, and here is where the chamber for the CO_2 measurements was placed. A static cuvette made of transparent polyacrylics (30x40x35cm) was used for this. An infrared CO_2 probe (GMP343 diffusion model, Vaisala, Vantaa, Finland) was installed inside the cuvette and connected to a handheld control and logger unit (MI70 Indicator, Vaisala) to record the camber CO_2 concentration. To facilitate air mixing inside the cuvette, a moderate turbulence was created by a small fan (0.5-0.8 $m\,s^{-1}$). To isolate the system from the atmosphere during the measurement, a cell foam band was used to seal the cuvette to the frame. A two minutes measurement period per frame was conducted by

measuring changes in CO_2 concentration at five seconds intervals. By selecting a brief measurement period, it was possible to reduce the impact of changing ambient conditions inside the chamber and prevent the cuvette from fogging up from high evapotranspiration rates. Under clear skies only, measurements were performed during the day between two hours before and after solar noon (NEE_{day}). At night, measurements started at least one hour after sunset (NEE_{night}). Soil temperature was recorded at 10cm depth during each flux measurement using a handheld electric thermometer.

For this project, 12 measuring campaigns have been conducted approximately every two weeks, from June 2022 (14.06.2022) to June 2023 (06.06.2023), with a winter break between November (7.11.2022) and April (18.04.2022).

2.5.2 Estimation of Gross Primary Productivity and Ecosystem Respiration

Relationship between soil temperature and ecosystem respiration

Nearly all of the CO_2 that is produced in soils comes from microbial decomposition of organic materials and root respiration. These processes, just like all chemical and biological reactions, depend on temperature (Davidson & Janssens 2006).

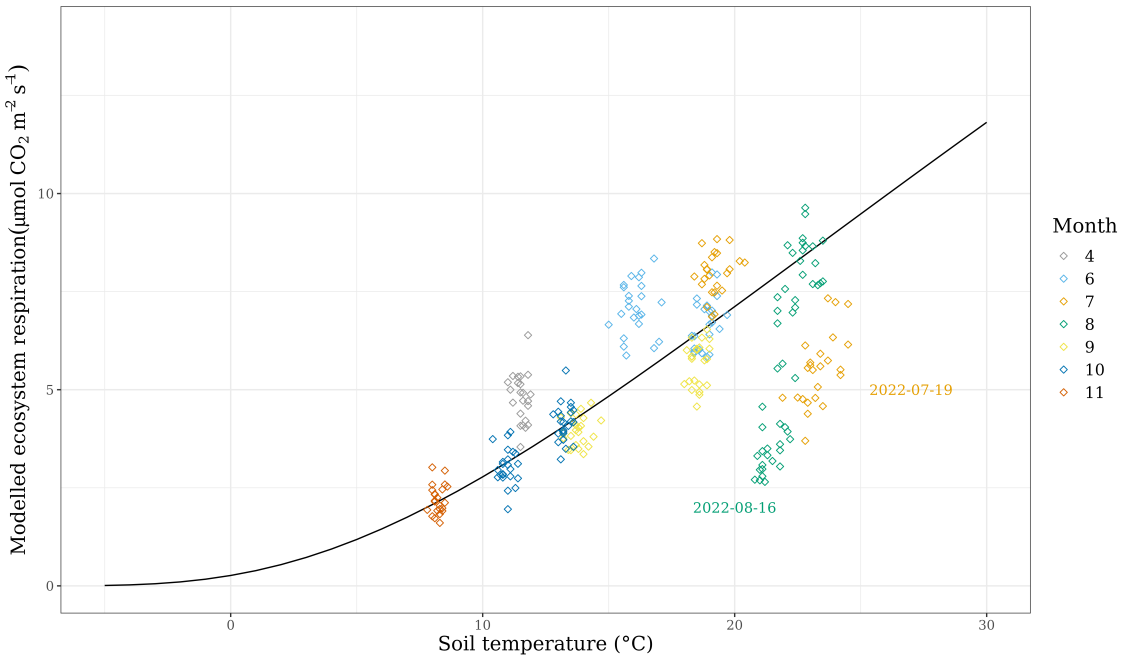

Figure 9: Ecosystem respiration during the campaigns plotted with the Arrhenius curve. The colours of the data points, described in the legend, represent the month of the measurements. The Arrhenius line (in black) is suitable for describing the relationship between ecosystem respiration and temperatures for most points. There are, however, points from the campaigns of 19 July 2022 and 16 August 2022 that do not follow the line. The summer of 2022 was very dry (DWD et al. 2022) and, therefore, the ecosystem respiration on these dates was lower than expected due to water limitation (Cook & Orchard 2008, Davidson & Janssens 2006).

The Arrhenius equation (5) was used to describe the temperature dependence of ecosystem respiration

(ER) (Figure 9) (Bahn et al. 2008, Davidson & Janssens 2006, Hofmann et al. 2016, Hussain et al. 2011, Lloyd & Taylor 1994, Rogger et al. 2022). The values for the equation parameters were already determined in earlier experiments on (pre)alpine grassland by Matthias Volk and adopted for the measurements in Muldain.

$$R(T_{soil}) = R_{10}\ exp\ \left[E_0\ \left(\frac{1}{10°C - T_0} - \frac{1}{T_{soil} - T_0}\right)\right] \tag{5}$$

where:

T_{soil}: Soil temperature (°C)

R_{10} (2.78 µmol CO_2 m^{-2} s^{-1}): Respiration rate at reference temperature of 10 °C

E_0 (73.3 °C): Activation energy

T_0 (260 °C): Growth characteristic of the exponential function

Relationship between soil moisture and ecosystem respiration

ER is not only affected by soil temperature but by soil moisture as well. Water constraint also affects microbial decomposition and root respiration (Cook & Orchard 2008, Davidson & Janssens 2006). Figure 10 displays the positive linear relationship between ER_{10} and soil moisture for the mean values generated during 11 measuring campaigns (all except the last one, where no soil moisture data are available). For simplicity, ER_{10} has positive values here, as opposed to the usual values where the atmospheric perspective is considered.

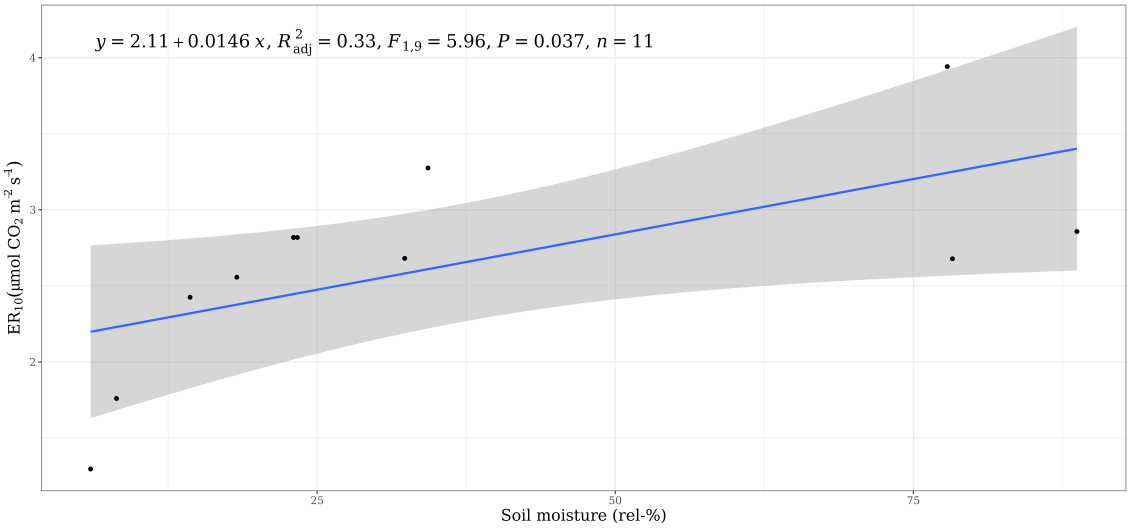

Figure 10: Positive linear relationship between ER_{10} and soil moisture. The black dots represent mean ER_{10} and soil moisture values (n=24) for the NEE measuring campaigns. The blue line is the fitting of the simple linear regression model, whose results are reported in the graph, with a confidence interval of 95% shown in transparent grey.

ER_{10}

As no photosynthesis happens without sunlight, the measured net ecosystem carbon exchange (NEE_{night}) was taken to reflect ER (Reco). The Arrhenius equation (5) was used to normalise NEE_{night} for temperature (10 °C at 10 cm soil depth) for each frame on each field parcel (ER_{10}). These normalised data take into

account the effects of seasonal fluctuations in substrate availability, heterotrophic and autotrophic biomass, and soil moisture availability (Volk et al. 2011).

GPP_{pot}

Using the Arrhenius equation (5), a normalised daily R_{eco} ($Reco_{day}$) was interpolated using the R_{eco} obtained during night measurements ($Reco_{night}$) and the soil temperature recorded at the time of the NEE measurements during the day (NEE_{day}) (Volk et al. 2011).

$$GPP_{pot} = NEE_{day} - Reco_{day} \tag{6}$$

Equation 6 was applied to estimate GPP_{pot} using NEE_{day} data and ER data normalised for temperature during the day ($Reco_{day}$). NEE_{day} measurements at mid-day and under clear sky conditions depict an environment without a radiation assimilation limit. Thus, these GPP estimates represent the potential GPP (GPP_{pot}) at maximum radiation at seasonal solar altitude (Volk et al. 2011).

2.6 Statistical analysis and data visualisation

The data were processed and prepared for analysis using Microsoft Excel (2016). All data visualisation and statistical analysis were performed in the R environment (R Core Team, 2023, version 4.3.0). The packages used are indicated in italics in brackets.

Minimum, mean, and maximum values for the different variables were calculated with the summary function *base*, and the standard error and standard deviation were calculated with the package *stats*.

To establish the existence of a linear relationship between two variables, a simple regression model was run, for the example between time and yield (*stats*). The linearity of the relationship was assessed using the Pearson correlation (*stats*) and simple visualisations of scatter plots (*graphics*). A general check of all linear model assumptions was performed using a Top-level function for Global Validation of Linear Models Assumptions (*gvlma*). If some assumptions were not met, data underwent log or square-root transformation, and the model requisites were re-checked. For the analysis of monotonic trends in time series, the non-parametric Mann-Kendall trend test (*Kendall*) was applied when the linear regression model's assumptions were not met. For this test, the presence of (partial) autocorrelation was checked (*stats*).

To detect the presence of differences between two groups concerning a particular variable (e.g. for weather indices between years with high and years with low yields), a two-tailed T-test was performed (*stats*). If the T-test assumptions were not met, the Mann-Whitney-U-Test (Wilcoxon rank-sum test) was applied.

To detect the presence of differences between more than two groups regarding a certain variable (for example, differences in yield between productivity categories), a two-way Analysis of Variance (ANOVA) for randomised complete block design was performed, treating the field replicate as a blocking variable (*stats*). If the ANOVA assumptions were not met, the Friedman rank sum test was applied as a non-parametric alternative. The repeated measures ANOVA was used to compare means across one or more variables based on repeated observations (e.g. comparison of ER between measuring campaigns).

A pairwise comparison was performed using the Tukey's Honest Significant Difference method (*stats*). Letters of the pairwise comparison were created for later presentation in plots (*multcompView*).

For all statistical analyses, the necessary assumptions were tested. Homoscedasticity was tested with the Breusch-Pagan test (*car*) or with Levene's test (*rstatix*) and by visual observation of the Residuals vs Fitted plot (*graphics*). Normality was checked with the Shapiro-Wilk Normality Test (*stats*) and by visualising the Q-Q plot of the residuals (*graphics*).

A significance level of $\alpha = 0.05$ was chosen for all the statistical analyses. The packages used for data visualisation were *ggplot2*, *ggpubr* and *patchwork*. Results of linear regression models were reported on graphics with the package *ggpmisc*. Examples of the R code used for the various data analyses and visualisations can be found in the Appendix (Section .5).

The study area maps were created with the free and open source geographic information system QGIS (version Hannover 3.16.7, 14.05.2021), using geodata from the Federal Office of Topography (©swisstopo).

3 Results

Premise

To avoid burdening the text, it will not always be repeated that a certain result is statistically significant. It will only be specified if a statistical analysis does not generate a significant result. When mean values (with standard error) are given for a certain variable, an n of 4 refers to the average of the four field replicates of a productivity category, an n of 24 to the average between the 24 field plots (six fertiliser combinations repeated four times). Other n refers to the average between the number of years in the period under consideration or to something else specified in the text.

3.1 Aboveground productivity

3.1.1 Yield and fertilisation treatment combinations

ANOVA was used to test if different fertilisation treatments lead to different aboveground productivity. Data was averaged over time for every field parcel, and then the means of these averaged yields (n=4) were compared between productivity categories. Figure 11 shows that mean yield (n=4) differed as a result of different P and K applications. Table 2 summarises the mean dry yield for the six productivity categories and the corresponding period.

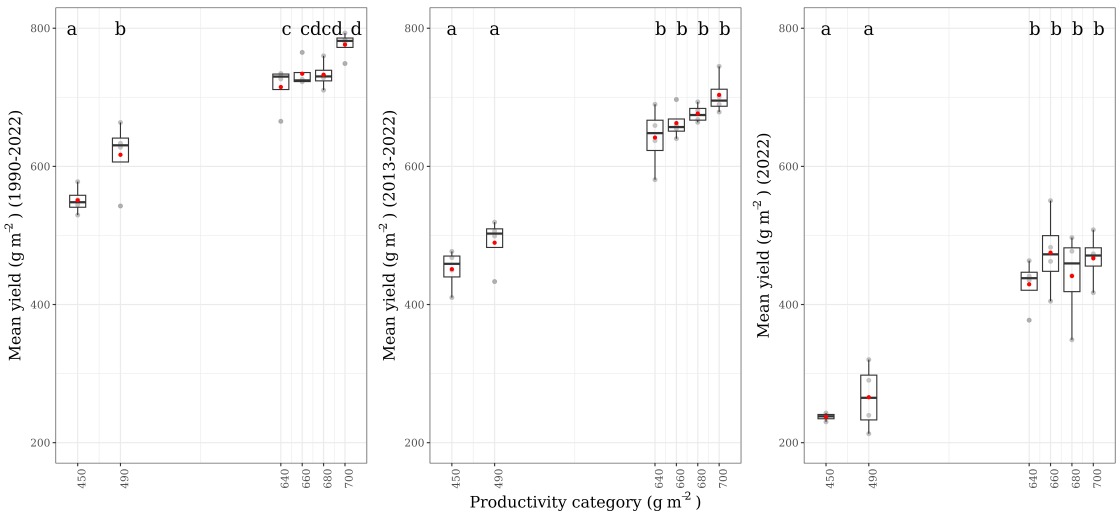

Figure 11: Differences in mean yield between productivity categories. The red dots indicate mean values (n=4), while the four grey dots represent the average yield for the indicated period for the four field replicates of the respective productivity category. The black horizontal lines within the boxplots represent the median values, and the letters above are the pairwise comparison results.

However, depending on the period considered (1990-2022, 2013-2022, 2022), these differences in yield vary, which is visible by the different results of the pairwise comparisons (indicated with different letters). Even though only six out of the 16 treatment combinations have been selected for this research, the gradient between the lowest and the highest mean yield obtained is apparent.

Table 2: Mean yield (±SE, n = 4) of the six productivity categories for three time periods (1990-2022, 2013-2022, 2022).

Productivity category	Mean aboveground dry yield ($g\,m^{-2}$)		
	1990 - 2022	2013 - 2022	2022
450	550.9 ±10.1 [a]	451.2 ±14.8 [a]	237.3 ±2.8 [a]
490	616.8 ±25.9 [b]	489.5 ±19.2 [a]	265.8 ±24.2 [a]
640	714.9 ±16.7 [c]	641.7 ±23.0 [b]	429.3 ±18.4 [b]
660	734.1 ±10.3 [cd]	662.7 ±12.1 [b]	475.1 ±30.0 [b]
680	732.7 ±10.3 [cd]	676.5 ±6.7 [b]	441.2 ±32.8 [b]
700	776.3 ±9.6 [d]	703.5 ±14.5 [b]	466.8 ±18.8 [b]

3.1.2 Yield over time

General trend

A simple linear regression was applied to test whether there was a significant linear relationship between time (years) and mean annual yield (n=24). It was found that time explained 16% of the variability in yield and that during the last 33 years, yield decreased on average by about 6 $g\,m^{-2}$ per year (Figure 12). The Mann-Kendall test confirmed this decreasing trend over time (tau = -0.307, $p<0.05$). However, when performing the simple linear regression model and the Mann-Kendall test separately for the six productivity categories, it was found that a significant decrease in yield is only true for the three lowest productivity categories. These results are reported in the Appendix (Figure 26 and Table 12). More details on mean annual yield are to be found in Table 8 (Appendix).

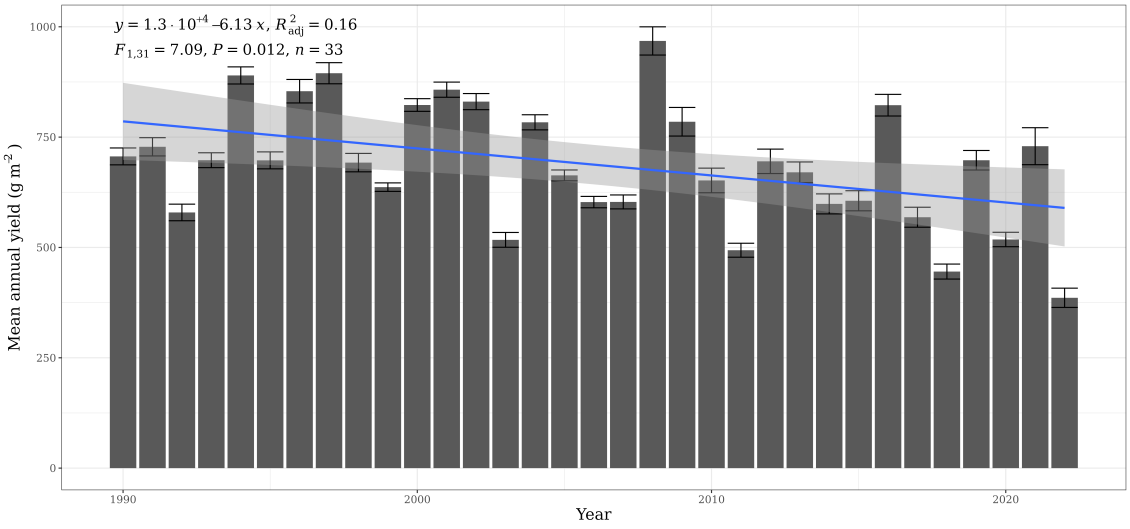

Figure 12: Decreasing mean yield over time (1990-2022). The dark grey bars represent the mean annual yield (n=24) together with the standard error. The blue line fits the simple linear regression model, whose results are reported in the graph, with a confidence interval of 0.95 shown in transparent grey.

3.1.3 Yield and weather

Correlation between mean yield and climatic parameters

Mean annual yield (n=24) was found to negatively correlate (Pearson) with temperature-based climatic parameters, especially with GDD_{sum} during the GS. No correlation was found between mean yield and GSL. A moderate (>0.4) positive correlation was found with P_{tot} between May and July as well as with IDM. More details can be found in the Appendix (Table 11).

Simple linear regression models to explain yield with climatic parameters

A simple linear regression model was performed between yield and all climatic variables that showed at least a moderate correlation (Pearson) with yield. It was found that higher temperatures, especially during the GS and, in particular, during April and July, led to lower harvests (Figure 13). In contrast, higher precipitation rates, especially between May and July, supported greater yields (Figure 13). This ties in with the positive linear relationship between yield and IDM during the GS (Table 11 in the Appendix). The more light (RelS) and the warmer, the higher the probability of drought conditions which impede plant growth. No relationship was found between yield and the GLS. The results of the performed simple linear regression models are summarised in the Appendix (Table 13).

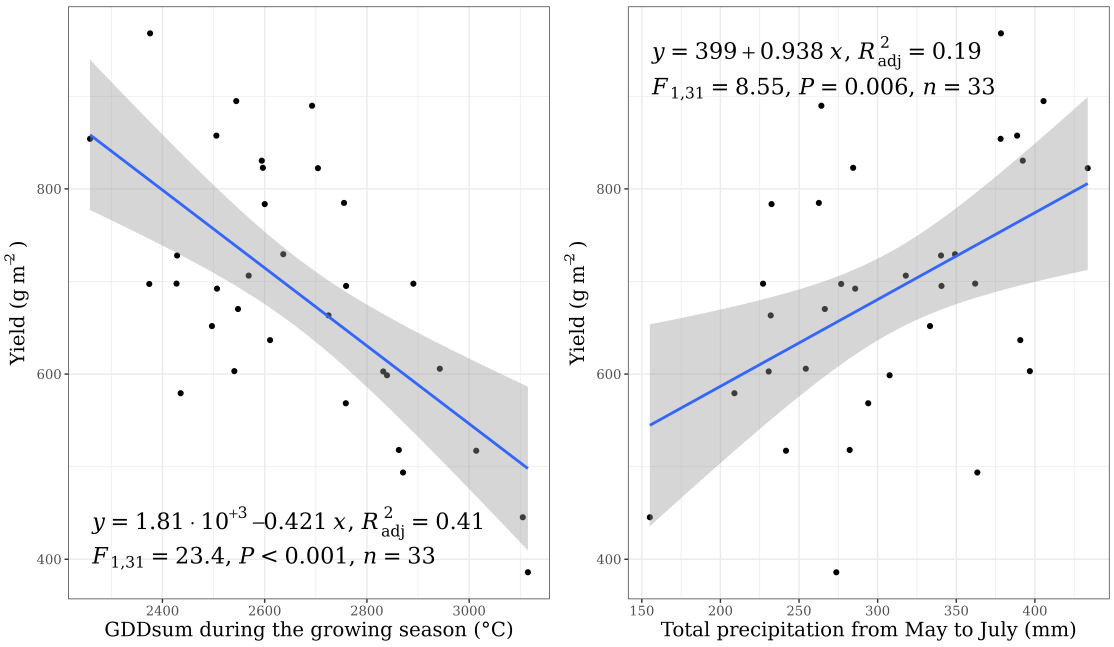

Figure 13: GDD_{sum} during the GS and P_{tot} between May and July predict yield. The left figure shows the negative relationship between yield and GDD_{sum} during the GS, while the right figure shows the positive relationship between P_{tot} from May to July and yield. The black dots are the values for mean annual yield (n=24) and the respective climate variable for the 33 years between 1977 and 2022. The blue lines are the fit of the simple linear regression models whose results are reported in the graphs, with the confidence interval of 0.95 shown in transparent grey.

Weather comparison between years with particularly high and low yield

By plotting the mean yield (n=24) over time, it is clear that interannual variations are present (Figure 12). Mean yields (n=24) ranged between 386 ±22 (2022) and 968 ±32 g m^{-2} (2008) for the period between 1990 and 2022, with mean values around 688 g m^{-2}. There were years where the mean yield was lower than the average yield (1990-2022) for the lowest productivity category (551 g m^{-2}), where no P or K were applied. On the contrary, there were years in which the mean yield exceeded mean yield (1990-2022) of the highest productivity category (776 g m^{-2}) (Figure 14).

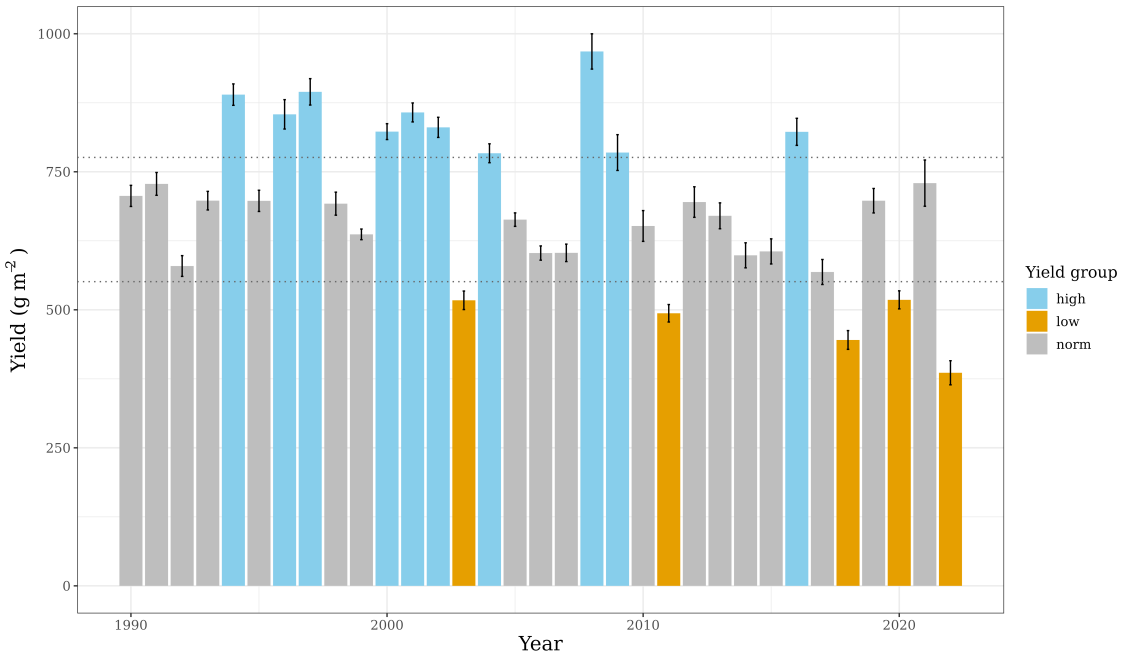

Figure 14: Years with particularly high and low yield. The graph columns represent the mean annual yield (n=24), together with standard error bars. Grey years represent mean yield values in the norm, between 551 and 776 g m^{-2}. Mean yields lower than 551 g m^{-2} (group "low") are depicted in orange and mean yields higher than 776 g m^{-2} (group "high") are coloured in light blue. The thresholds of 551 and 776 g m^{-2} for the lowest and highest productivity categories, respectively, are shown with horizontal grey dotted lines.

The two-tailed T-test was applied to test which weather parameters differed between years with mean yields higher than 776 ("high") and years with mean yields lower than 551 g m^{-2} ("low") (Figure 15). It was found that GDD_{sum} during the GS, in April and in August and RelS during the GS were significantly higher in years with low yields compared to years with high yields. In addition, in years with low yields, P_{tot} in March and April was lower compared to years with high yields. Summarising, extremely high GDD_{sum} during the GS and low precipitation rates in spring led to lower aboveground biomass production.

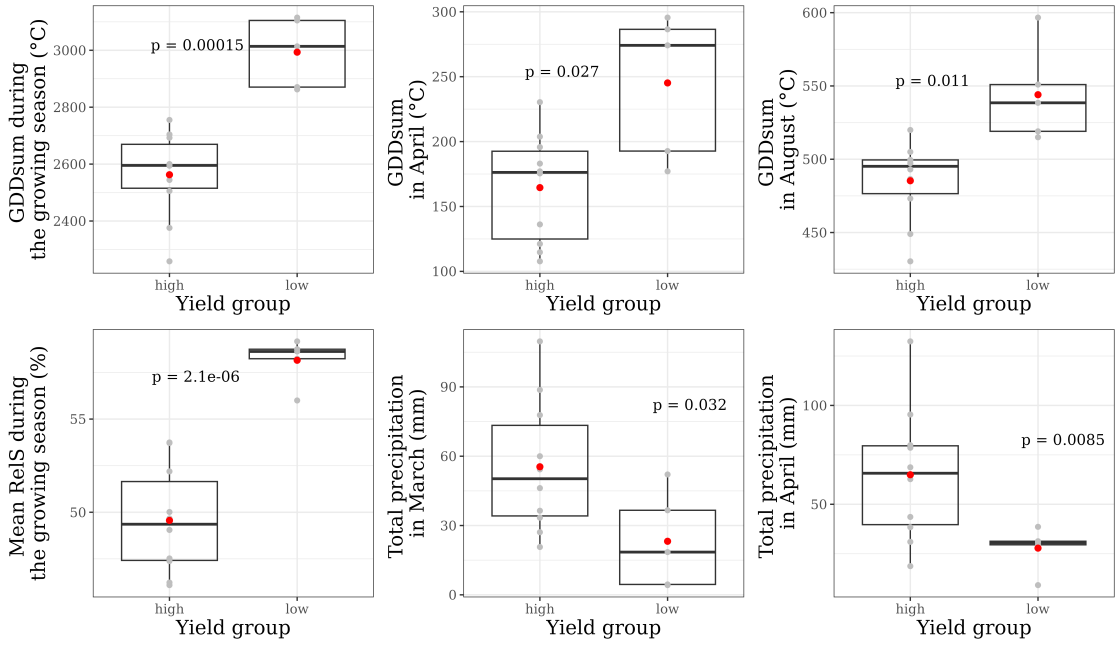

Figure 15: Weather parameters in years with particularly high and low yield. The red dots indicate mean values (n=10 four of the "high" group and n=5 four of the "low" group). The grey dots represent the values of the respective climate variables in the respective years with particularly high and low yields. The black horizontal lines within the boxplots represent the median values, and the p-value of the two-sided T-test is reported.

3.2 Soil organic carbon stocks

3.2.1 SOC stocks and productivity

ANOVA was used to test if mean SOC stocks during three chosen periods (1990-2022, 2013-2022 and 2022) differed between the six productivity categories. Table 3 summarises mean SOC stocks for the six productivity categories and the corresponding period.

Table 3: Mean SOC stocks for three time periods and their relative change over time (1990-2022) of the six productivity categories. Letters report the results of the non-significant pairwise comparisons.

Productivity category	Mean SOC stocks ($kg\,m^{-2}$)				Relative change (%)
	1990	1990-2022	2013-2022	2022	1990-2022
450	9.03 ±0.27 [a]	8.85 ±0.27 [a]	8.29 ±0.24 [a]	7.70 ±0.44 [a]	-14.89 ±3.05 [a]
490	9.39 ±0.80 [a]	9.33 ±0.70 [a]	8.70 ±0.67 [a]	8.57 ±0.48 [a]	-7.99 ±2.90 [a]
640	9.99 ±0.97 [a]	9.60 ±0.84 [a]	8.99 ±0.81 [a]	8.45 ±0.56 [a]	-14.71 ±2.72 [a]
660	10.27 ±0.94 [a]	9.58 ±0.90 [a]	9.09 ±0.86 [a]	8.31 ±0.50 [a]	-18.43 ±2.72 [a]
680	10.05 ±0.59 [a]	9.55 ±0.50 [a]	9.01 ±0.51 [a]	7.96 ±0.56 [a]	-20.47 ±5.67 [a]
700	9.25 ±0.33 [a]	9.04 ±0.09 [a]	8.48 ±0.11 [a]	8.20 ±0.23 [a]	-11.12 ±3.28 [a]

Figure 16 shows that the mean SOC stocks (n=4) did not differ between productivity categories, regardless

of the period considered. The same is true when comparing the change in SOC stocks (%) relative to the initial values (1990) (Figure 17). The relative change in SOC stocks was calculated by dividing the difference in SOC stocks between 2022 and 1990 with the starting SOC stocks in 1990 and multiplying by 100.

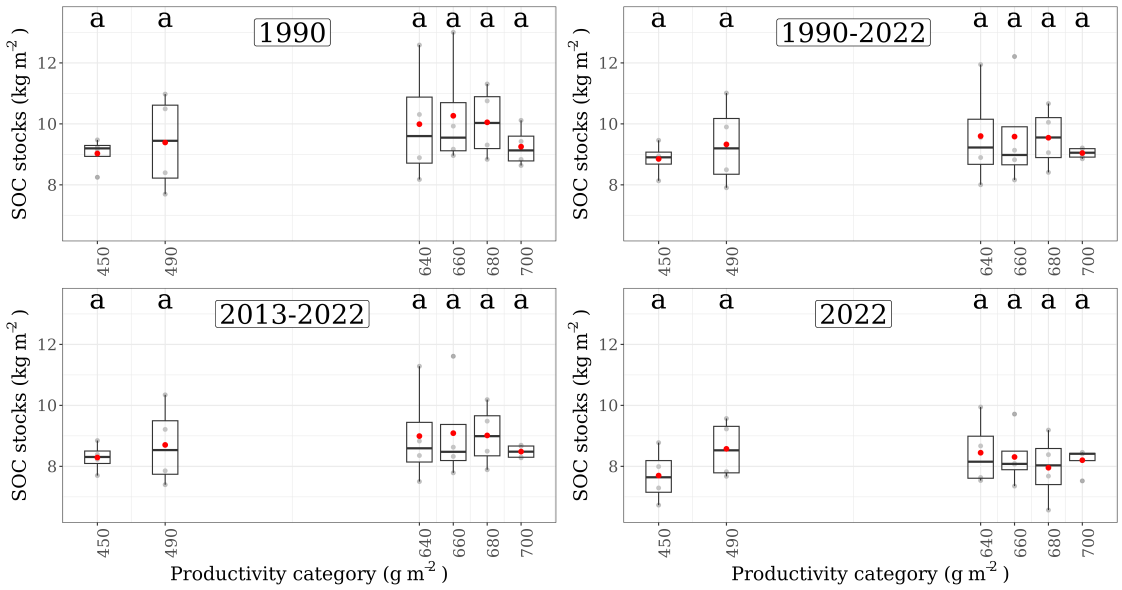

Figure 16: No differences in SOC stocks between productivity categories. The red dots indicate mean values (n=4), while the four grey dots represent the average SOC stocks for the indicated period for the four field replicates of the respective productivity category. The black horizontal lines within the boxplots represent the median values, and the letters above are the results of the (non-significant) pairwise comparisons.

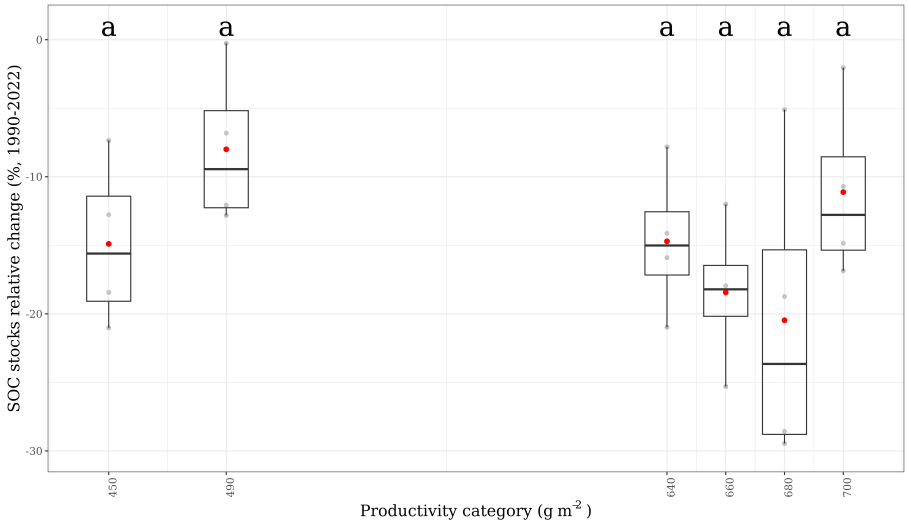

Figure 17: No differences between productivity categories regarding SOC stocks relative change. The understanding of the facets of Figure 16 also applies here.

Pearson correlation and simple linear regression models were run to identify possible positive relationships between increasing productivity and SOC stocks. No correlation was found, indicating that higher produc-

tivity did not lead to higher SOC stocks. Figure 18 shows a general visualisation with boxplots for SOC stocks and mean yield for the six productivity categories. From this visualisation, it is clear that there is no dependency. Another visualisation can be found in the Appendix (Figure 28).

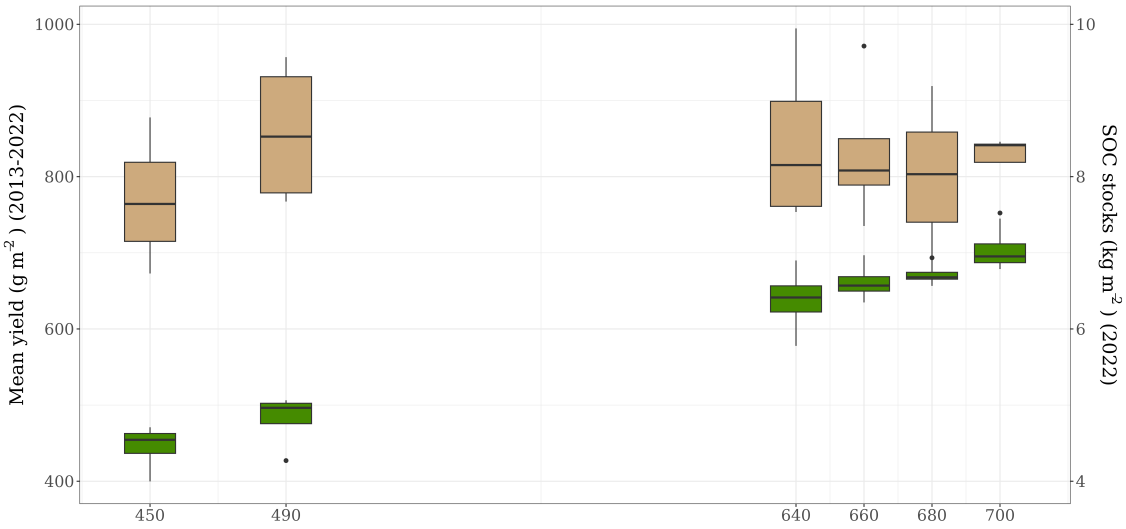

Figure 18: No relationship between mean yield (2013-2022) and final SOC stocks (2022) for the six productivity categories. The green boxplots represent the mean yield, and mean SOC stocks are shown with the brown boxplots. The increasing productivity from the lowest category, 450, to the highest, 700, is visible. Conversely, SOC stocks do not differ between productivity categories and do not follow an increasing trend with increasing productivity.

3.2.2 SOC stocks over time

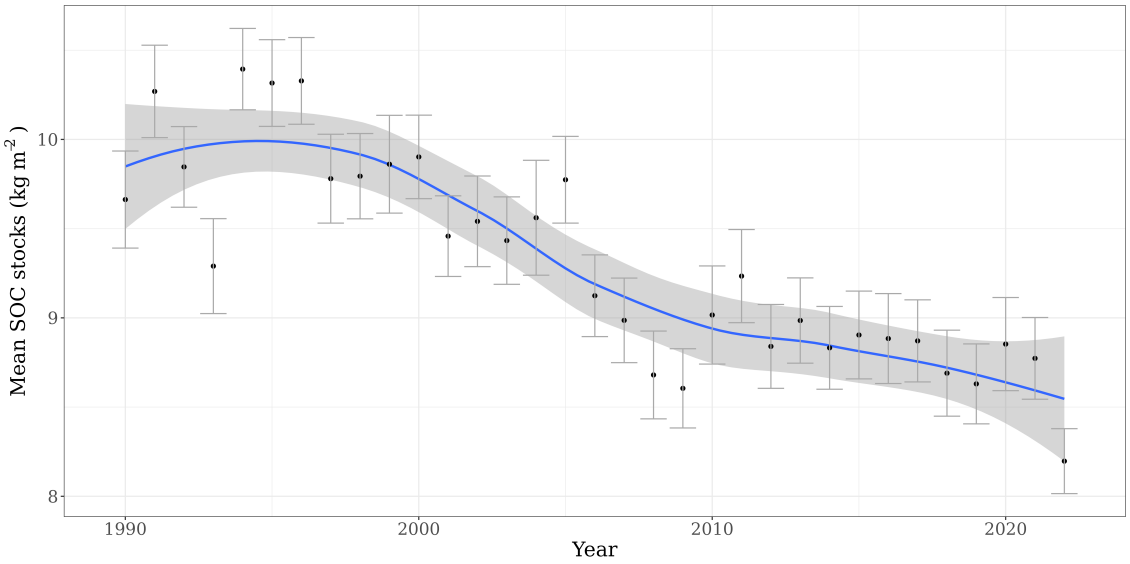

Figure 19: Decreasing mean SOC stocks (n=24) over time (1990-2022). The black dots represent the mean annual SOC stocks, together with the standard errors in grey. The blue line is the fitted loess curve (local polynomial regression) with a percentage confidence interval of 0.95 shown in transparent grey.

The Mann-Kendall test was performed to test whether mean annual SOC stocks (n=24) showed a trend over time. A moderate-strong decreasing trend was found (tau = -0.678, $p<0.05$) (Figure 19). The Mann-Kendall test was also performed separately for the six productivity categories, to test if the decreasing trend in SOC stocks applies independent from the aboveground productivity. It was found that SOC stocks strongly decreased (tau-statistics < -0.6, $p<0.05$) for all productivity categories. These results are presented in the Appendix (Figure 27). More data regarding annual SOC stocks over time are to be found in Table 8 (Appendix).

3.2.3 SOC stocks and weather

Over the entire period, SOC stocks decreased, showing a negative linear relationship with increasing temperatures and a positive linear relationship with decreasing soil N_{tot} as well as with decreasing yield. However, these relationships are only evident over a longer period of time and not from year to year and could be spurious. Only GDD_{sum} in May was found to correlate significantly with annual losses of SOC stocks. Between annual relative changes in SOC stocks and other weather parameters, no additional linear correlations were discovered when assessed with Pearson correlation coefficients and simple linear regression models. More details are reported in the Appendix (Figure 29 and Table 11).

3.3 Ecosystem carbon fluxes

3.3.1 Comparison between measuring campaigns

CO_2 fluxes were compared between the 12 measurement campaigns using ANOVA. GPP_{pot}, ER_{10} (µmol CO_2 $m^{-2}\,s^{-1}$) and their ratio (unitless) were not constant over time but showed variations between measurement dates. Mean values (±SE, n=24) are summarised in Table 5 for each measurement campaign, along with soil moisture (rel-%) on the day of the measurements and soil temperature (°C) during night and day.

Table 4 summarises minimum, maximum and mean values (n = 12 campaigns) for ER, ER_{10} and GPP_{pot} (µmol CO_2 $m^{-2}\,s^{-1}$). Minimum and maximum values correspond to the mean values (n=24) during a certain campaign. Figure 20 shows the mean CO_2 fluxes (n=24) over time along with soil moisture and soil temperature. Figure 21 visualises the mean GPP_{pot}/ER_{10} (n=24) over time. More details are reported in Table 5).

Table 4: Minimum, maximum and mean GPP_{pot}, ER_{10} and their ratio for the six productivity categories. µmol CO_2 m^{-2} s^{-1} is the unit for GPP_{pot} and ER_{10}, while the ratio GPP_{pot}/ER_{10} is unit less.

CO_2 flux	Minimum	Maximum	Mean (n=12)
ER	-2.21 ±0.07 *7.11.2022*	-8.08 ±0.16 *2.8.2022*	-5.23 ±0.56
ER_{10}	-1.30 ±0.06 *16.08.2022*	-3.94 ±0.11 *18.04.2023*	-2.74 ±0.21
GPP_{pot}	1.89 ±0.28 *19.07.2022*	15.33 ±0.45 *8.7.2022*	9.24 ±1.07

Table 5: Soil temperature (ST, °C) and moisture (SM, %) together with CO_2 fluxes (µmol CO_2 m^{-2} s^{-1}) and the ratio between GPP_{pot} and ER_{10} on the different measuring campaigns. Mean values refer to the average between the field parcels for every campaign (n=24). Letters represent the results of the pairwise comparisons.

Date	SM	ST_{night}	ER_{10}	ST_{day}	GPP_{pot}	GPP_{pot}/ER_{10}
2022-06-14	23.34	18.9	-2.8 ±0.05 ^{de}	19.9	10.1 ±0.3 ^{cde}	3.6 ±0.08 ^{bc}
2022-07-08	34.30	19.2	-3.3 ±0.05 ^{f}	18.7	15.3 ±0.5 ^{f}	4.7 ±0.15 ^{e}
2022-07-19	8.17	23.3	-1.8 ±0.05 ^{b}	21.9	1.9 ±0.3 ^{a}	1.1 ±0.15 ^{a}
2022-08-02	32.34	22.7	-2.7 ±0.05 ^{cde}	20.8	10.1 ±0.3 ^{cd}	3.8 ±0.10 ^{cd}
2022-08-16	6.00	21.5	-1.3 ±0.06 ^{a}	19.5	3.1 ±0.3 ^{a}	2.4 ±0.25 ^{c}
2022-09-05	14.34	18.5	-2.4 ±0.05 ^{c}	17.4	10.7 ±0.3 ^{de}	4.4 ±0.11 ^{de}
2022-09-20	18.27	13.8	-2.6 ±0.05 ^{cd}	12.2	9.2 ±0.2 ^{c}	3.6 ±0.10 ^{bc}
2022-10-04	78.28	11.0	-2.7 ±0.08 ^{cde}	12.0	8.8 ±0.3 ^{c}	3.3 ±0.08 ^{bc}
2022-10-19	23.02	13.3	-2.8 ±0.07 ^{de}	12.3	8.9 ±0.3 ^{c}	3.2 ±0.09 ^{bc}
2022-11-07	88.72	8.2	-2.9 ±0.1 ^{e}	7.5	6.1 ±0.2 ^{b}	2.2 ±0.09 ^{b}
2023-04-18	77.84	11.6	-3.9 ±0.1 ^{g}	9.5	11.5 ±0.3 ^{e}	3.0 ±0.10 ^{bc}
2023-06-06	-	16.1	-3.7 ±0.1 ^{g}	14.9	14.1 ±0.3 ^{f}	3.8 ±0.10 ^{cd}

Figure 20: GPP_{pot} and ER_{10} compared between measurement campaigns. The grey dots represent ER_{10} and GPP_{pot}, respectively, for the 24 parcels on the indicated date. The red dots indicate mean values (n=24), while the black horizontal lines within the boxplots are the median values. The letters above the boxplots refer to the results of the pairwise comparisons. The orange line shows the daily mean values for soil temperature, while the blue line shows the daily mean values for soil moisture. Harvest dates (25.05.2022, 19.07.2022 and 22.09.2022) are indicated by the vertical green dashed lines.

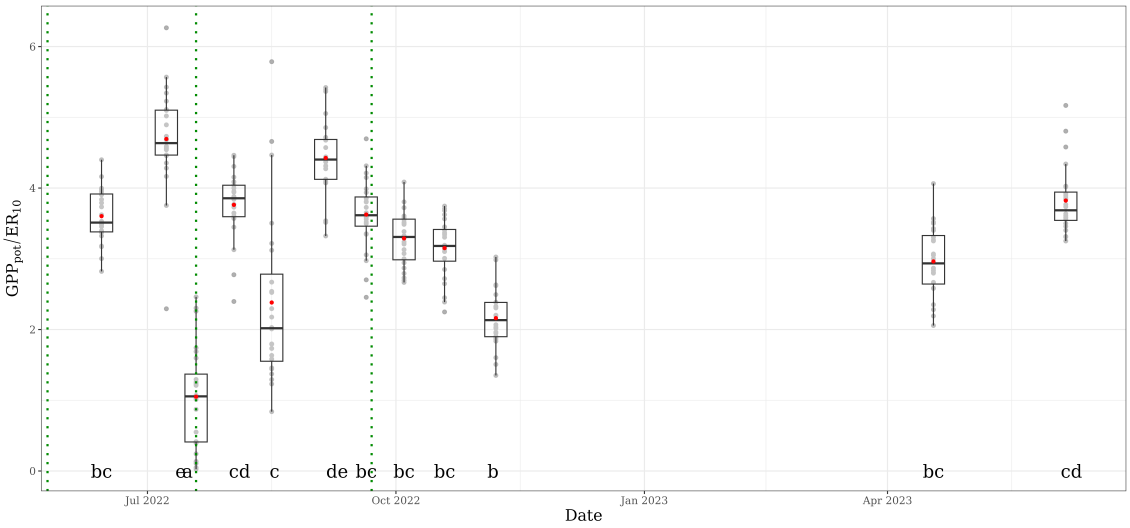

Figure 21: GPP_{pot}/ER_{10} compared between measuring campaigns. The understanding of the facets of the graph in Figure 20 also applies here.

3.3.2 Comparison between productivity categories

GPP_{pot}, ER_{10} and GPP_{pot}/ER_{10} were averaged over the measuring campaigns (n=12) for every of the 24 field parcels. With ANOVA, it was found that mean GPP_{pot}, ER_{10} and their ratio did not differ between the six productivity categories. Figure 22 visualises and Table 6 report these results.

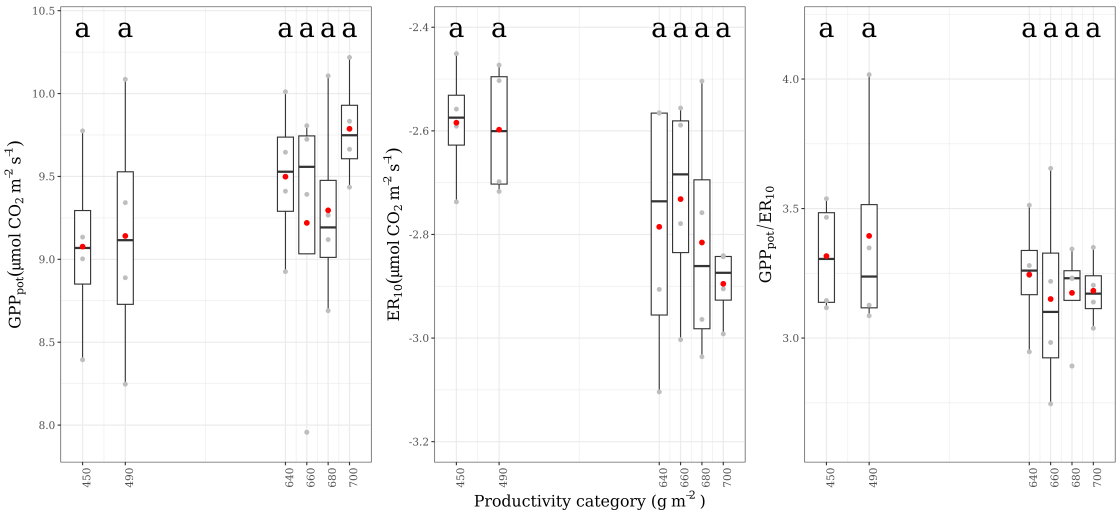

Figure 22: GPP_{pot}, ER_{10} and GPP_{pot}/ER_{10} compared between productivity categories. The red dots indicate mean values (n=4), while the four grey dots represent the average GPP_{pot}, ER_{10} and their ratio for the four field replicates of the respective productivity category. The black horizontal lines within the boxplots represent the median values, and the letters above are the results of the (non-significant) pairwise comparisons.

Table 6: Mean GPP_{pot}, ER_{10} (µmol CO_2 m^{-2} s^{-1}) and their ratio for the six productivity categories.

Productivity category	GPP_{pot}	ER_{10}	GPP_{pot}/ER_{10}
450	9.08 ±0.28 [a]	-2.584 ±0.06 [a]	3.32 ±0.11 [a]
490	9.14 ±0.39 [a]	-2.598 ±0.06 [a]	3.39 ±0.22 [a]
640	9.50 ±0.23 [a]	-2.785 ±0.13 [a]	3.25 ±0.12 [a]
660	9.22 ±0.43 [a]	-2.732 ±0.10 [a]	3.15 ±0.19 [a]
680	9.30 ±0.30 [a]	-2.816 ±0.12 [a]	3.18 ±0.10 [a]
700	9.79 ±0.17 [a]	-2.895 ±0.04 [a]	3.18 ±0.07 [a]

3.4 Relationship between SOC stocks and carbon fluxes

Simple linear regression analysis was performed to detect significant linear relationships between:

- SOC stocks in 2022 and the ratio GPP_{pot}/ER_{10};
- Relative changes in SOC stocks (1990-2022) and the ratio GPP_{pot}/ER_{10}.

No linear relationship, nor of any other type, was found between relative changes in SOC stocks (1990-2022) and GPP_{pot}/ER_{10} (Figure 23). The same is true between SOC stocks (2022) and GPP_{pot}/ER_{10} (Figure 30 in the Appendix). Therefore, the ratio between GPP_{pot}/ER_{10} measured in 2022 cannot be used to predict changes in SOC stocks nor to explain possible differences in final SOC stocks (2022). The weak or non-existent relationships between carbon fluxes and SOC stocks (changes) can be seen in Table 14 (Appendix) according to the very low Pearson correlation coefficients.

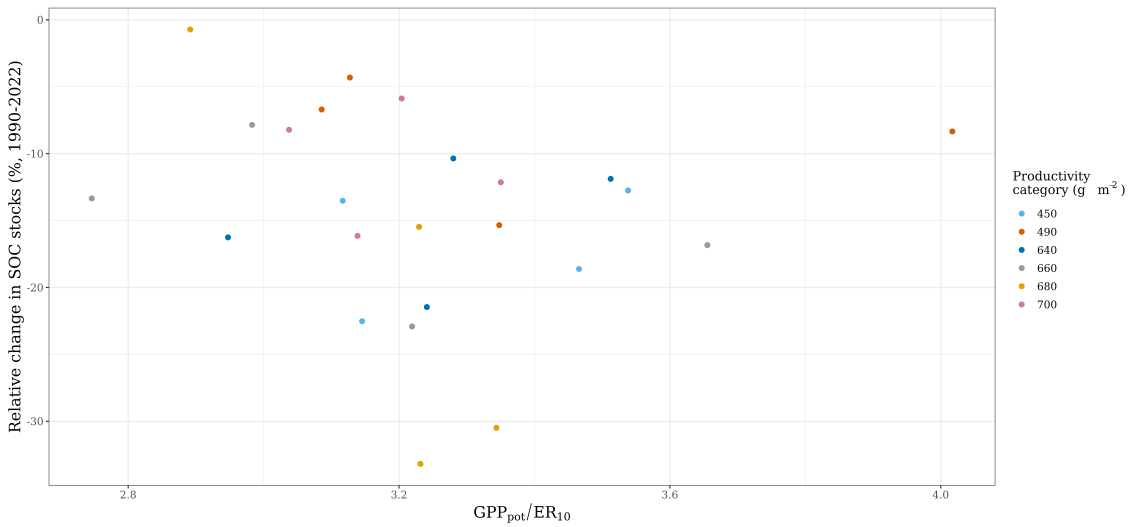

Figure 23: No relationship between GPP_{pot} / ER_{10} and SOC stocks relative change (%). Every point represents the SOC stocks relative change between 1990 and 2022 and the mean (averaged over the measuring campaigns) ratio between GPP_{pot} / ER_{10} for the corresponding field parcel. The dots colour corresponds to the productivity category.

4 Discussion

4.1 Grassland productivity

4.1.1 Yield differences between fertilisation treatment combinations

European alpine and pre-alpine grasslands provide essential ecological services such as the promotion of biodiversity and soil conservation and the support the economy by providing livestock fodder. Due to the need for high yields, fertilisers are employed every year to alleviate nutrient limitations and so stimulate plant growth (Bernhardt-Römermann et al. 2011, Botter et al. 2020, Crowther et al. 2019, Eze et al. 2018). Not only the amount of fertiliser applied is important, but also the type, rates and combination of the several nutrients determine the productive potential of grasslands (Poeplau 2021, Samuil et al. 2018).

The grassland in Muldain showed different yields depending on the combination of N, P and K in the fertiliser application (Figure 11 and Table 2). Increasing productivity with higher nutrient supply is recognisable. However, these differences varied depending on the period chosen. In the last decade, the yield differences between the productivity categories have been less pronounced. The reasons for this might be climate warming and increasing dryness in combination with the decreasing soil N_{tot} concentration. These aspects will be discussed further in the next two chapters (4.1.2 and 4.1.3).

4.1.2 Yield changes with weather variability

As climatic conditions influence grassland productivity, aboveground biomass is characterised by interannual variations (Grigulis & Lavorel 2020, Samuil et al. 2018). The lowest mean yields were found in Muldain for the years 2003, 2011, 2018, 2020 and 2022 (Figure 14), in line with other studies reporting yield losses due to drought for the same years (Emadodin et al. 2021, Finger et al. 2013, Sweeney et al. 2019). Other studies confirm the fact that grassland aboveground productivity is reduced under warmer and drier conditions, also in subalpine regions (Addy et al. 2022, De Boeck et al. 2016, Qi et al. 2018, Schmid 2017, Wu et al. 2021). The fact that lower yields are mainly caused by water limitation is also consistent with the results of the T-test comparison of the weather parameters between years with the highest and years with the lowest yields (Figure 15), in which years with the lowest harvests were characterised by high temperatures and low spring precipitation, possibly leading to drought.

Yield in 2022

As a result of drought, especially in May, July and August, caused by above-average temperatures and a prolonged period of low rainfall (DWD et al. 2022), the mean yield in 2022 was the lowest since measurements began in 1990 and, depending on the productivity category, was about 28-47% below the norm (2013-2022) (Figure 12 and Table 2).

4.1.3 Decreasing yield with climate change and decreasing soil nitrogen

Effects of climate change on yield

If warming is accompanied by a decline in water availability, the potential benefits of warmer temperatures on plant growth in mountain regions through extended growing seasons may be countered by the negative impacts of drought, which would result in a lower aboveground biomass production (Schuchardt et al. 2021, Volk et al. 2021). No linear relationship between yield and the length of the growing season was found in Muldain for the period 1990-2022. Several studies identify climate change, with its increasing dryness caused by changing precipitation patterns and rising temperatures, as the main cause of declining grassland productivity (Brookshire & Weaver 2015, Emadodin et al. 2021).

These results are consistent with the positive linear relationship between yield and P_{tot} between May and July and the negative linear relationship between yield and GDD_{sum} during the growing season found in Muldain for 1990-2022 (Figure 13). Yields were lower at higher temperatures and at low precipitation rates in spring and summer, which is confirmed by the positive linear relationship between yield and IDM during the agricultural year (yield = 360.16 + 5.96*IDM, R^2_{adj} = 1.13, $F_{1,\ 31}$ = 5.84, p-value = 0.022*, n=33).

The summer climate in the European Alps is expected to become warmer and drier, making extreme events such as prolonged droughts more likely (De Boeck et al. 2016, Finger et al. 2013, Schmid 2017), so that further yield declines are predicted for the future (Addy et al. 2022, Carozzi et al. 2022).

Influence of decreasing soil total nitrogen on yield

Important premise: The elemental analyser provided the N_{tot} present in the soil samples, which does not correspond to the plant-available N in the inorganic form of nitrate (NO_3^--N) and ammonium (NH_4^+-N) (Fernandez & Kaiser 2021). In the absence of data on N in the chemical forms that are readily available for plant roots, N_{tot} is used, assuming that a constant proportion of N_{tot} represents plant-available N and that a decrease in N_{tot} in the soil leads to a deficiency in plant-available N (Capriel 2013).

As shown in Figure 7, N_{tot} decreased over time (about 10% in the last 30 years), and this trend is true for all productivity categories. There are two possible explanations for this decline in soil N_{tot}. The first can be attributed to agricultural management practices. Since the grassland under study is extensively managed, only limited amounts of N were applied through fertilisers. The 25 $kg\,ha^{-1}\,year^{-1}$ applied are even lower than the usual values of 50 $kg\,ha^{-1}\,year^{-1}$ applied on likewise extensively managed pre-alpine grasslands (Botter et al. 2020). Moreover, pasture management involved three annual harvests, during which the nutrients were removed by the grass cuttings. This N could, therefore, not replace the N used by vegetation for its growth and was lost by the removal of aboveground plant biomass (Turner 2021). This translocated N was unlikely to be compensated for by the low fertiliser application of N (Bernhardt-Römermann et al. 2011). The second possible explanation is related to the decline in productivity of the field, which may have led to a decrease in N input to the soil due to declining plant residues and their decomposition (Capriel 2013).

The declining soil N_{tot}, assuming it is representative of plant available N, may have contributed to the decreasing grassland productivity in Muldain (Figure 12). Several nutrients are required for plant growth,

with N being a key player (Botter et al. 2020, Crowther et al. 2019, Fay et al. 2015). The availability of a balanced supply of N, P and K is crucial for the efficient development of vegetation, as grassland productivity can be limited by an imbalance between supply and demand of plant nutrients, e.g. due to N deficiency in the soil (Puche et al. 2023, Zhang et al. 2007). This is consistent with Liebig's law, which holds that a plant's ability to grow is dependent on the resources, particularly nutrients, available in minimum quantity (Fornara et al. 2013, Hanson et al. 1985). In addition, water availability and plant nutrient uptake are strongly linked (Bernhardt-Römermann et al. 2011). It could be that with increasing drought conditions during the GS, plants had additional difficulties taking up the available nutrients, including N, due to water limitation.

Stronger yield decrease for low nutrient treatments

The declining yield trend was found to be statistically significant only for the three treatments with the lowest nutrient levels. Similar findings of greater yield decline in less productive grasslands are reported by Samuil et al. (2018) and Bernhardt-Römermann et al. (2011). In the field plots that received high nutrient treatments, nutrient removal with harvest was, at least partly, compensated for by fertiliser application. On the other hand, in the plots that received low nutrient treatments, nutrient replacement and removal through haymaking may no longer be in balance, which may have led to a greater decline because of more pronounced nutrients deficiency (Bernhardt-Römermann et al. 2011).

4.2 Soil organic carbon stocks

SOC stocks comparison with other studies

The mean SOC stocks (n=24) in Muldain (0-20 cm soil depth) ranged from 8.439 ±0.238 to 9.017 ±0.546 $\mathrm{kg\,m^{-2}}$ for the period between 2013 and 2022 (Table 3). These values can be compared with similar results from Moll-Mielewczik et al. (2023), who report mean SOC stocks of 8.14 $\mathrm{kg\,m^{-2}}$ for 24 long-term monitoring sites distributed across Switzerland (1985-2014, soil depth 0-20 cm). This study also includes an extensively managed grassland in Graubünden at an altitude of 1818 m a.s.l., where mean SOC stocks of 9.17 $\mathrm{kg\,m^{-2}}$ were found. In another study conducted in Switzerland, mean SOC contents of 9.3-11.7 $\mathrm{kg\,m^{-2}}$ (varying soil depth) were determined for various selected grassland areas (Bolliger et al. 2008). These SOC contents are more similar to the initial (1990) SOC stocks in Muldain (Table 3). Ammann et al. (2009) report 6.1-6.5 $\mathrm{kgC\,m^{-2}}$ values for their experiment in the Swiss Plateau (450 m a.s.l., soil depth: 100cm). These SOC stocks are lower than those found in Muldain, nonetheless in the same order of magnitude. Similar SOC stocks, 7.1 ±3.7 $\mathrm{kg\,m^{-2}}$ (soil horizon A), were found by Wiesmeier et al. (2013) when sampling 333 grassland soils in Bavaria in south-eastern Germany. In contrast, much lower SOC stocks (1-5 $\mathrm{kg\,m^{-2}}$, 0-20cm) are reported by Pendall et al. (2018) in their report on the situation in US grasslands in 2005. Differences between the SOC stocks found in Muldain and those reported by other studies might be due to different agricultural management and different location characteristics regarding weather, climate, soil and elevation. In addition, not all the studies cited considered only the upper soil (0-20 cm), and used identical sampling techniques in the same period.

4.2.1 Reasons for interannual SOC stocks change

Climatic conditions, i.e. temperature and precipitation, are the most important drivers of SOC stock change, as they influence both OC input into and output from the soil by affecting grassland productivity and microbial decomposition of soil organic matter (SOM). Weather fluctuations thus lead to changes in SOC stocks (Fuchslueger et al. 2019, Puche et al. 2023, Wiesmeier et al. 2018). However, the correlation between changes in SOC stocks and weather variability, and between changes in SOC stocks and aboveground productivity, could only be described on a longer time scale and not for each year (Figure 29 in the Appendix). The increase or decrease in SOC stocks in some years could not be linked to particular weather conditions or yield in the same year of sampling. This could be due to three aspects.

First, a complex interplay of many factors determines changes in SOC stocks. Besides weather and aboveground productivity, many drivers influence the carbon cycle, such as soil pH, water, oxygen and nutrients availability, as well as SOM stability and substrate availability, among others (Hofmann et al. 2016, Wiesmeier et al. 2013).

Second, lag effects may play an important role in the change of SOC stocks. The weather and productivity in one year may not only influence the changes in SOC stocks in the same year but possibly in subsequent years as well. Similarly, the changes in SOC stocks observed between two consecutive years are not only due to the weather conditions and aboveground biomass of that period but also to the weather and productivity of previous years (Trumbore 2000). These aspects can explain why a direct correlation between the change in SOC stocks and the weather and between the change in SOC stocks and productivity could not be described statistically, as was the case with yield variations over time.

Third, SOC stocks in agricultural landscapes are characterised by a large spatial heterogeneity at the small scale, which could affect the detection of interannual variations in SOC stocks by the applied sampling method. Indeed, the in time repeated sampling approach of soils is suitable for studying treatment variations over a longer period of time, but not intended for detecting short-term temporal dynamics of changes in SOC stocks (Hofmann et al. 2016).

4.2.2 Reasons for and consequences of SOC losses over a longer time period

SOC losses: comparison with other studies

Climate change not only implies rising temperatures but also leads to weather extremes such as droughts, and, together with agricultural management, affects grassland productivity and the carbon cycle. The relationship between climate change and terrestrial carbon reservoirs, particularly the role of soils as potential carbon sources or sinks, has been extensively discussed during the past 20 years (Gubler et al. 2019). Sun et al. (2022) performed a meta-analysis with the results of 136 studies that conducted warming experiments on various ecosystem types worldwide, including grasslands. They found that warming resulted in a significant decrease in SOC in most studies. SOC losses between 8 and 20% were found in Muldain between 1990 and 2022 (Figure 19 and Table 3). This is in line with the findings of other studies (Capriel 2013, Puche et al. 2023, Sochorová et al. 2016, Volk et al. 2021, Wiesmeier et al. 2016).

Reasons for SOC losses

Several factors and their interaction could have caused the SOC losses observed in Muldain between 1990 and 2022. The net balance of C input and output determines the SOC content. Primary production and OM decomposition, influenced by weather variability and climate change, biologically regulate carbon fluxes. In addition, grassland production and OM decomposition are influenced by soil factors, including texture, nutrients, and water availability, which control the OM flow into the soil, its quality, and its decomposition rates (Capriel 2013, Garcia-Pausas et al. 2007, Volk et al. 2021).

A first explanation for the decreasing SOC stocks in Muldain might be the observed rising temperature (Figure 4). Because of the dependency of microbial activity on soil temperature, higher temperatures might enhance the decomposition of plant residues and so lead to greater SOC losses (Poeplau 2021, Puche et al. 2023, Sun et al. 2022, Volk et al. 2021). This confirms the first hypothesis that the SOC stocks may shrink with rising temperatures and subsequently increasing microbial respiration.

A second possible reason for decreasing SOC stocks lies in the declining aboveground productivity, which is affected by weather variability, more occurring dry seasons, with climate change, and declining soil N_{tot}. Lower aboveground plant productivity translates into lower possible carbon inputs into the soil through plant residues decomposition, and so to decreasing SOC stocks over time, by stable or increasing ER (Crowther et al. 2019, Eze et al. 2018, Puche et al. 2023).

In addition to a decline in aboveground biomass production, agricultural management includes harvesting. Even though carbon input also occurs from roots and harvest residues, possible carbon inputs to the soil are limited because of grass removal after every cutting (Wiesmeier et al. 2013, Wilts et al. 2004), which according to the literature accounts for about 80-95% of the aboveground biomass (Puche et al. 2023, Seeber et al. 2022). Because there were no other sources of OC input, such as manure treatments for fertilisation, photosynthetic assimilates were the only source of OC in the grassland in Muldain (Eze et al. 2018, Soussana et al. 2007, Volk et al. 2021). Poeplau et al. (2018) and Carozzi et al. (2022) state that biomass removal, for example with crop yield and residues export, can convert the grassland into net carbon sources, if crop residues are not returned to the soil.

Consequences of SOC losses

SOC losses have consequences for soil quality and climate warming. SOC has numerous beneficial effects on soil properties because it affects many soil functions and processes, such as the cycling and storage of nutrients, soil fertility, the filtering of pollutants and water holding capacity, and helps to reduce soil erosion (Gubler et al. 2019, Sochorová et al. 2016). As a crucial measure of soil quality, SOC losses are considered as soil degradation (Capriel 2013, Garcia-Pausas et al. 2007, Lal 2004, Poeplau 2021). In addition, as SOC represents the largest carbon pool in terrestrial ecosystems, even slight changes in SOC content can have a significant impact on the atmospheric CO_2 concentration, contributing significantly to climate warming (Capriel 2013, Deng et al. 2021, Poeplau 2021, Wiesmeier et al. 2016).

4.2.3 No differences in SOC stocks between productivity categories

The second hypothesis of this thesis was that the SOC stock increases with increasing productivity in the different management forms because the OC input is greater than the combined ecosystem carbon losses (Davidson & Janssens 2006, FAO 2010, Paustian et al. 2016, Poeplau et al. 2016, Rumpel et al. 2020). Several studies report increased SOC stocks with grassland mineral fertilisation and the consequently increased yields (Conant et al. 2001, Poeplau 2021, Sanderman et al. 2017, Sochorová et al. 2016). It is believed that the accelerated microbial decomposition caused by climate warming could be counterbalanced by higher grassland productivity, thus leading to a positive relationship between aboveground biomass and SOC stocks (Seeber et al. 2022). However, this hypothesis could not be confirmed for Muldain, as no significant differences in SOC stocks and their change over time were found between productivity categories (Figures 16 and 17, Table 3). Additionally, no apparent relationship between increasing productivity and SOC stocks was found, indicating that higher productivity did not lead to higher SOC stocks (Figure 18 and Figure 28 in the Appendix).

SOC stocks were not significantly different between productivity categories at the beginning of the experiment (1990) and are still similar, even though lower compared to initial values, between productivity categories (2022). Because SOC stocks in individual years can be affected by weather conditions and sampling techniques (Fuchslueger et al. 2019, Puche et al. 2023, Wiesmeier et al. 2018), SOC stocks for two different time periods (1990-2022 and 2013-2022) were also included as these are considered to be more representative. There was no gradual increase in SOC stocks with increasing productivity; the mean SOC stocks for productivity categories 450 and 700 were nearly identical to each other for all time periods considered, as well as to the other productivity categories. Although the lowest SOC stocks were found in productivity category 450 for all periods considered, the highest were not found in the highest productivity category (700); the highest mean SOC stocks, although not significantly different from the other productivity categories, were found in the middle productivity categories (Table 3). The non-significant differences between productivity categories regarding initial and final SOC stocks agree with the fact that no significant differences were found in SOC losses during the last 30 years (1990-2022) between productivity categories (Figure 17). This is not an isolated case, as other studies report a lack of a consistent relationship between higher productivity, obtained with more nutrients application through fertilisation, and SOC stocks, as well as with changes in SOC stocks (Crowther et al. 2019, Fornara et al. 2011, Harmens & Mills 2012). For this lack of relationship between productivity and SOC stocks, there might be several possible explanations.

Role of nutrients application

The grassland field under study is characterised by low N and a gradient of P and K fertiliser applications. Poeplau et al. (2016) report SOC losses for all PK fertilisation levels in the absence of N, but SOC stocks increase following productivity, if N fertilisation is provided. A following paper by Poeplau et al. (2018) confirms similar conclusions, where N application was strongly correlated with the accumulated SOC stocks. Similar results are provided by Eze et al. (2018), where SOC stocks were increased only when N fertiliser was applied. Application of other nutrients had no effect on SOC stocks when N fertiliser was not applied,

even though it increased grassland productivity. Comparable outcomes are shown by Fornara et al. (2013), who show that multi-nutrient application might lead to lower carbon sequestration in permanent grasslands. Because, in Muldain, the same and limited amount of N was applied to all plots regardless of productivity category, differences in aboveground productivity may not translate into differences in SOC stocks. If N is so decisive even in Muldain's grassland, being limited, applications of P and K could not lead to differences in SOC stocks despite productivity differences.

Effect of harvest and possible contribution of belowground biomass

Another possible explanation for the lack of correlation between SOC stock and productivity is the grassland management. With harvest, most of the aboveground biomass is exported. As a result, differences in aboveground productivity may not lead to differences in OC input to the soil (Poeplau 2021, Poeplau et al. 2018). This is because, following harvest, the biomass that remains available for decomposition may be similar between productivity categories. Consequently, the influence of nutrients addition to SOC sequestration might be blurred (Fornara et al. 2013).

Related to harvest is the possible role of plant roots. Some scientists claim that because most of the aboveground biomass is exported from mown grasslands, most of the carbon that reaches the soil is derived from the roots (Poeplau 2021, Poeplau et al. 2018). In addition, in some grasslands, belowground biomass might be higher than aboveground biomass (Eze et al. 2018). The question is whether, in Muldain, belowground biomass differs between productivity categories and, if yes, whether higher aboveground productivities translate into higher belowground productivities as well or if the opposite happens. Fornara et al. (2013) report, for example, similar root mass across different nutrient treatments, highlighting that root mass generally decreased when various nutrients were added and increased only when N was applied. In this study, for example, nutrient treatments had different impacts on aboveground productivity than on belowground mass. Similar findings are reported by Poeplau (2021), who explain the lower root biomass found in fertilised plots compared to unfertilised plots with a shift of the root:shoot ratios towards shoots. Unfortunately, no data concerning the belowground biomass are available for Muldain. Therefore it is impossible to confirm the hypothesis that root biomass might counteract differences in aboveground productivity, in terms of SOC sequestration.

Importance of initial SOC stocks and soil properties

In addition to the possible explanations mentioned before, no relationship between productivity and SOC stocks change between 1990 and 2022 might be present because of non-different initial SOC stocks (1990). Initial SOC stocks are crucial to predict and describe changes in SOC over time in many ecosystems (Bellamy et al. 2005, Capriel 2013, Hanegraaf et al. 2009, Moll-Mielewczik et al. 2023). This would support the hypothesis that SOC stocks changed equally, and independently of productivity, because starting SOC stocks (1990) did not substantially differ between productivity categories (Figure 16 and Table 3).

High variability between field replicates

A final possible factor hampering the detection of an eventual positive relationship between productivity and SOC stocks might be the high variation in SOC stocks between the four replicates, which could be greater than the treatment effects. The two-way ANOVA, which considered the field replicate as a blocking factor, found no significant differences in SOC stocks between productivity categories. However, significant differences between field replicates were detected, possibly affecting the statistical power of the ANOVA (Blainey et al. 2014). A similar issue was encountered by Poeplau et al. (2018).

4.3 CO_2 fluxes

CO_2 fluxes comparison with other studies

ER between June 2022 and June 2023 ranged between -2.21 ±0.07 and -8.08 ±0.16, with mean values of -5.23 ±0.56 µmol CO_2 m^{-2} s^{-1}. ER_{10} ranged between -1.30 ±0.06 and -3.94 ±0.11, with mean values of -2.74 ±0.21 µmol CO_2 m^{-2} s^{-1}. GPP_{pot} ranged between 1.89 ±0.28 and 15.33 ±0.47, with mean values of 9.34 ±1.07 µmol CO_2 m^{-2} s^{-1} (Table 5). These results align with the ecosystem CO_2 fluxes reported by other studies (Bahn et al. 2008, Flanagan & Johnson 2005, Gilmanov et al. 2007, Rogger et al. 2022). Flanagan & Johnson (2005) report ER rates of -9 µmol CO_2 m^{-2} s^{-1} for a moist year (2022) and -5 µmol CO_2 m^{-2} s^{-1} for a drier year (2001) in a native Canadian grassland. Bahn et al. (2008) provide ER for 20 European grasslands across a climatic transect. Maximum rates of ER ranged from -1.9 to -15.9 µmol CO_2 m^{-2} s^{-1}, while ER_{10} ranged between -0.3 and -5.5 µmol CO_2 m^{-2} s^{-1}. Rogger et al. (2022) conducted an experiment on a medium intensively managed grassland in central Switzerland at 1000 m above sea level and measured CO_2 fluxes for 15 years (2005-2019). ER ranged from -3.3 to -3.5 µmol CO_2 m^{-2} s^{-1}, while GPP ranged from 8.0 to 9.6 µmol CO_2 m^{-2} s^{-1}. Differences in CO_2 fluxes with these studies might lie in the used measuring technique (eddy covariance vs static chambers vs flexible chambers), in the period and site under study, and in the grassland management.

4.3.1 Reasons for differences between measuring campaigns

Environmental parameters

The magnitude of ER is determined by root respiration and microbial decomposition of OM, processes that strongly depend on temperature (Davidson & Janssens 2006, Volk et al. 2021). Because of the dependence of ER on temperature, the greatest values were found at the highest soil temperatures (02.08.2022), while the smallest values at the lowest temperatures (07.11.2022) (Figure 20).

By constant environmental conditions, ER_{10} would be similar over the year. However, ER_{10} in Muldain showed important variations over time. Seasonal changes in ER_{10} are due to the fact that the ability of an ecosystem for respiration is not only temperature dependent but influenced by other factors such as soil moisture (Figure 10) (Davidson & Janssens 2006, Flanagan & Johnson 2005, Hussain et al. 2011). Depending on soil moisture, ER might vary greatly even at the same temperature (Reichstein et al. 2003, Rogger et al. 2022). The smallest ER_{10} was measured on 16.08.2022, by a very low relative soil moisture of 6%. On the

contrary, the greatest ER_{10} was measured on 18.04.2023, by a much higher relative soil moisture of 78% (Figure 20, Table 5 and Table 4). This is in line with the findings of Flanagan & Johnson (2005), who explained a large part of the seasonal and interannual variation in ER_{10} data with soil moisture changes.

GPP_{pot} is determined by seasonal temperature. Higher values are normally to be found by a more developed canopy at higher temperatures. However, GPP_{pot} is also influenced by soil moisture (Rogger et al. 2022, Volk et al. 2021). As indicated in Figure 20, the lowest GPP_{pot} was measured on 19.07.2022, by very low relative soil moisture (8.17 %). At similar temperatures, the highest values were measured, but at a relative soil moisture of 34.30 %. Several studies identified drought as the cause for GPP declines in 2003 (Harmens & Mills 2012, Heyburn et al. 2017).

Aboveground biomass

Not only seasonal temperature and soil moisture determine the magnitude of GPP_{pot} and ER_{10}. Canopy development plays an important role as well (Volk et al. 2021). The amount and activity of aboveground biomass may also impact variations in GPP_{pot} and ER_{10}, with larger values likely to correlate with peak biomass levels (Gilmanov et al. 2007, Schmitt et al. 2010). However, because the grassland under study is managed, harvesting has an impact on the natural phenological plant development and hence decouples it from the seasonal change in environmental conditions (Wohlfahrt et al. 2008). As it is clear by looking at Figure 20, GPP_{pot} and ER_{10} were much smaller right after the second harvest on 19.07.2022. Similar findings are reported by Bahn et al. (2008) and Rogger et al. (2022). Harvest leads to a strong decline in CO_2 assimilation by reducing the available amount of assimilating plant materials. Additionally, the exported biomass is unavailable for decomposition and ER (Hussain et al. 2011).

Variations in the ratio GPP_{pot}/ER_{10}

The ratio GPP_{pot}/ER_{10} helps to understand the relative importance of carbon uptake through photosynthesis and carbon release through respiration. However, this ratio is not the ecosystem carbon balance, as carbon lost through harvesting is not taken into account (Table 15 in the Appendix) and the CO_2 fluxes data are only available for 12 measurement campaigns and not for the whole year.

Variations in GPP_{pot} and ER_{10} affect the GPP_{pot}/ER_{10} ratio if GPP_{pot} and ER_{10} do not change to a similar extent in response to variations in environmental parameters, such as soil moisture (SM) and soil temperature (ST). However, for example, the GPP_{pot}/ER_{10} ratio did not differ significantly between the campaigns 14.06.2022 (SM = 23.34%, ST = 18.9 - 19.9 °C), 19.10.2022 (SM = 23. 02%, ST = 12.3 - 13.3 °C) and 18.04.2023 (SM = 77.84%, ST = 9.5 - 11.6 °C), despite different times of the year (Figure 21 and Table 5). This could be due to the complex interaction of soil temperature, soil moisture, canopy development stage and available substrate for decomposition (Flanagan & Johnson 2005, Reichstein et al. 2003). For example, on 18.04.2023 the soil temperature was lower than on 14.06.2022 and 19.10.2022, but the soil moisture was much higher, so with an impact on the resulting CO_2 fluxes (Table 5).

In addition, the effect of harvesting on GPP_{pot} and ER_{10} is also evident from the GPP_{pot}/ER_{10} ratio, especially due to the decrease in GPP_{pot}. The lowest ratio was found on 19.07.2022 (1.1 $\pm$0.15 µmol CO_2

$m^{-2}\,s^{-1}$), immediately after the second harvest. In contrast, the highest ratios at the highest aboveground biomass were on 8.7.2022 (4.7 µmu mol CO_2 $m^{-2}\,s^{-1}$), between the first and second harvests, and on 5.9.2022 (4.4 ±0.11 µmol CO_2 $m^{-2}\,s^{-1}$), before the second and last harvests.

4.3.2 No differences in CO_2 fluxes between productivity categories

The third hypothesis of this thesis was that CO_2 fluxes differ between productivity categories and increase with aboveground productivity, as different yields affect carbon cycling (Bahn et al. 2008). When looking at Figure 22 and Table 6, mean GPP_{pot} and mean ER_{10} (n=4) were greater by categories with higher productivity, as expected. Especially obvious is the visual difference in mean GPP_{pot} and mean ER_{10} between productivity categories 450 and 700, as smallest values are to be found in the lowest productivity category. However, these differences are not statistically significant, so the initial hypothesis can not be confirmed.

The ratio of OC inputs to outputs was similar and independent of aboveground productivity during the measurement period since GPP_{pot}/ER_{10} did not differ between productivity groups. Additionally, the ratio GPP_{pot}/ER_{10} was higher than 1 for all measuring campaigns, implying that more carbon was assimilated than lost. Whether this defines the grassland under study as a net carbon sink is not possible to state based on 12 campaigns. An interpolation over the year would be needed, and 2022 was a dry year, possibly misrepresenting the general pattern. Furthermore, it is impossible to determine whether a grassland is a carbon sink or source by considering only GPP_{pot} and ER_{10} and neglecting other OC inputs and outputs, such as harvesting (Table 15). This aspect will be further discussed in Chapter 4.4.

Possible reasons for no differences in ER_{10}

Similarly to Dornbush & Raich (2006) and Ward et al. (2017), who did not find any correlation between aboveground productivity and ER rates in central Iowa grasslands and three long-term grassland experiments in South Africa, respectively, ER_{10} did not significantly differ between productivity categories in Muldain. For this, there might be several possible explanations.

First, ER is not only controlled by aboveground productivity but is the result of complex interactions of environmental and biotic factors (Flanagan & Johnson 2005, Reichstein et al. 2003). Soil temperature, soil water availability, substrate quality, and changes in above- and below-ground vegetation and fauna are all significant ER drivers (Reichstein et al. 2003). Because all these factors were similar across the different productivity categories, they might have minimised possible differences in ER_{10} caused by different productivity.

Second, the management of grasslands with regard to harvesting and fertilisation may alter the spatial variability in nutrient availability and species composition, hence affecting the effects on above- and below-ground processes (Reichstein et al. 2003, Schmitt et al. 2010). Regarding fertilisation in the grassland under study, productivity categories differed in terms of P and K applied, but the same amount of N was applied to all field parcels. Ward et al. (2017) found no significant change in ER depending on P addition but reported significant differences in ER due to levels of N fertiliser. Similarly, Zhai et al. (2017) and Peng et al. (2011)

found increased ER with higher N application. The fact that in Muldain, soil N_{tot} does not differ between productivity categories could have hampered an eventual effect of different aboveground productivity on ER_{10}. Regarding harvest, the frequent removal of aboveground biomass may have weakened the relationship between grassland productivity and ER. Harvesting the aboveground biomass can directly impact the OC input to the soil and subsequently affect ER. It is possible that the removal of biomass could have had similar effects across all productivity categories, leading to comparable ER_{10} rates (Hussain et al. 2011). Related to this is the possible role played by belowground biomass. Unfortunately, no data are available regarding roots biomass and activity, but a hypothesis based on the literature is that compensatory processes were occurring within the grassland ecosystem. For example, plots with lower aboveground productivity might have experienced higher belowground productivity, leading to comparable overall ER_{10} rates. Such compensation effects could have masked the expected differences in ER_{10} between productivity categories (Dornbush & Raich 2006)

Third, 2022 was a dry year in Muldain (DWD et al. 2022). Because soil moisture availability strongly limits ER, ER_{10} might have been lower overall for all productivity categories. Drought might therefore have masked any potential expected differences in ER_{10} between productivity categories (Hussain et al. 2011).

Finally, a high variability characterises ER_{10} data within each productivity category (Figure 22). It is, therefore, more challenging to detect significant differences between productivity categories when ER_{10} significantly varies between field replicates. Additionally, data were averaged between campaigns to perform the ANOVA; this data loss, together with the low sample size for each productivity category, might have limited the statistical power of the analysis and so affected the detection of eventual differences.

Possible reasons for no differences in GPP_{pot}

Remarkably, GPP_{pot} did not vary with aboveground productivity, despite significant yield differences depending on the nutrients applied (Figure 11). Similarly, Skinner & Adler (2010) were unable to determine any relationship between GPP and aboveground biomass production and suggested that variations in belowground biomass and related root characteristics, such as depth and density, may be a factor influencing GPP fluctuations. However, these are merely speculations since there are no data on the belowground biomass in Muldain.

Another possible explanation is that drought leads to reduced GPP, similar to ER. The experiment experienced drought conditions in 2022 when most campaigns took place, which could have masked the expected differences in GPP_{pot} between productivity categories. Drought stress can affect all plants, regardless of their initial productivity levels, leading to a convergence in GPP_{pot} values (Farooq et al. 2012).

Finally, as was the case with ER_{10}, the high data variability within productivity categories could have complicated the detection of significant differences in GPP_{pot} between productivity categories (Blainey et al. 2014).

Possible reasons for no differences in GPP_{pot}/ER_{10}

No differences were found in GPP_{pot}/ER_{10} between productivity categories. This might firstly be because

there were no significant differences in the carbon inputs and outputs between productivity categories. Secondly, this balance, like GPP_{pot} and ER_{10}, is influenced by temperature, soil moisture, nutrient availability, and microbial activity, which might have been relatively consistent across the different productivity categories, thus leading to similar GPP_{pot}/ER_{10} ratios. Another possible reason is the variability in GPP_{pot} and ER_{10} measurements, and potential errors or uncertainties in their estimation, which could have contributed to the lack of detected differences in the GPP_{pot}/ER_{10} ratio (Blainey et al. 2014).

4.3.3 No relationship between GPP_{pot}/ER_{10} and SOC stocks

The last hypothesis of this work was that higher ratios between GPP_{pot} and ER_{10} would be found in field parcels with higher SOC stocks, indicating a higher net carbon gain by the ecosystem. This could be because, either more carbon can be assimilated through photosynthesis and/or less carbon is lost to the atmosphere via ecosystem respiration (Davidson & Janssens 2006). However, no relationship was found between the ratio of GPP_{pot}/ER_{10} and SOC stocks, when considering the relative change in SOC stocks between 1990 and 2022 (Figure 23) and the SOC stocks in 2022 (Figure 30 in the Appendix). This is confirmed by the low Pearson correlation coefficients found (Table 14 in the Appendix). Possible reasons might explain the lack of this relationship.

Firstly, the absence of a relationship between SOC stocks and GPP_{pot}/ER_{10} could be related to the complex dynamics and feedback mechanisms between plants, soil microorganisms, and carbon cycling processes. Strong coupling and interaction between soil's physical characteristics, chemical composition, belowground components like plant roots and live microorganisms, and with above-ground factors like plant litter and biodiversity, exist within soil systems (Flanagan & Johnson 2005, Hofmann et al. 2016, Reichstein et al. 2003, Wiesmeier et al. 2013). SOC stocks and the ratio GPP_{pot}/ER_{10}, as well as the relationship between them, are influenced by various factors. One of these factors is the weather. The year of CO_2 fluxes measurements, 2022, was characterised by drought conditions, possibly affecting the resulting GPP_{pot}/ER_{10} (Forte et al. 2023). CO_2 fluxes measured in 2022 might, therefore, not represent the ecosystem because of soil moisture deficiency, thus potentially masking or overriding a potential relationship between SOC stocks and GPP_{pot}/ER_{10}. Comparing CO_2 fluxes of more and more diverse years with changes in SOC stocks might lead to a different result.

Secondly, the time scale mismatch may have played a role. Values for GPP_{pot} and ER_{10} are available only for 12 dates between June 2022 and June 2023. On the contrary, information on SOC stocks ranges between 1990 and 2022. The measured CO_2 fluxes may not be suitable to explain and interpret the final SOC stocks (2022), because changes in SOC stocks in response to weather and to OC input from yield residues, might take more time. Similarly, final SOC stocks were not only influenced by processes occurring in 2022 but also by carbon inputs and outputs from previous years (Trumbore 2000). The mismatch in time scales could thus make it difficult to detect a relationship between SOC stocks and GPP_{pot} and ER_{10}.

Thirdly, N limitation can directly impact GPP_{pot} and ER_{10} by reducing photosynthesis, biomass production, microbial activity, and litter decomposition rates (Puche et al. 2023, Zhang et al. 2007). These

direct effects can subsequently influence the GPP_{pot}/ER_{10} ratio through changes in carbon use efficiency and feedback mechanisms. The impact of N limitation on GPP_{pot}, ER_{10} and their ratio could have contributed to a decoupling between SOC stocks and the GPP_{pot}/ER_{10} ratio.

Finally, the presence of high variability in SOC stocks and in the GPP_{pot}/ER_{10} ratio within each productivity category, combined with a relatively small sample size, could have reduced the statistical power to detect a relationship. Larger sample size or additional data points may be required to detect a potential relationship that is obscured by this high variability (Blainey et al. 2014). Related to this are possible measurement errors or limitations in the quantification of SOC stocks or the GPP_{pot}/ER_{10} ratio that affect the ability to detect a relationship. These aspects are further discussed in Chapter 4.4 "Possible limitations".

4.4 Possible limitations

4.4.1 Dry 2022

As already mentioned, the drought in 2022 may have affected the results of the measurements of CO_2 fluxes and, consequently, the interpretation of the lack of relationship between GPP_{pot}/ER_{10} and SOC stocks, as well as the lack of differences in GPP_{pot}, ER_{10} and their ratio between productivity categories. As discussed in several studies, droughts and the terrestrial carbon cycle are closely linked. Drought can have a significant impact on the magnitude and patterns of carbon cycling over different time periods in grasslands. This, by affecting vegetation productivity and, thus, OC input to the soil and, consequently microbial decomposition, which in turn determines ER and carbon output (Deng et al. 2021, Fuchslueger et al. 2019, Hussain et al. 2011, Lei et al. 2020). Repeating the same experiment in a second, wetter year might be interesting to validate the results of this work, or to draw alternative conclusions.

4.4.2 Field sampling, measurement technology and calculations

SOC stocks estimation

The first aspect that leads to uncertainty in SOC stock estimates is soil sampling. Since 1989, seven cores for the top 20 cm have been randomly collected yearly for every field plot. The measurement accuracy of soil sampling, which is influenced by sampling strategy and design, is primarily responsible for the associated uncertainty in spatial and temporal SOC dynamics. Samples were not collected from the same location each year, and it may be difficult to detect spatial variability in SOC stocks and represent it similarly over time (Hofmann et al. 2016, Moll-Mielewczik et al. 2023). However, this uncertainty should be minimised given the seven samples per plot.

Secondly, additional uncertainty may lie in the assumption of constant C_{min} over time (Paragraph 2.3.1). SOC concentrations were calculated as the difference between C_{tot} and C_{min}. The simple linear regression model was used to test if time significantly predicted mean C_{min} concentration (n=24). The overall regression was not statistically significant, meaning that the mean C_{min} concentration was constant over time. The Mann-Kendall test was performed separately for every field parcel to detect possible trends in C_{min} over time.

In most field parcels, C_{min} stayed constant over time. However, in field parcels 19, 29, 30, 33, 36 and 42 a non-parametric significant decreasing trend in C_{min} was found. This could have led to a possible overestimation of SOC concentration for these parcels for the years 1990-2005 and 2022, as the SOC calculations assumed constant C_{min} values in every field parcel.

Finally, for calculating SOC stocks in the historical soil samples, the mean soil density (n=24) determined with the soil samples taken in 2022 was used. This underlies two assumptions. The first one is that mean soil density (n=24) is representative of the soil density for every soil sample. Despite the fact that only two samples per parcel were taken in 2022, them also not being entirely representative of the entire field parcel, this solution was more appropriate than applying separate soil densities to each field parcel (Poeplau et al. 2016). The second assumption is that soil density is constant over time, given the extensive grassland management. However, possible differences in bulk density over time might play an important role, thus affecting the calculated SOC stocks (Moll-Mielewczik et al. 2023, Poeplau et al. 2018).

Deep SOC

Further uncertainty lies in the fact that for this study, SOC stocks refer only to the top 20 cm of soil. While SOC concentrations are often higher in surface soils than in deeper layers, soils also store carbon throughout the depth of the soil profile (Lal et al. 2015, Lorenz & Lal 2021). Most studies tend to focus on the topsoil because, technical difficulties and higher costs associated with sampling deep soils aside, it is generally acknowledged that the topsoil contains most of the SOM (Lorenz & Lal 2021, Ward et al. 2016). Deep SOC is considered important, primarily because of its greater protection from degradation and consequent longer residence time, so that despite low carbon concentrations in deep soil horizons, it contributes to more than half of total SOC stocks overall (Rumpel & Kögel-Knabner 2011). However, in Muldain, SOC stocks below the first 20 cm are not expected to reverse the results because soils in Swiss mountain regions are typically shallow (Hoffmann et al. 2014). This could be observed during sampling, where it was manually not possible to sample deeper with the technique used due to the high stone content and higher soil density. Deeper soil sampling using adaptive techniques could provide insights into deep SOC. It could be interesting to investigate whether most of the SOC in Muldain is stored in the top 20 cm or whether deeper soil layers contribute strongly to the overall SOC.

Separation of NEE into GPP and ER

Additional uncertainty may lie in the partitioning of NEE into GPP and ER (Equation 6). GPP_{pot} was calculated by extending the relationship between temperature and NEE_{night} (determined by using the Arrhenius equation 5), when GPP_{pot} is zero, to daytime conditions. This approach could have led to an overestimation of daytime ER, because leaf respiration is reduced during the day compared to dark conditions, and because the temperature sensitivity of ER calculated from long-term data sets does not necessarily correspond to the short-term temperature sensitivity useful for converting ER measured in the night to ER during the day (Reichstein et al. 2004, Wohlfahrt et al. 2005).

Winter measurements of CO_2 fluxes

It is generally recognised that CO_2 fluxes during the GS are the main driver of annual carbon balances and provide essential information on mechanisms of carbon exchange. There is general agreement, nevertheless, that respiratory losses during the cold season might cancel out the carbon budget determined during the GS. This is because of considerable amounts of CO_2 released by heterotrophic respiration in the soil even when it is covered in snow (Merbold et al. 2012). Winter CO_2 fluxes have not been measured in Muldain for several reasons. Firstly, it is logistically and methodologically challenging to measure GHG fluxes in winter, because the snow-covered site is more difficult to access, and because the cold temperatures make it challenging for people and equipment to operate (Merbold et al. 2013). Secondly, the scope of this thesis was not to estimate an annual net ecosystem carbon balance. For this aim, winter CO_2 fluxes could be interpolated. For comparing GPP_{pot} and ER_{10} between productivity categories, winter fluxes were assumed not to bring significant differences in CO_2 fluxes depending on the aboveground productivity. However, this hypothesis could only be tested with available data from winter measurements.

Interpolation of CO_2 fluxes between campaigns

This work aims to answer the third and fourth research questions based solely on 12 measurement campaigns of CO_2 fluxes, all during the GS and under similar daytime sunlight conditions. For a complete understanding of the carbon sink capacity of the grassland studied, and for detecting possible differences in GPP_{pot} and ER_{10} between productivity categories, interpolation of CO_2 fluxes between campaigns would be needed. This could be done using available data for soil temperature, soil moisture, relative sunshine duration (light response curve) and canopy development (Volk et al. 2011). However, such an analysis is beyond the scope of this thesis.

4.4.3 Grassland management and field design

Grassland management and field design could also contribute to uncertainties. The low N application rate since 1989, which is below the norm for extensively managed grassland, is one factor contributing to N limitation in the soil (Botter et al. 2020). Because of potential N depletion, plant growth is limited (Botter et al. 2020, Crowther et al. 2019, Fay et al. 2015). Consequently, the grassland in Muldain, also in terms of SOC stocks and CO_2 fluxes, might not be representative of an extensively managed Swiss mountain grassland.

In addition, despite the small study area, the field design established in 1989 is characterised by a fairly high variability in soil properties between field replicates. The blocking effect of the field replicates was accounted for in the statistical analysis. However, the limited number of replicates and the variability between them could have affected the results by masking possible differences between productivity categories (Blainey et al. 2014). Nevertheless, this should have been minimised by considering the completely randomised block design in the statistical analyses.

5 Conclusion

Despite the recognised importance of grasslands as global carbon sinks, it is still uncertain which effects global warming will have on the carbon budgets of such ecosystems. The influence of productivity on SOC stocks and ecosystem carbon exchange with the atmosphere is understudied. It is important to find the most suitable management practices in agriculture that can sustain the desired yields and increase SOC stocks globally, or at least mitigate SOC losses to the atmosphere. Hence this thesis aimed to investigate if and how the aboveground productivity of an extensively managed pre-alpine grassland affects the SOC stock, respectively, if and how the carbon sequestration depends on the fertilisation management practice. Furthermore, the goal was to show which fertilisation management is most suited to achieve carbon sequestration in grassland soils, thus mitigating climate change and compensating for GHG emitted by agriculture.

The first research question was: Is the SOC stock in the chosen Swiss mountain grassland site shrinking or rising with climate warming? The formulated hypothesis that SOC stocks may shrink with rising temperatures and subsequently increasing microbial respiration could be confirmed. SOC stocks losses were found for all productivity categories between 1990 and 2022. Additionally to warming, possible reasons may be the decreasing yield, and the consequent reduced OC input to the soil, caused by more often occurring drought periods, together with decreasing soil N_{tot}.

The second research question was: Does higher productivity translate into lower SOC losses? The formulated hypothesis that SOC stock increases with increasing productivity in the different management forms (because the OC input is greater than the combined ecosystem carbon losses) could not be confirmed. Despite differences in aboveground productivity, no differences in SOC stocks were found between productivity categories. This might be because many factors are involved in the complexity of the carbon cycling. Weather variability, climate change, the harvesting practice, nutrients availability, and possible differences in belowground biomass may have masked a possible relationship between productivity and SOC stocks or stronger determined changes in SOC stocks.

The third research question was: Are there differences in GPP_{pot}, ER_{10} and GPP_{pot}/ER_{10} between different productivity categories? The hypothesis that CO_2 fluxes differ between productivity categories and increase with aboveground productivity could not be confirmed. Similarly to the lacking of a relationship between productivity and SOC stocks, the complexity of the ecosystem may have influenced these results. Additionally, the drought that characterised 2022 and the high data variability might have affected these results.

The last research question was: Is there a positive relationship between the SOC stocks and the ratio GPP_{pot}/ER_{10}? The hypothesis that higher GPP_{pot}/ER_{10} ratios are found in field parcels with higher SOC stocks, indicating a higher net carbon gain by the ecosystem, could not be confirmed. This could be because similar amounts of carbon were assimilated through photosynthesis and lost to the atmosphere via ER. Additionally, the year 2022 might not be representative, because of the drought.

6 Outlook

It is crucial to further study the relationship between grassland productivity and SOC stocks to find the most appropriate management form to maintain the carbon sink potential of grasslands with climate change. Additional measurements, which are beyond the scope of this thesis, could be performed. First, information on belowground biomass and root carbon could be useful; integrating aboveground and belowground components may provide a more comprehensive understanding of ecosystem carbon dynamics and productivity. Roots data could be used to test whether differences in aboveground productivity translate into differences in root biomass and what thrives more SOC changes. Second, fertilisation and climate change may affect plant species composition, which in turn influences productivity and possibly nutrients and carbon cycling (Poeplau et al. 2018, Ward et al. 2017). Data on the plant species composition, the respective yield and changes over time might be relevant. Finally, it might be interesting to repeat measurements of CO_2 fluxes in several years with different weather conditions.

7 Bibliography

Addy, J. W., Ellis, R. H., MacLaren, C. et al. (2022), 'A heteroskedastic model of Park Grass spring hay yields in response to weather suggests continuing yield decline with climate change in future decades', *Journal of the Royal Society Interface* **19**(193).

Agroscope (2021), 'The STYCS Trials – Another Soil, Another Fertilisation Approach'.
URL: *https://www.agroscope.admin.ch/agroscope/en/home/topics/environment-resources/monitoring-analytics/long-term-trials/stycs.html*

Ammann, C., Spirig, C., Leifeld, J. et al. (2009), 'Assessment of the nitrogen and carbon budget of two managed temperate grassland fields', *Agriculture, Ecosystems and Environment* **133**(3-4), 150–162.

Bahn, M., Rodeghiero, M., Anderson-Dunn, M. et al. (2008), 'Soil respiration in European grasslands in relation to climate and assimilate supply', *Ecosystems* **11**(8), 1352–1367.

Bellamy, P. H., Loveland, P. J., Bradley, R. I. et al. (2005), 'Carbon losses from all soils across England and Wales 1978-2003', *Nature* **437**(7056), 245–248.

Bernhardt-Römermann, M., Römermann, C., Sperlich, S. et al. (2011), 'Explaining grassland biomass - the contribution of climate, species and functional diversity depends on fertilization and mowing frequency', *Journal of Applied Ecology* **48**(5), 1088–1097.

Blainey, P., Krzywinski, M. & Altman, N. (2014), 'Points of significance: Replication', *Nature Methods* **11**, 879–880.

Bolliger, J., Hagedorn, F., Leifeld, J. et al. (2008), 'Effects of land-use change on carbon stocks in Switzerland', *Ecosystems* **11**(6), 895–907.

Botter, M., Zeeman, M., Burlando, P. et al. (2020), 'Impacts of fertilization on grassland productivity and water quality across the European Alps under current and warming climate: Insights from a mechanistic model', *Biogeosciences* **18**(6), 1917–1939.

Brookshire, E. N. & Weaver, T. (2015), 'Long-term decline in grassland productivity driven by increasing dryness', *Nature Communications* **6**(7148).

Bürli, S., Theurillat, J. P., Winkler, M. et al. (2021), 'A common soil temperature threshold for the upper limit of alpine grasslands in European mountains', *Alpine Botany* **131**(1), 41–52.

Capriel, P. (2013), 'Trends in organic carbon and nitrogen contents in agricultural soils in Bavaria (south Germany) between 1986 and 2007', *European Journal of Soil Science* **64**(4), 445–454.

Carozzi, M., Martin, R., Klumpp, K. et al. (2022), 'Effects of climate change in European croplands and grasslands: Productivity, greenhouse gas balance and soil carbon storage', *Biogeosciences* **19**(12), 3021–3050.

Conant, R. T., Paustian, K. & Elliott, E. T. (2001), 'Grassland management and conversion into grassland: effects on soil carbon', *Ecological Applications* **11**(2), 343–355.

Cook, F. J. & Orchard, V. A. (2008), 'Relationships between soil respiration and soil moisture', *Soil Biology and Biochemistry* **40**(5), 1013–1018.

Crowther, T. W., Riggs, C., Lind, E. M. et al. (2019), 'Sensitivity of global soil carbon stocks to combined nutrient enrichment', *Ecology Letters* **22**(6), 936–945.

Davidson, E. A. & Janssens, I. A. (2006), 'Temperature sensitivity of soil carbon decomposition and feedbacks to climate change', *Nature* **440**(7081), 165–173.

De Boeck, H. J., Bassin, S., Verlinden, M. et al. (2016), 'Simulated heat waves affected alpine grassland only in combination with drought', *New Phytologist* **209**(2), 531–541.

Deng, L., Peng, C., Kim, D. G. et al. (2021), 'Drought effects on soil carbon and nitrogen dynamics in global natural ecosystems', *Earth-Science Reviews* **214**.

Dornbush, M. E. & Raich, J. W. (2006), 'Soil temperature, not aboveground plant productivity, best predicts intra-annual variations of soil respiration in central Iowa grasslands', *Ecosystems* **9**(6), 909–920.

DWD, MeteoSchweiz & ZAMG (2022), Alpenklima Sommerbulletin 2022: Klimazustand in den Zentral- und Ostalpen, Technical report.

Emadodin, I., Corral, D. E. F., Reinsch, T. et al. (2021), 'Climate change effects on temperate grassland and its implication for forage production: A case study from Northern Germany', *Agriculture (Switzerland)* **11**(232).

Eze, S., Palmer, S. M. & Chapman, P. J. (2018), 'Soil organic carbon stock in grasslands: Effects of inorganic fertilizers, liming and grazing in different climate settings', *Journal of Environmental Management* **223**, 74–84.

FAO (2010), Challenges and opportunities for carbon sequestration in grassland systems, Technical report.

Farooq, M., Hussain, M., Wahid, A. et al. (2012), *Drought stress in plants: An overview*, Springer-Verlag Berlin Heidelberg, pp. 1–33.

Fay, P. A., Prober, S. M., Harpole, W. S. et al. (2015), 'Grassland productivity limited by multiple nutrients', *Nature Plants* **1**(7).

Fernandez, F. & Kaiser, D. (2021), 'Understanding nitrogen in soils', `https://extension.umn.edu/nitrogen/understanding-nitrogen-soils`. [Accessed 20-Jul-2023].

Finger, R., Gilgen, A. K., Prechsl, U. E. et al. (2013), 'An economic assessment of drought effects on three grassland systems in Switzerland', *Regional Environmental Change* **13**(2), 365–374.

Flanagan, L. B. & Johnson, B. G. (2005), 'Interacting effects of temperature, soil moisture and plant biomass production on ecosystem respiration in a northern temperate grassland', *Agricultural and Forest Meteorology* **130**(3-4), 237–253.

Fornara, D. A., Banin, L. & Crawley, M. J. (2013), 'Multi-nutrient vs. nitrogen-only effects on carbon sequestration in grassland soils', *Global Change Biology* **19**(12), 3848–3857.

Fornara, D. A., Steinbeiss, S., Mcnamara, N. P. et al. (2011), 'Increases in soil organic carbon sequestration

can reduce the global warming potential of long-term liming to permanent grassland', *Global Change Biology* **17**(5), 1925–1934.

Forte, T. G. W., Carbognani, M., Chiari, G. et al. (2023), 'Drought timing modulates soil moisture thresholds for CO_2 fluxes and vegetation responses in an experimental alpine grassland', *Ecosystems* .

Fuchslueger, L., Wild, B., Mooshammer, M. et al. (2019), 'Microbial carbon and nitrogen cycling responses to drought and temperature in differently managed mountain grasslands', *Soil Biology and Biochemistry* **135**, 144–153.

Garcia-Pausas, J., Casals, P., Camarero, L. et al. (2007), 'Soil organic carbon storage in mountain grasslands of the Pyrenees: Effects of climate and topography', *Biogeochemistry* **82**(3), 279–289.

Gilmanov, T. G., Soussana, J. F., Aires, L. et al. (2007), 'Partitioning European grassland net ecosystem CO_2 exchange into gross primary productivity and ecosystem respiration using light response function analysis', *Agriculture, Ecosystems and Environment* **121**(1-2), 93–120.

Grigulis, K. & Lavorel, S. (2020), 'Simple field-based surveys reveal climate-related anomalies in mountain grassland production', *Ecological Indicators* **116**.

Grotzinger, J. & Jordan, T. (2017), *Allgemeine Geologie*, 7 edn, Springer, Berlin, Heidelberg.

Gubler, A., Wächter, D., Schwab, P. et al. (2019), 'Twenty-five years of observations of soil organic carbon in Swiss croplands showing stability overall but with some divergent trends', *Environmental Monitoring and Assessment* **191**(277).

Hanegraaf, M. C., Hoffland, E., Kuikman, P. J. et al. (2009), 'Trends in soil organic matter contents in Dutch grasslands and maize fields on sandy soils', *European Journal of Soil Science* **60**(2), 213–222.

Hanson, J. D., Parton, W. J. & Innis, G. S. (1985), 'Plant growth and production of grassland ecosystems: a comparison of modelling approaches', *Ecological Modelling* **29**, 131–144.

Harmens, H. & Mills, G. (2012), Ozone Pollution: Impacts on carbon sequestration in Europe, Technical report, Centre for Ecology and Hydrology, Wales.

Heyburn, J., McKenzie, P., Crawley, M. J. et al. (2017), 'Effects of grassland management on plant C:N:P stoichiometry: Implications for soil element cycling and storage', *Ecosphere* **8**(10).

Hoffmann, U., Hoffmann, T., Jurasinski, G. et al. (2014), 'Assessing the spatial variability of soil organic carbon stocks in an alpine setting (Grindelwald, Swiss Alps)', *Geoderma* **232-234**, 270–283.

Hofmann, M., Jurisch, N., Garcia Alba, J. et al. (2016), 'Detecting small-scale spatial heterogeneity and temporal dynamics of soil organic carbon', *Biogeosciences* **14**, 1003–1019.

Hörtnagl, L., Barthel, M., Buchmann, N. et al. (2018), 'Greenhouse gas fluxes over managed grasslands in Central Europe', *Global Change Biology* **24**(5), 1843–1872.

Hussain, M. Z., Grünwald, T., Tenhunen, J. D. et al. (2011), 'Summer drought influence on CO_2 and water fluxes of extensively managed grassland in Germany', *Agriculture, Ecosystems and Environment* **141**(1-2), 67–76.

Lal, R. (2004), 'Soil carbon sequestration impacts on global climate change and food security', *Science* **304**(5677), 1623–1627.

Lal, R. (2008), 'Sequestration of atmospheric CO_2 in global carbon pools', *Energy and Environmental Science* **1**(1), 86–100.

Lal, R., Negassa, W. & Lorenz, K. (2015), 'Carbon sequestration in soil', *Current Opinion in Environmental Sustainability* **15**, 79–86.

Lei, T., Feng, J., Zheng, C. et al. (2020), 'Review of drought impacts on carbon cycling in grassland ecosystems', *Frontiers of Earth Science* **14**(2), 462–478.

Lloyd, J. & Taylor, J. A. (1994), 'On the Temperature Dependence of Soil Respiration', *Functional Ecology* **8**(3), 315–323.

Lorenz, K. & Lal, R. (2021), 'The depth distribution of soil organic carbon in relation to land use and management and the potential of carbon sequestration in subsoil horizons', *Advaneces in Agronomy* **88**, 35–66.

Mcmaster, G. S. & Wilhelm, W. W. (1997), 'Growing degree-days: one equation, two interpretations', *Agricultural and Forest Meteorology* **87**(4), 291–300.

Merbold, L., Rogiers, N. & Eugster, W. (2012), 'Winter CO_2 fluxes in a sub-alpine grassland in relation to snow cover, radiation and temperature', *Biogeochemistry* **111**(1-3), 287–302.

Merbold, L., Steinlin, C. & Hagedorn, F. (2013), 'Winter greenhouse gas fluxes (CO_2, CH_4 and N_2O) from a subalpine grassland', *Biogeosciences* **10**(5), 3185–3203.

Mesterházy, I., Mészáros, R., Pongrácz, R. et al. (2018), 'The analysis of climatic indicators using different growing season calculation methods – An application to grapevine grown in Hungary', *Idojaras* **122**(3), 217–235.

Moll-Mielewczik, J., Keel, S. G. & Gubler, A. (2023), 'Organic carbon contents of mineral grassland soils in Switzerland over the last 30 years', *Agriculture, Ecosystems and Environment* **342**.

Nelson, D. W. & Sommers, L. E. (1996), Total Carbon, Organic Carbon, and Organic Matter, *in* D. Sparks, A. Page, P. Helmke et al., eds, 'Methods of Soil Analysis: Part 3 Chemical Methods', Soil Science Society of America and American Society of Agronomy, Madison, chapter 34.

Paustian, K., Lehmann, J., Ogle, S. et al. (2016), ''Climate-smart' soils: a new management paradigm for global agriculture', *Nature* **532**(7597), 49–47.

Pendall, E., Bachelet, D., Conant, R. T. et al. (2018), Chapter 10: Grasslands, Technical report, U.S. Global Change Research Program, Washington, DC.

Peng, Q., Dong, Y., Qi, Y. et al. (2011), 'Effects of nitrogen fertilization on soil respiration in temperate grassland in Inner Mongolia, China', *Environmental Earth Sciences* **62**(6), 1163–1171.

Poeplau, C. (2021), 'Grassland soil organic carbon stocks along management intensity and warming gradients', *Grass and Forage Science* **76**(2), 186–195.

Poeplau, C., Bolinder, M. A., Kirchmann, H. et al. (2016), 'Phosphorus fertilisation under nitrogen limitation can deplete soil carbon stocks: Evidence from Swedish meta-replicated long-term field experiments', *Biogeosciences* **13**(4), 1119–1127.

Poeplau, C., Vos, C. & Don, A. (2017), 'Soil organic carbon stocks are systematically overestimated by misuse of the parameters bulk density and rock fragment content', *SOIL* **3**(1), 61–66.

Poeplau, C., Zopf, D., Greiner, B. et al. (2018), 'Why does mineral fertilization increase soil carbon stocks in temperate grasslands?', *Agriculture, Ecosystems and Environment* **265**, 144–155.

Puche, N. J., Kirschbaum, M. U., Viovy, N. et al. (2023), 'Potential impacts of climate change on the productivity and soil carbon stocks of managed grasslands', *PloS one* **18**(4).

Qi, A., Holland, R. A., Taylor, G. et al. (2018), 'Grassland futures in Great Britain – Productivity assessment and scenarios for land use change opportunities', *Science of the Total Environment* **634**, 1108–1118.

R Core Team (2023), *R: A Language and Environment for Statistical Computing*, R Foundation for Statistical Computing, Vienna, Austria.
URL: *https://www.R-project.org/*

Reichstein, M., Falge, E., Baldocchi, D. et al. (2004), 'On the separation of net ecosystem exchange into assimilation and ecosystem respiration: review and improved algorithm', *Global Change Biology* **11**(9), 1424–1439.

Reichstein, M., Rey, A., Freibauer, A. et al. (2003), 'Modeling temporal and large-scale spatial variability of soil respiration from soil water availability, temperature and vegetation productivity indices', *Global Biogeochemical Cycles* **17**(4).

Rogger, J., Hörtnagl, L., Buchmann, N. et al. (2022), 'Carbon dioxide fluxes of a mountain grassland: Drivers, anomalies and annual budgets', *Agricultural and Forest Meteorology* **314**.

Romano, G., Schaumberger, A., Piepho H.P. et al. (2014), 'Optimal base tempearture for computing growing degree-day sums to predict forage quality of mountain permanent meadow in South Tyrol', *Grassland Science in Europe* **19**, 655–657.

Rumpel, C., Amiraslani, F., Chenu, C. et al. (2020), 'The 4p1000 initiative: Opportunities, limitations and challenges for implementing soil organic carbon sequestration as a sustainable development strategy', *Ambio* **49**(1), 350–360.

Rumpel, C. & Kögel-Knabner, I. (2011), 'Deep soil organic matter-a key but poorly understood component of terrestrial C cycle', *Plant and Soil* **338**(1), 143–158.

Samuil, C., Stavarache, M., Sîrbu, C. et al. (2018), 'Influence of Sustainable Fertilization on Yield and Quality Food of Mountain Grassland', *Not Bot Horti Agrobo* **46**(2), 410–417.

Sanderman, J., Creamer, C., Baisden, W. T. et al. (2017), 'Greater soil carbon stocks and faster turnover rates with increasing agricultural productivity', *SOIL* **3**(1), 1–16.

Schmid, S. (2017), Impacts of Climate Change on Alpine Grassland Ecosystems: Responses in Structure and Function, PhD thesis, ETH Zürich, Zürich.

Schmitt, M., Bahn, M., Wohlfahrt, G. et al. (2010), 'Land use affects the net ecosystem CO_2 exchange and its components in mountain grasslands', *Biogeosciences* **7**(8), 2297–2309.

Scholz, K., Hammerle, A., Hiltbrunner, E. et al. (2018), 'Analyzing the Effects of Growing Season Length on the Net Ecosystem Production of an Alpine Grassland Using Model–Data Fusion', *Ecosystems* **21**(5), 982–999.

Schuchardt, M. A., Berauer, B. J., von Heßberg, A. et al. (2021), 'Drought effects on montane grasslands nullify benefits of advanced flowering phenology due to warming', *Ecosphere* **12**(7).

Seeber, J., Tasser, E., Rubatscher, D. et al. (2022), 'Effects of land use and climate on carbon and nitrogen pool partitioning in European mountain grasslands', *Science of the Total Environment* **822**.

Skinner, R. H. & Adler, P. R. (2010), 'Carbon dioxide and water fluxes from switchgrass managed for bioenergy production', *Agriculture, Ecosystems and Environment* **138**(3-4), 257–264.

Sochorová, L., Jansa, J., Hejcman, M. et al. (2016), 'Long-term agricultural management maximizing hay production can significantly reduce belowground C storage', *Agriculture, Ecosystems & Environment* **220**, 104–114.

Soussana, J. F., Allard, V., Pilegaard, K. et al. (2007), 'Full accounting of the greenhouse gas (CO_2, N_2O, CH_4) budget of nine European grassland sites', *Agriculture, Ecosystems and Environment* **121**(1-2), 121–134.

Sun, Y., Wang, C., Chen, H. Y. et al. (2022), 'A global meta-analysis on the responses of C and N concentrations to warming in terrestrial ecosystems', *Catena* **208**.

Sweeney, D. W., Farney, J. K. & Moyer, J. L. (2019), 'Nitrogen Fertilizer Timing and Phosphorus and Potassium Fertilization Rates for Established Endophyte-Free Tall Fescue', *Kansas Agricultural Experiment Station Research Reports* **5**(2).

Trumbore, S. (2000), 'Age of soil organic matter and soil respiration: radiocarbon constraints on belowground C dynamics', *Ecological Applications* **10**(2), 399–411.

Turner, B. L. (2021), 'Soil as an archetype of complexity: A systems approach to improve insights, learning, and management of coupled biogeochemical processes and environmental externalities', *Soil Systems* **5**(3).

Volk, M., Obrist, D., Novak, K. et al. (2011), 'Subalpine grassland carbon dioxide fluxes indicate substantial carbon losses under increased nitrogen deposition, but not at elevated ozone concentration', *Global Change Biology* **17**(1), 366–376.

Volk, M., Suter, M., Wahl, A. L. et al. (2021), 'Subalpine grassland productivity increased with warmer and drier conditions, but not with higher N deposition, in an altitudinal transplantation experiment', *Biogeosciences* **18**(6), 2075–2090.

Ward, D., Kirkman, K., Hagenah, N. et al. (2017), 'Soil respiration declines with increasing nitrogen fertiliza-

tion and is not related to productivity in long-term grassland experiments', *Soil Biology and Biochemistry* **115**, 415–422.

Ward, S. E., Smart, S. M., Quirk, H. et al. (2016), 'Legacy effects of grassland management on soil carbon to depth', *Global change biology* **22**(8), 2929–2938.

Wiesmeier, M., Hübner, R., Barthold, F. et al. (2013), 'Amount, distribution and driving factors of soil organic carbon and nitrogen in cropland and grassland soils of southeast Germany (Bavaria)', *Agriculture, Ecosystems and Environment* **176**, 39–52.

Wiesmeier, M., Poeplau, C., Sierra, C. A. et al. (2016), 'Projected loss of soil organic carbon in temperate agricultural soils in the 21 st century: Effects of climate change and carbon input trends', *Scientific Reports* **6**.

Wiesmeier, M., Urbanski, L., Hobley, E. et al. (2018), 'Soil organic carbon storage as a key function of soils-A review of drivers and indicators at various scales', *Geoderma* **333**, 149–162.

Wilts, A. R., Reicosky, D. C., Allmaras, R. R. et al. (2004), 'Long-Term Corn Residue Effects: Harvest Alternatives, Soil Carbon Turnover, and Root-Derived Carbon', *Soil Science Society of America Journal* **68**, 1342–1351.

Wohlfahrt, G., Bahn, M., Haslwanter, A. et al. (2005), 'Estimation of daytime ecosystem respiration to determine gross primary production of a mountain meadow', *Agricultural and Forest Meteorology* **130**(1-2), 13–25.

Wohlfahrt, G., Hammerle, A., Haslwanter, A. et al. (2008), 'Seasonal and inter-annual variability of the net ecosystem CO_2 exchange of a temperate mountain grassland: Effects of weather and management', *Journal of Geophysical Research Atmospheres* **113**(8).

Wu, G. L., Cheng, Z., Alatalo, J. M. et al. (2021), 'Climate Warming Consistently Reduces Grassland Ecosystem Productivity', *Earth's Future* **9**(6).

Zhai, Z. W., Gong, J. R., Luo, Q. P. et al. (2017), 'Effects of nitrogen addition on photosynthetic characteristics of Leymus chinensis in the temperate grassland of Nei Mongol, China', *Chinese Journal of Plant Ecology* **41**(2), 196–208.

Zhang, K., Greenwood, D. J., White, P. J. et al. (2007), 'A dynamic model for the combined effects of N, P and K fertilizers on yield and mineral composition; Description and experimental test', *Plant and Soil* **298**(1-2), 81–98.

Acknowledgments

While working on this thesis, I received a lot of help and collected many great memories. First and foremost, I would like to thank my amazing supervisor, Matthias Volk (Climate and Agriculture, Agroscope Zurich), who supported me throughout the project with his knowledge and experience and patiently gave helpful advice. His encouragement and belief in my abilities cannot be overstated. Furthermore, I would like to thank my faculty member Prof. Michael Schmidt (Soil science and Biogeochemistry, University of Zurich) for the valuable expertise imparted to me during my studies. I would also like to thank Robin Giger (Climate and Agriculture, Agroscope Zurich) for his invaluable help with the field work, his musical accompaniment and for driving the van during the night while I could not avoid falling asleep. Further, I would like to thank the lab staff of Agroscope (Zurich) for their availability, explanations and technical support, especially Martin Zuber (Environmental analysis), Diane Bürge (Environmental chemistry), Patricia Peier (Environmental chemistry) and Steven Kaufmann (Environmental analysis). Thanks also to the entire Climate and Agriculture group, especially Pierluigi Calanca, Cyrill Zosso, Marcio Dos Reis Martins and Christoph Ammann, for their valuable suggestions and interesting exchanges. Special thanks to Juliane Hirte and Hans-Ulrich Zbinden and their group (Water protection and substance flows, Agroscope Zurich) for providing essential data for my research and for sharing the archived soil samples. Thanks also to the MeteoSwiss staff for interpolating the weather data for Muldain and thanks to Alexandra and Mirco Städler (Städler's Organic Farm, Voa Dal, Muldain) for letting us use part of the grassland of their organic farm for this research. Furthermore, I would like to thank Juliane Hirte, Annina Cincera (Institute of Mathematics, University of Zurich) and Rocco Bagutti (Department of Geography, University of Zurich) for their precious support with statistics and programming in R. Special thanks go to Larry Hackett, my former English teacher in Ireland, and Nadja Hertel for proofreading my work. Last but not least, I would like to thank from the bottom of my heart my supporting family, my loving boyfriend and my funny friends for believing in me and for cheerful distractions.

Appendix

.1 Theoretical base

.1.1 Carbon cycling

What is a greenhouse gas?

Methane (CH_4) and carbon dioxide (CO_2) are examples of GHG, which are substances in the atmosphere that absorb heat radiation reflected from the earth's surface. The climate warms if organisms produce more CO_2 and CH_4 than they consume, while the climate cools if the opposite occurs (Davidson & Janssens 2006, Grotzinger & Jordan 2017).

What is a biogeochemical cycle?

The movement of a chemical element or compound through the biological and environmental elements of an ecosystem is referred to as a biogeochemical cycle. The biosphere contributes to biochemical cycles through the respiration process, the intake of nutrients from the hydrosphere and lithosphere, and the release of these nutrients following the death and decomposition of organisms (Grotzinger & Jordan 2017).

Where is carbon stored?

The four main reservoirs for the carbon cycle are the atmosphere, the Earth's oceans including their organisms, the land surface including all land plants and soils (biosphere), and the deeper lithosphere (Grotzinger & Jordan 2017). These pools are linked together by the carbon flow between them, which is significantly impacted by human disturbances (Lal 2008).

Which are the ways for gas exchange?

The carbon cycle can be divided in four sub-processes (Grotzinger & Jordan 2017):

- The exchange of gases between the atmosphere and the ocean's surface;
- The transportation of carbon dioxide from the biosphere to the atmosphere via photosynthesis, respiration, and direct oxidation;
- The movement of dissolved organic carbon from surface waters to the oceans;
- The weathering and precipitation of calcium carbonate.

Gas exchange atmosphere-biosphere

The photosynthetic abilities of plants in terrestrial ecosystems are primarily responsible for the conversion of carbon into organic binding forms. The degradation of all organic materials is carried out by soil organisms. The exchange of CO_2 between the terrestrial biosphere and the atmosphere during photosynthesis, respiration, and decomposition results in this sub-cycle, which has the biggest flux of carbon material. About half of the CO_2 that plants absorb during photosynthesis is released back into the atmosphere during respiration. The

remaining half is integrated as OC into the tissues of the plant, including its leaves, wood, roots, and seeds. Animals consume plants, and microorganisms regulate their decomposition. Both procedures cause the plant tissue to oxidise, thus releasing CO_2. The soils store the majority of the organic carbon produced during this process. Another portion is directly oxidised by forest fires and other combustion processes, entering the atmosphere. A little amount of the CO_2 that is taken up by plant tissue is dissolved in surface waters and transported by rivers to the oceans, where it is is returned to the atmosphere through respiration of marine organisms, before being taken up again by plants during photosynthesis (Davidson & Janssens 2006, FAO 2010, Grotzinger & Jordan 2017).

What does carbon sequestration mean?

Carbon sequestration refers to the process of transferring atmospheric CO_2 into long-lasting pools and safely storing it to prevent immediate re-emission. Carbon sequestration occurs through several processes, which are based in the chemical, geologic, oceanic and terrestrial systems. The natural process of photosynthesis, by transferring atmospheric CO_2 into plant biomass, serves as the foundation for carbon sequestration in terrestrial ecosystems. The potential to offset a sizeable portion of current GHG emissions may lie in the sequestration of carbon as soil organic matter through changes in land use and better land management. Carbon sequestration is thus understood as being a way of mitigating the increasing atmospheric CO_2 concentrations (Lal 2004, 2008, Paustian et al. 2016, Sanderman et al. 2017).

.2 Some methodology in more details

.2.1 Calcimeter and soil mineral carbon

Figure 24: Analysis of historical soil samples (2006-2021) for C_{min} with the calcimeter.

The measurement procedure used to determine the C_{min} concentration of soil samples is explained in more detail in the following steps:

1. Sample preparation: The archived samples were already prepared for this analysis by drying them at 40°C and sieving them to 2mm. No further preparation was needed.

2. pH estimation: To determine how much soil material should be weighed in for the analysis, the pH was estimated by pouring a few drops of hydrogen chloride on a small amount of soil. The smaller the reaction of the soil with the acid, the larger the required weight of the soil sample. This step was repeated for every soil sample.

3. Operating the measuring device: The required amount of soil or calcium carbonate was weighed into an Erlenmeyer flask and 20mL of water were added. A small tube was filled with 5mL hydrochloric acid and placed in the Erlenmeyer. The Erlenmeyer was tightly sealed with the rubber stopper on the calcimeter. The liquid level in the columns was adjusted to zero by moving the adjustment vessel. The magnetic stirrer was switched on. Then the Erlenmeyer was kipped carefully so that the acid would run out of the tube. The resulting carbon dioxide pushed the liquid level down. After 20 minutes, the liquid level, which corresponds to the amount of carbon dioxide in mL, was read off (Figure 24).

4. Running in the measuring device: Before each measuring series (every day), all columns of the device must be run in with a calcareous sample so that the water/gas interface is saturated. For this purpose, 0.3g $CaCO_3$ were weighed into 5 Erlenmeyer flasks and weighed out as described under point 3.

5. Calibration of the measuring device: The calibration was done with pure water and calcium carbonate. A blank value was first measured on each column. For this purpose, the water and the acid were added to the Erlenmeyer flasks and measured as described in point 3. Then calcium carbonate samples were used as standards. First 0.15g calcium carbonate was measured on all columns and then 0.3g.

6. Measurement of control samples for quality assurance: In each measurement series, a control soil with a known lime content was measured on each column after calibration.

7. Measuring the lime content in soil samples: The estimated amount of soil (point 2) was weighed into the Erlenmeyer flask and the measurement was carried out as described in point 3.

8. Calculation of $CaCO_3$ concentrations: For the evaluation of the measured volume levels, the calculation was done according to the ISO method 10693 (7).

$$\mathrm{CaCO_3}[\%] = 100 * \frac{m_S * (V_P - V_B)}{m_P * (V_S - V_B)} \tag{7}$$

where:

m_S = Average weight of the standards used

V_S = Average volume of the standards used

V_B = Average volume of the blank samples

m_P = Weight of the sample to be analysed

V_P = Volume of the sample to be analysed

9. Calculation of mineral carbon concentration (%-mass): Based on the molecular mass of $CaCO_3$ (100.0869 g/mol) and the molar mass of carbon (12.0107 g/mol), the mineral carbon concentration was derived from the calcium carbonate values: 12% of $CaCO_3$ mass consists in carbon.

.2.2 SOC stocks calculation

The following steps illustrate in more detail how the SOC stocks were calculated, according to Garcia-Pausas et al. (2007), Poeplau et al. (2017) and (Eze et al. 2018):

1. SOC (%, 2022) = C_{tot} - C_{min} for every sample (24 field parcels, North and South replicates, depths 0-10, 10-20 and rest).

2. Determination of the fine soil mass, by subtracting coarse fragments (roots and mineral parts > 2 mm) from the total soil mass.

3. Conversion of the dry soil mass from gr to kg.

4. Calculation of the sample volume by multiplying the area of the coring device (r=5cm, $r^2 * \pi$) with the sample depth. Volume conversion from cm^{-3} to m^{-3}.

5. Calculation of the soil bulk density ($kg\,m^{-3}$) by dividing the fine soil sample mass with its volume. For the samples collected in 2022 specific soil density was used for every single sample. For the historical samples, a mean value of 8.84 $kg\,L^{-1}$ was used.

6. Calculation of the soil mass for the given depth under $1m^{-2}$.

7. For every depth range and parcel, the SOC stocks ($kg\,m^{-2}$) were calculated by multiplying the soil mass (under $1m^{-2}$) with the SOC concentration.

8. Sum of the SOC stocks of the two depths (0-10 and 10-20cm), to obtain SOC stocks for the first 20cm soil depth.

9. Average of the soil density between depths 0-10 and 10-20cm. The calculation was repeated for the soil samples of every year (1989-2021), by applying the mean soil density (0-20cm) calculated in 2022. As the grassland is extensively managed, a constant soil density over time was assumed.

.3 Additional figures

.3.1 Soil sampling in 2022

Figure 25: Soil sampling (01.11.2022), with Robin Giger in the picture, using sampling tubes to collect probes with a defined volume.

.3.2 Yield over time for different productivity

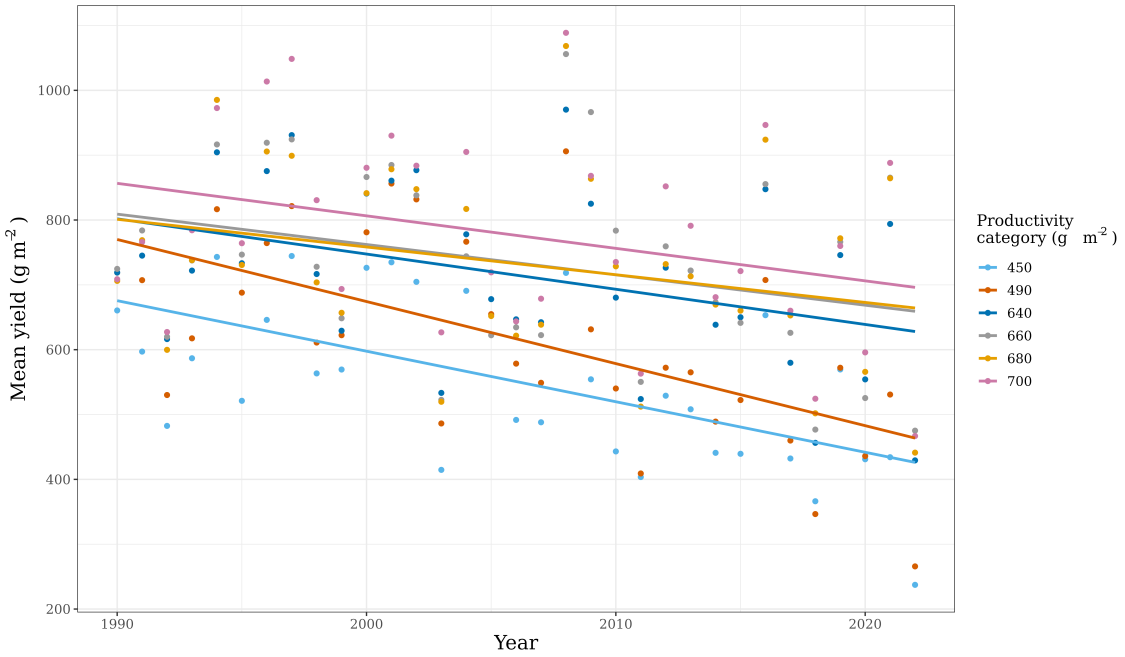

Figure 26: Yield (g m^{-2}) over time (1990-2022) for the six productivity categories. The dots represent the mean annual yield (n=4) of the respective productivity category to which a different colour is assigned. The lines are the fitted simple linear regression models, which are only significant for the three lowest productivity categories.

.3.3 SOC stocks over time for different productivity

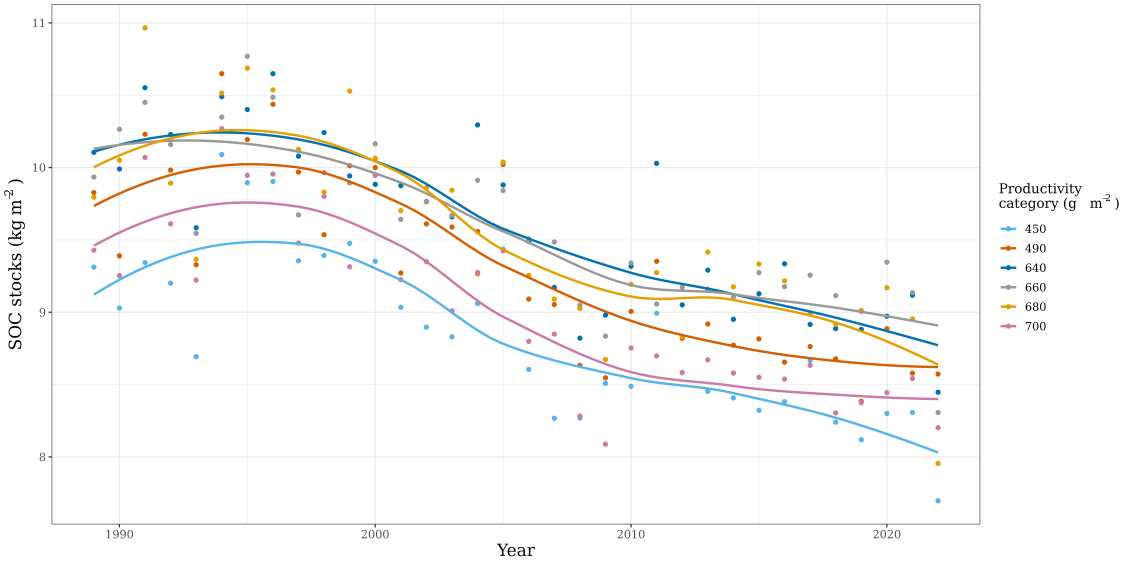

Figure 27: SOC stocks (kg m^{-2}) over time (1990-2022) for the six productivity categories. The dots represent the mean annual yield (n=4) of the respective productivity category to which a different colour is assigned. The lines are the fitted loess curves, which show a significant non-parametric decreasing trend for all productivity categories.

.3.4 Productivity and SOC stocks

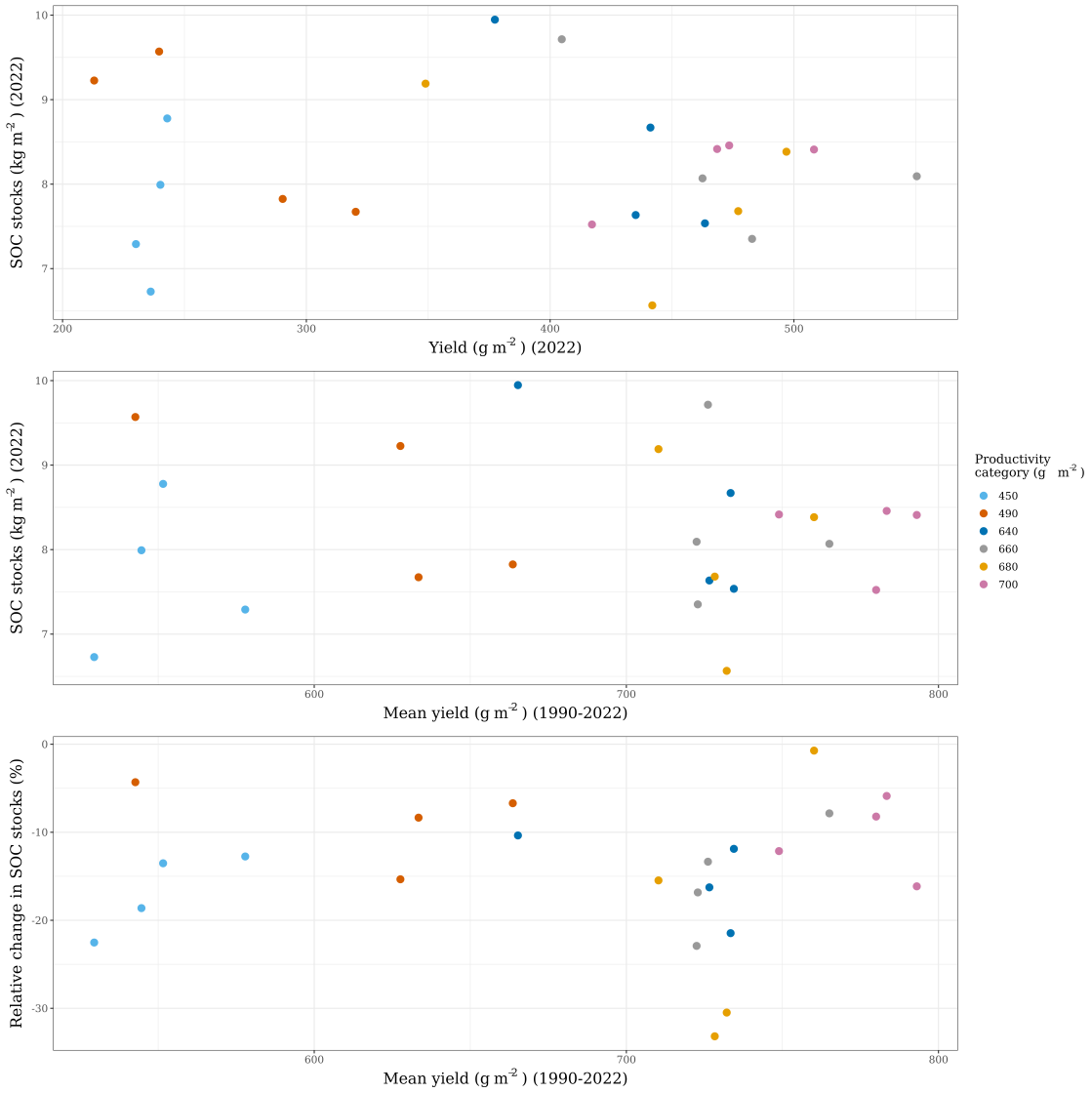

Figure 28: No relationship between productivity and SOC stocks. Each graph comprises 24 dots, each representing the mean SOC stocks and yields for the periods indicated. The colours indicate the productivity categories.

.3.5 SOC stocks and yield over time with weather parameters

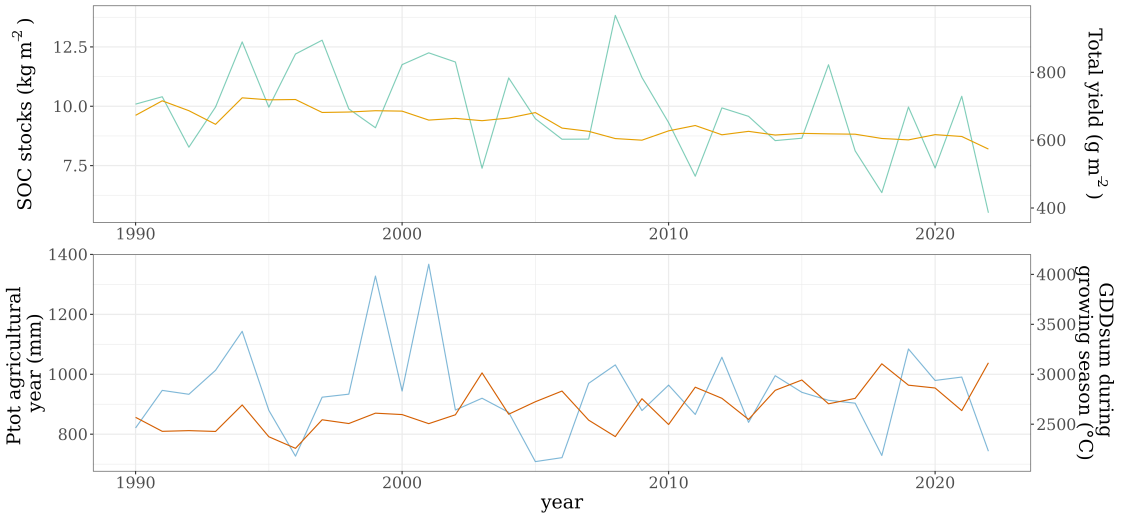

Figure 29: Mean annual SOC stocks and yield over time (n=24, 1990-2022) together with temperature and precipitation based parameters. For the mean SOC stocks, no correlation with either yield or weather is apparent.

.3.6 No relationship between final SOC stocks (2022) and GPP_{pot}/ER_{10}

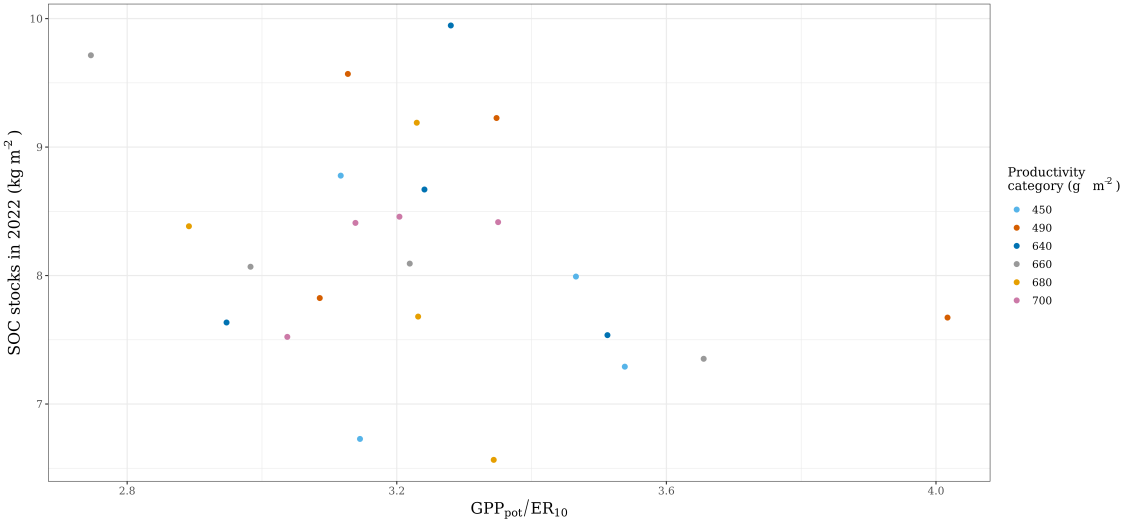

Figure 30: No relationship between GPP_{pot} / ER_{10} and final SOC stocks (2022). Every point represents the SOC stocks in 2022 and the mean (averaged over the measuring campaigns) ratio GPP_{pot}/ER_{10} for the corresponding field parcel. The dots colour corresponds to the productivity categories.

.4 Additional tables

.4.1 Weather in Valbella from January 2022 to June 2023

Table 7: Monthly minimum, maximum and mean temperature, P_{tot} and mean RelS in Valbella (January 2022 - June 2023).

Month	T_{min} (°C)	T_{max} (°C)	T_{mean} (°C)	P_{tot} (mm)	$RelS_{mean}$ (%)
January 2022	-6	1.3	-2.5	21.7	48
February	-6.5	1.9	-2.2	42.3	50
March	-3.6	5.2	0.8	1.9	72
April	-1.6	7.2	2.8	30.6	58
May	5.2	13.6	9.4	61.4	45
June	8.2	18.5	13.3	137.4	58
July	9.8	19.2	14.5	79.7	69
August	9.4	18	13.9	60.6	71
September	4.3	11.5	7.9	95.8	46
October	5.5	14	9.4	93	55
November	-1.2	5.4	2	29.5	41
December	-4.8	1.7	-1.5	31.4	38
January 2023	-6.5	-0.3	-3.6	5.3	35
February	-4.8	2.4	-1.3	10.5	60
March	-3.1	5.1	0.7	43.2	48
April	-1.7	5	1.4	70.5	36
May	3.9	11.3	7.5	93.9	38
June	8.2	17.6	13.2	19.5	59

.4.2 Mean yield and SOC stocks over time

Table 8: Mean (±SE) annual yield and SOC stocks (n=24) over time (1990-2022).

Year	Mean yield ($g\,m^{-2}$)	Mean SOC stocks ($kg\,m^{-2}$)
1990	706 ±19	9.66 ±0.27
1991	728 ±21	10.27 ±0.26
1992	579 ±19	9.85 ±0.23
1993	698 ±17	9.29 ±0.27
1994	890 ±19	10.39 ±0.23
1995	697 ±19	10.32 ±0.24
1996	854 ±27	10.33 ±0.24
1997	895 ±24	9.78 ±0.25
1998	692 ±21	9.79 ±0.24
1999	637 ±10	9.86 ±0.27
2000	823 ±14	9.90 ±0.23
2001	858 ±17	9.46 ±0.23
2002	830 ±18	9.54 ±0.25
2003	517 ±17	9.43 ±0.25
2004	784 ±17	9.56 ±0.32
2005	663 ±12	9.77 ±0.24
2006	603 ±13	9.12 ±0.23
2007	603 ±16	8.99 ±0.24
2008	968 ±32	8.68 ±0.25
2009	785 ±32	8.61 ±0.22
2010	652 ±28	9.02 ±0.28
2011	494 ±16	9.23 ±0.26
2012	695 ±28	8.84 ±0.24
2013	670 ±23	8.99 ±0.24
2014	599 ±23	8.83 ±0.23
2015	606 ±23	8.90 ±0.25
2016	822 ±25	8.88 ±0.25
2017	568 ±23	8.87 ±0.23
2018	445 ±17	8.69 ±0.24
2019	698 ±22	8.63 ±0.22
2020	518 ±16	8.85 ±0.26
2021	729 ±42	8.77 ±0.23
2022	386 ±22	8.20 ±0.18

.4.3 Pearson correlations

Table 9: Weather parameters over time. Reported are the coefficients of the Pearson correlation test and the tau-statistics of the Mann-Kendall test. Stars represent the significance of the tests.

Weather parameter	Year	
	Pearson correlation coefficient	Mann Kendall (tau statistics)
MAT (°C)	0.639***	0.447***
T_{mean} agricultural year (log) (°C)	0.638***	0.455***
GSL (Days)	0.250	0.159
GDD_{sum} during GS (°C)	0.669***	0.489***
T_{mean} during GS (°C)	0.525**	0.383**
GDD_{sum} in January (°C)	-0.074	-0.011
GDD_{sum} in February (log) (°C)	-0.186	-0.086
GDD_{sum} in March (°C)	0.075	0.057
GDD_{sum} in April (log) (°C)	0.558***	0.413***
GDD_{sum} in May (°C)	0.030	0.019
GDD_{sum} in June (°C)	0.558***	0.455***
GDD_{sum} in July (°C)	0.352*	0.239
GDD_{sum} in August (°C)	0.137	0.148
GDD_{sum} in September (°C)	0.299	0.201
GDD_{sum} in October (°C)	0.322	0.246*
GDD_{sum} in November (°C)	0.429*	0.282*
GDD_{sum} in December (°C)	0.366*	0.248*
RelS in during GS (%)	0.421*	0.269*
RelS agricultural year (%)	0.189	0.106

Continued on next page.

Table 10: Weather parameters over time: Pearson correlation test and Mann Kendall test (Continued).

Weather parameter	Year	
	Pearson correlation test	Mann Kendall (tau statistics)
P_{tot} during GS (mm)	-0.101	-0.057
P_{tot} agricultural year (log) (mm)	-0.115	-0.023
P_{tot} in January (log) (mm)	0.372*	0.242*
P_{tot} in February (log) (mm)	-0.132	-0.063
P_{tot} in March (log) (mm)	-0.151	-0.057
P_{tot} in April (mm)	-0.178	-0.159
P_{tot} in May (log) (mm)	0.155	0.064
P_{tot} in June (log) (mm)	-0.138	-0.076
P_{tot} in July (mm)	-0.189	-0.135
P_{tot} in August (mm)	0.117	0.059
P_{tot} in September (log) (mm)	-0.078	-0.038
P_{tot} in October (mm)	0.041	0.049
P_{tot} in November (log) (mm)	-0.230	-0.121
P_{tot} in December (mm)	0.031	0.053
P_{tot} in May, June and July (mm)	-0.163	-0.102
IDM during GS	-0.177	-0.087
IDM agricultural year (log)	-0.271	-0.197

Table 11: Pearson correlation test of weather parameters with mean annual yield and SOC stocks (n=24), respectively. The resulting Pearson correlation coefficients are reported with the significance of the test.

Weather parameter	Pearson correlation coefficient		
	Yield ($g\,m^{-2}$)	SOC stocks ($kg\,m^{-2}$)	SOC annual change (%)
MAT (°C)	-0.517**	-0.580***	-0.145
T_{mean} agricultural year (log) (°C)	-0.467**	-0.597***	-0.131
GSL (Days)	-0.143	-0.168	0.120
GDD_{sum} during GS (°C)	-0.656***	-0.589***	-0.070
T_{mean} during GS (°C)	-0.583***	-0.532**	-0.244
GDD_{sum} in January (°C)	-	-0.027	-0.167
GDD_{sum} in February (log) (°C)	-	0.150	0.436
GDD_{sum} in March (°C)	-0.116	-0.029	0.199
GDD_{sum} in April (log) (°C)	-0.554***	-0.493**	-0.017
GDD_{sum} in May (°C)	-0.264	-0.200	-0.403*
GDD_{sum} in June (°C)	-0.310	-0.490**	-0.141
GDD_{sum} in July (°C)	-0.396*	-0.250	0.152
GDD_{sum} in August (°C)	-0.281	-0.177	0.000
GDD_{sum} in September (°C)	-0.265	-0.214	0.070
GDD_{sum} in October (°C)	-0.137	-0.262	-0.239
RelS during GS (%)	-0.523**	-0.404*	-0.094
RelS agricultural year (%)	-0.345*	-0.311	-0.247
P_{tot} during GS (mm)	0.322	0.075	0.035
P_{tot} agricultural year (log) (mm)	0.320	0.068	0.107
P_{tot} in January (log) (mm)	-0.141	-0.255	0.086
P_{tot} in February (log) (mm)	-0.024	0.040	-0.123
P_{tot} in March (log) (mm)	0.401*	0.140	0.016
P_{tot} in April (mm)	0.414*	0.038	-0.261
P_{tot} in May (log) (mm)	0.105	-0.020	0.311
P_{tot} in June (log) (mm)	0.148	0.026	-0.106
P_{tot} in July (mm)	0.448**	0.096	-0.261
P_{tot} in August (mm)	0.072	0.000	0.087
P_{tot} in September (log) (mm)	-0.097	0.097	0.266
P_{tot} in October (mm)	-0.260	-0.199	-0.268
P_{tot} in May, June and July (mm)	0.465**	0.095	-0.084
IDM during GS	0.379*	0.151	0.060
IDM agricultural year (log)	0.427*	0.215	0.135

.4.4 Yield over time in relation to productivity categories and weather

Table 12: Statistics results of mean yield over time for the six productivity categories. The results of the simple linear regression model and the Mann-Kendall test are reported. The two-tailed T-test compared the mean yield between the first and the second half of the period under study (1990-2005 and 2006-2022).

Statistical test	Simple linear regression model			Mann Kendall test		Two tailed t-test
Productivity category	Slope	R^2_{adj}	p-value	tau statistics	p-value	p-value
450	- 8*year	0.327	<0.0005	-0.439	< 0.0005	< 0.0005
490	- 10*year	0.347	<0.0005	-0.428	< 0.0005	< 0.0005
640	- 5*year	0.125	<0.05	-0.242	< 0.05	< 0.05
660	- 5*year	0.066	<0.1	-0.205	< 0.1	> 0.1
680	- 4*year	0.050	>0.1	-0.205	< 0.1	> 0.1
700	- 5*year	0.073	<0.1	-0.201	> 0.1	< 0.1

Table 13: Simple linear regression models to explain yield variations with weather. The table presents the results of the linear regression analysis between selected weather parameters and the mean annual yield (n=24).

Explanatory variable	Regression coefficients from simple linear regression models				
	F	df	Estimate	p-value	R^2_{adj}
GDD_{sum} during GS (°C)	23.36	31	-0.42074	3.46e-05	0.4114
T_{mean} during GS (°C)	15.93	31	-106.92	0.000374	0.3182
GDD_{sum} in April (°C)	13.01	31	-1.4061	0.00107	0.273
GDD_{sum} in July (°C)	5.757	31	-1.0900	0.0226	0.1294
P_{tot} May-July (mm)	8.547	31	0.9377	0.006414	0.1908
IDM during GS	5.205	31	7.978	0.029543	0.1161
LGS (Days)	0.6447	31	-1.164	0.42813	-0.01123

.4.5 Correlation between SOC stocks and carbon fluxes

Table 14: Pearson correlation test between SOC stocks ($kg\,m^{-2}$) and CO_2 fluxes (µmol CO_2 $m^{-2}\,s^{-1}$). The resulting Pearson correlation coefficients are reported; a significant negative correlation was only found between final SOC stocks and GPP_{pot}.

CO_2 fluxes	SOC stocks 2022	SOC relative change (%)
ER_{10}	0.22	0.07
GPP_{pot}	-0.44*	-0.28
GPP_{pot}/ER_{10}	-0.32	-0.14

.4.6 Plant carbon content lost through harvest

Grass cut during the three harvests in 2022 was analysed for carbon content. For each harvest, the amount of plant carbon content (g) for 1 kg of grass was determined. This amount was averaged to determine what percentage of the grass is made of carbon. The amount of plant carbon content lost to cutting was also summed between the three harvests, and scaled by the actual yield to obtain the net plant carbon content (g) lost in 2022. Table 15 reports the results of plant carbon content lost with harvest (in % and in g) for the 24 field parcels of interest.

Table 15: Plant carbon content lost through the three harvests in 2022 (25 May, 19 July, 22 September). Mean values (n=4) are reported for the six productivity categories.

Productivitycategory	Plant carboncontent lost (%)	Plant carboncontent lost (g)
450	47.161 ±0.018 ^{a}	111.926 ±1.301 ^{a}
490	46.617 ±0.257 ^{ab}	123.762 ±10.815 ^{a}
640	46.369 ±0.146 ^{b}	198.976 ±7.950 ^{b}
660	46.020 ±0.172 ^{b}	218.563 ±13.376 ^{b}
680	46.295 ±0.170 ^{b}	204.263 ±15.239 ^{b}
700	46.193 ±0.143 ^{b}	215.629 ±8.526 ^{b}

.5 R code

The following figures illustrate some selected R codes as an example of the analysis performed.

```
# Packages
```{r}
library(ggplot2)
library(lmtest)
library(dplyr)
library(Kendall)
library(gt)
library(gvlma)
library(readxl)
library(ggpubr)
library(tibble)
library(car)
library(tidyverse)
library(rstatix)
library(patchwork)
library(ggpmisc)
library(emmeans)
library(multcompView)
```
```

Figure 31: R code used to load the necessary packages.

```
# Data
```{r}
# Example: soil pH and clay content for the selected 24 field parcels (1989,
soil depth: 0-20cm)
data_pH_clay <- read_excel("data/1989_pH_clay.xlsx", sheet=2)
```


Summary statistics
```{r}
# Example for clay content of soil samples (1989)
summary(data_pH_clay$clay_percent) #min, max, mean, median

data_pH_clay %>% #mean and standard error (se)
  get_summary_stats(clay_percent, type = "mean_se")

# Example for GPPpot: average by grouping for variable(s) (in this case, for
DATE)
data_campaigns %>%
  group_by(date) %>%
  summarise_at(vars(GPPpot),
               list(GPPpot_mean = mean, GPPpot_se=se)) %>%
  as.data.frame()
```
```

Figure 32: R code used to read the data saved in .xlsx format.

```
# Pearson correlation
```{r}
# Example: correlation between yield and climatic variables

## 1. Check normal distribution of variables
data_climate_1990_2022 %>%
  shapiro_test(mean_yield, MAT_celsius, MAT_agricultural_year,
length_growing_season_days, GDD_sum_during_LGS, Tmean_during_LGS, GDDsum_March,
GDDsum_April, GDDsum_May, GDDsum_June, GDDsum_July, GDDsum_August,
GDDsum_September, GDDsum_October, RelS_mean_during_LGS,
RelS_mean_agricultural_year, Ptot_during_LGS, tot_P_agricultural_year,
Ptot_March, Ptot_April, Ptot_May, Ptot_June, Ptot_July, Ptot_August,
Ptot_September, Ptot_October, Ptot_May_June_July, IDM_mean_during_LGS,
IDM_agricultural_year)


## 2. Log transformation of variables that are not normally distributed
cols <- c("IDM_agricultural_year", "Ptot_June", "Ptot_March", "Ptot_May",
"Ptot_September", "tot_P_agricultural_year", "MAT_agricultural_year",
"GDDsum_April")

data_climate_1990_2022[cols] <- log(data_climate_1990_2022[cols])

## 3. Second normality check
data_climate_1990_2022 %>%
  shapiro_test(IDM_agricultural_year, Ptot_June, Ptot_March, Ptot_May,
Ptot_September, tot_P_agricultural_year, MAT_agricultural_year, GDDsum_April) #
Ptot_March is not normally distributed after log transformation!

## 4. Perform Pearson correlation test between yield and climatic variables
(separately)
cor.test(data_climate_1990_2022$mean_yield,
data_climate_1990_2022$tot_P_agricultural_year, method="pearson")
```
```

Figure 33: R code used to compute some summary statistics, such as average and standard error.

```
# Simple linear regression model
```{r}
# Example for linear relationship between mean yield and time

## 1. Perform simple linear regression model
model <- lm(mean~year, data = data_yield_mse_year)

## 2. Check assumptions of simple linear regression model
plot(data_yield_mse_year$year,data_yield_mse_year$mean) #linear relationship
cor(data_yield_mse_year$year, data_yield_mse_year$mean) #moderate negative
correlation between year and yield

par(mfrow=c(2,2))
plot(model) # diagnostic plots to analyze the residuals of the model
par(mfrow=c(1,1))

ggboxplot(data_yield_mse_year, y = "mean") #variance in data

ncvTest(model) # heteroscedasticity (Breusch-Pagan test)
shapiro.test(residuals(model)) # normality of model residuals

gvlma(model) ### general check of model assumptions

## 3. Results
summary(model)

tab_model(model, emph.p=TRUE,  dv.labels = "Yield over time", file =
paste("tables/", "Yield_over_time", ".html", sep="")) # save model results as
table

############################################################
```

Figure 34: R code used to check the assumptions of the simple linear regression model, perform the analysis and save the results as a table.

```
# For loop: example for linear relationship between mean yield and selected
climatic variables
## 1. Define list of variables for analysis in for loop
colnames(data_climate_1990_2022)

colnames <- list_("MAT_celsius_previous_year", "GDD_sum_during_LGS",
"GDDsum_March", "GDDsum_May", "GDDsum_July", "RelS_mean_during_LGS",
"Ptot_during_LGS",  "Ptot_May_June_July", "length_growing_season_days",
"GDDsum_June",  "GDDsum_August",  "tot_P_agricultural_year",
"IDM_calendar_year")

## 2. Check linear regression model assumptions
for (col_name in colnames) {
  cat("---", col_name, "---", "\n")
  model <- lm(mean_yield ~ get(col_name), data=data_climate_1990_2022)
  par(mfrow=c(2,2))
  plot(model)
  par(mfrow=c(1,1))
  print(gvlma(model))
}

## 3. Print linear regression model results
for (col_name in colnames) {
  cat("---", col_name, "---", "\n")
  model <- lm(mean_yield ~ get(col_name), data=data_climate_1990_2022)
  print(summary(model))
}

############################################################
```

Figure 35: R code used to run several simple linear regression model in for-loops, repeating the analysis for multiple variables. A first example.
```

```r
# For loop: example of linear trend over time in yield for all productivity
categories (separately)
# 1. Average and se annual yield between 4 replicates
data_yield_mse_year_yield <- data_yield_24 %>%
  group_by(year, productivity) %>%
  get_summary_stats(yield_tot_year_gm2, type = "mean_se") %>%
  as.data.frame()

# 2. Define list of productivity categories
productivity_groups <- list(450, 490, 640, 660, 680, 700)

# 3. Check linear model assumptions and run linear model for all productivity
categories
for (productiviti in productivity_groups) {
  cat("PRODUCTIVITY", productiviti, "\n")
  subset_yield <- filter(data_yield_mse_year_yield, productivity ==
productiviti)
  model_yield <- lm(mean~year, data = subset_yield)
  plot(model_yield)
  print(ncvTest(model_yield))
  print(shapiro.test(residuals(model_yield)))
  print(gvlma(model_yield))
  print(summary(model_yield))
}
```

Figure 36: R code used to run several simple linear regression model in for-loops, repeating the analysis for multiple variables. A second example.

```r
# Mann Kendall test
```{r}
# Example for non-parametric trend over time in SOC stocks
## 1. Check Mann Kendall test assumptions
par(mfrow=c(2,1))
acf(data_SOC_mse_year$mean) # no autocorrelation
pacf(data_SOC_mse_year$mean) # no partial autocorrelation

## 2. Perform Mann-Kendall test and print results
summary(MannKendall(data_SOC_mse_year$mean))

############################################################

# For loop: example of non-parametric trend in SOC stocks over time separately
for the 6 productivity categories
## 1. Define list with productivity groups
productivity_groups <- list(450, 490, 640, 660, 680, 700)

## 2. Check assumptions and perform Mann Kendall test in for loop for all
productivity categories
for (productiviti in productivity_groups) {
  cat("PRODUCTIVITY", productiviti, "\n")
  subset_treatment <- filter(data_SOCstocks_mse_year_treatment, productivity ==
productiviti)
  par(mfrow=c(2,1))
  acf(subset_treatment$mean)
  pacf(subset_treatment$mean)
  summary(MannKendall(subset_treatment$mean))
}
```
```

Figure 37: R code used to perform the Mann-Kendall test, for a single variable and in for-loop.

```
# Two tailed T-test
```{r}
# Example: differences in selected weather parameters between years with high
and years with low yield
## 1. Define list with weather variables
ttest_colnames <- list_("GDD_sum_during_LGS", "RelS_mean_during_LGS",
"Ptot_during_LGS", "Ptot_May_June_July", "length_growing_season_days",
"tot_P_agricultural_year")

## 2. Check t-test assumptions
### Normality
for (col_name in ttest_colnames) {
  cat("---", col_name, "---", "\n")
  shapiro <- data_yield_lowhigh_climate %>%
    group_by(group) %>%
    shapiro_test(col_name)%>%
    add_significance()
  print(shapiro)
}

### Homogeneity of variances
for (col_name in ttest_colnames) {
  cat("---", col_name, "---", "\n")
  levene <- data_yield_lowhigh_climate %>%
    levene_test(get(col_name) ~ as.factor(group))%>%
    add_significance()
  print(levene)
}
```

Figure 38: R code used to perform the two-tailed T-test. Continued in the next Figure.

```
### Outliers
for (col_name in ttest_colnames) {
  cat("---", col_name, "---", "\n")
  outlier <- data_yield_lowhigh_climate %>%
    group_by(group) %>%
    identify_outliers(col_name)
  print(outlier)
}

## 3. Perform two-tailed t-test and print results
for (col_name in ttest_colnames) {
  cat("---", col_name, "---", "\n")
  ttest <- t.test(get(col_name) ~ group, data=data_yield_lowhigh_climate,
var.equal=TRUE)
  print(ttest)
}

```
```

Figure 39: R code used to perform the two-tailed T-test (continued).

```
# Wilcoxon rank-sum test
```{r}
## 1. Define list
wilcoxontest_colnames <- list("Ptot_January", "Ptot_May", "Ptot_June",
"Ptot_September")

## 2. Perform test
for (col_name in wilcoxontest_colnames) {
  cat("---", col_name, "---", "\n")
  wilcox_test <- wilcox.test(get(col_name) ~ group,
data=data_yield_lowhigh_climate, var.equal=TRUE)
  print(wilcox_test)
}
```
```

Figure 40: R code used to perform the Wilcoxon rank-sum test, when the T-test assumptions were not fulfilled.

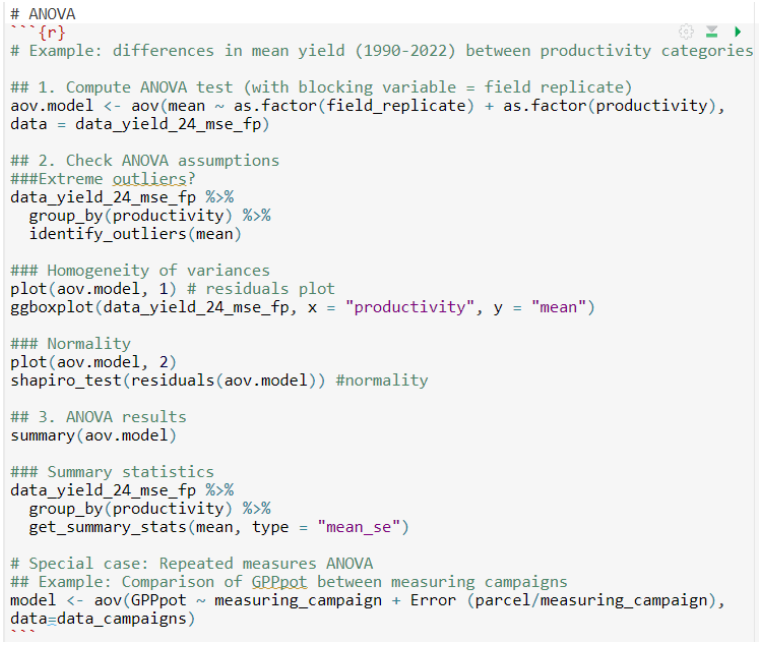

```
# ANOVA
```{r}
# Example: differences in mean yield (1990-2022) between productivity categories

## 1. Compute ANOVA test (with blocking variable = field replicate)
aov.model <- aov(mean ~ as.factor(field_replicate) + as.factor(productivity),
data = data_yield_24_mse_fp)

## 2. Check ANOVA assumptions
###Extreme outliers?
data_yield_24_mse_fp %>%
  group_by(productivity) %>%
  identify_outliers(mean)

### Homogeneity of variances
plot(aov.model, 1) # residuals plot
ggboxplot(data_yield_24_mse_fp, x = "productivity", y = "mean")

### Normality
plot(aov.model, 2)
shapiro_test(residuals(aov.model)) #normality

## 3. ANOVA results
summary(aov.model)

### Summary statistics
data_yield_24_mse_fp %>%
  group_by(productivity) %>%
  get_summary_stats(mean, type = "mean_se")

# Special case: Repeated measures ANOVA
## Example: Comparison of GPPpot between measuring campaigns
model <- aov(GPPpot ~ measuring_campaign + Error (parcel/measuring_campaign),
data=data_campaigns)
```
```

Figure 41: R code used to perform the Analysis of Variance (ANOVA). A special case regarding the repeated measures ANOVA, which is used to compare means across variables based on repeated observations, is reported.

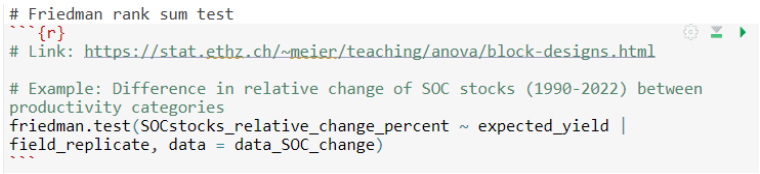

```
# Friedman rank sum test
```{r}
# Link: https://stat.ethz.ch/~meier/teaching/anova/block-designs.html

# Example: Difference in relative change of SOC stocks (1990-2022) between
productivity categories
friedman.test(SOCstocks_relative_change_percent ~ expected_yield |
field_replicate, data = data_SOC_change)
```
```

Figure 42: R code used to perform the Friedman rank sum test, as a non-parametric alternative when not all ANOVA assumptions were fulfilled.

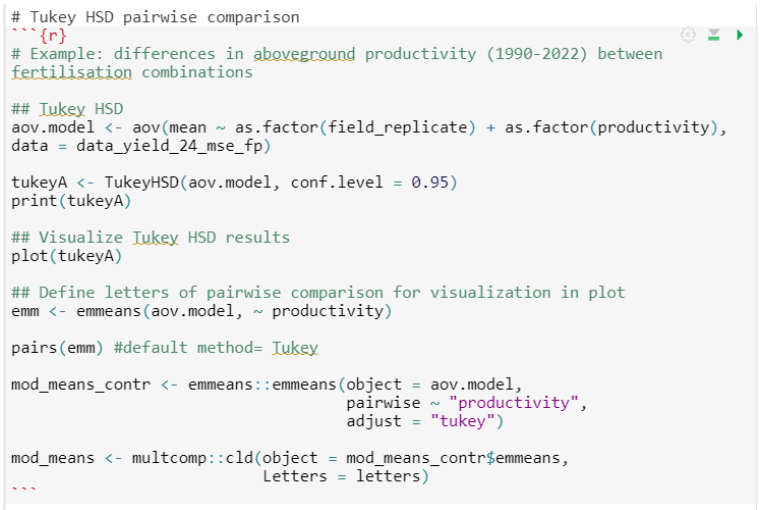

```
# Tukey HSD pairwise comparison
```{r}
# Example: differences in aboveground productivity (1990-2022) between
fertilisation combinations

## Tukey HSD
aov.model <- aov(mean ~ as.factor(field_replicate) + as.factor(productivity),
data = data_yield_24_mse_fp)

tukeyA <- TukeyHSD(aov.model, conf.level = 0.95)
print(tukeyA)

## Visualize Tukey HSD results
plot(tukeyA)

## Define letters of pairwise comparison for visualization in plot
emm <- emmeans(aov.model, ~ productivity)

pairs(emm) #default method= Tukey

mod_means_contr <- emmeans::emmeans(object = aov.model,
                                    pairwise ~ "productivity",
                                    adjust = "tukey")

mod_means <- multcomp::cld(object = mod_means_contr$emmeans,
                           Letters = letters)
```
```

Figure 43: R code used to perform multiple pairwise comparisons using the Tukey's HSD method.

```
# Plots
```{r}
# Example 1: Differences in mean yield between productivity categories
## 1. Add productivity column to mod_means in numeric format
mod_means$productivity_numeric <- c(450, 490, 640, 680, 660, 700)

## 2. Plot
ggplot(data_yield_24_mse_fp, aes(x=productivity, y=mean, group=productivity))+
  geom_point(color="grey")+
  geom_boxplot(alpha=0.1)+
  ylim(200, 800)+
  scale_x_continuous(breaks=c(450, 490, 640, 660, 680, 700))+
  scale_fill_manual(mod_means$.group)+
  stat_summary(fun.y=mean, geom="point", shape=20, size=2, color="red",
fill="red")+
  labs(x=bquote('Productivity category (g'~m^-2~')' ), y=bquote('Mean yield
(g'~m^-2~') (1990-2022)' ))+
  geom_text(size=6, family="serif", data=mod_means, aes(productivity_numeric,
upper.CL, label=.group), y=800, hjust =0.5)+
  theme_bw()+
  theme(axis.text=element_text(size=10,
family="serif"),axis.title=element_text(size=15, family="serif"), axis.title.x =
element_blank(), axis.text.x = element_text(angle = 90))
```

Figure 44: R code used to create plots. A first example.

```
# Example 2: MAT and MAP over time
## Plot MAT
plot_MAT_trend <- ggplot(data_climate, aes(year, MAT_celsius))+
  geom_point()+
  stat_poly_line() +
  stat_poly_eq(use_label(c("eq", "adj.R2")), family="serif", size=6,
label.y=0.9)+
  stat_poly_eq(use_label(c("f", "p", "n")), family="serif", size=6, label.y =
0.8)+
  labs(x="Year", y="MAT (°C)")+
  theme_bw()+
  theme(axis.text=element_text(size=10,
family="serif"),axis.title=element_text(size=15, family="serif"))

plot_MAT_trend

## Plot MAP
plot_MAP <- ggplot(data_climate, aes(year, MAP_deviation_mean_mm))+
  geom_col()+
  labs(x="Year", y="Annual total precipitation \ndeviation from the norm (mm)")+
  #annotate("label", x = 1987, y = 350, label = "Norm: mean total annual
precipitation \n (953 mm) for the period 1977-2022", size=3)+
  theme_bw()+
  theme(axis.text=element_text(size=10,
family="serif"),axis.title=element_text(size=15, family="serif"))

plot_MAP

## Combined plot
plot_climate <- plot_MAT_trend + plot_MAP
plot_climate

ggsave("plot_climate.png", plot_climate, path="figures", width = 14, height = 7,
dpi=600)
```
```

Figure 45: R code used to create plots. A second example.

Declaration of Originality

I hereby declare that the submitted Thesis is the result of my own, independent work. All external sources are explicitly acknowledged in the Thesis.

Zurich, 25.07.2023